UC San Diego

UC San Diego Electronic Theses and Dissertations

Title

DNA Guided Self-Assembly of Nanocrystals for Optoelectronic Devices /

Permalink

https://escholarship.org/uc/item/9w63w6p6

Author

Noh, Hyunwoo

Publication Date

2013

Peer reviewed|Thesis/dissertation

eScholarship.org Powered by the California Digital Library
University of California

UNIVERSITY OF CALIFORNIA, SAN DIEGO

DNA Guided Self-Assembly of Nanocrystals for Optoelectronic Devices

A dissertation submitted in partial satisfaction of the

requirements for the degree Doctor of Philosophy

in

Materials Science and Engineering

by

Hyunwoo Noh

Committee in Charge:

Professor Jennifer N. Cha, Chair
Professor Michael Heller
Professor Sungho Jin
Professor Yu-Hwa Lo
Professor Donald Sirbuly

2013

Copyright

Hyunwoo Noh, 2013

All rights reserved

The dissertation of Hyunwoo Noh is approved, and it is acceptable in quality and form for publication on microfilm:

Chair

University of California, San Diego

2013

DEDICATION

To my family

EPIGRAPH

When we are not sure, we are alive.

Graham Greene

TABLE OF CONTENTS

LIST OF FIGURES

LIST OF TABLES

ACKNOWLEDGEMENTS

This thesis would not have been possible without the extensive and generous support that I have received both personally and scientifically. First, and foremost, I would like to express my deepest gratitude and love to my wife, Miji, for always being there for me. Five years is not a short time to fully support someone without knowing his future outcome. However, she has always encouraged me when science is going well, reminded me to be realistic when I was too frustrated with things didn't work, and made the times outside of lab happier than I ever could have expected. Thanks as well to my daughter, Layla, for coming to us full of joy.

I would like to thank my family and in-laws for their love and support. My parents enabled me to pursue a graduate career without any concerns outside of lab. They have always shown their belief in me and given me inspiration in what I seek in my life. My sister and brother-in-law are always good friends as well as supporters.

I would like to express my sincere gratitude to my advisor, Prof. Jennifer N. Cha, for the immeasurable amount of support and guidance she has provided throughout this study. It was a great opportunity to work with her during my research career. A lot of fun was at the beginning of my graduate life with her while setting up the lab. This was followed by developing upon ideas which she has suggested when I first joined UCSD. Jen was a great mentor to my research as well as my life. She was always available whenever I got stuck and helped me find the answers with patience. I was always impressed that I walked into her office with confusion and uncertainty, but walked out with excitement and confidence.

I would like to thank my committee members, Prof. Sungho Jin, Prof. Michael Heller, Prof. Yu-Hwa Lo, Prof. Donald Sirbuly for helpful discussions and suggestions on my dissertation.

I would like to thank Prof. Andrew Goodwin for his valuable advice on my future and helping to edit all of my papers and Prof. Prashant Nagpal for useful discussion with my current project.

I am also thankful to all of former and current fellow group members - Prof. Albert Hung, Dr. Dylan Domaille, Ju Hun Lee, Lauren Forbes, Phyllis Xu, Matt Nakatsuka, Taeseok Oh, Michael Brasino, Ke Ma and Sam Goodman. It was my pleasure to work with them.

I would like to thank Dr. Chulmin Choi and Dr. Jin -Yeol Kim in Prof. Jin group for their help with the setup of our lab.

I would also like to thank all of my friends for making a long journey possible: Young Joo Kim, Sangkyu Nam, Hyunsu Kim's family, Youngjun Song, Junho Kim, Hyungman Cho's family, Heemin Kang, Jiwoo Kim's family, and Inkwan Park's family.

Finally, I would like to thank Charlotte Lauve for the administrative paperwork, invaluable advice, and numerous informative notices.

Chapter 1, in part, is a reprint of the material as it appears in Materials Today, 2013, in press. Xu, Phyllis F.[*]; Noh, Hyunwoo[*]; Lee, Ju Hun; Domaille, Dylan W.; Nakatsuka, Matthew A.; Goodwin, Andrew P.; Cha, Jennifer N. The dissertation author was the equally contributed primary investigator and author of this paper. Fig. 1.4 is a reprinted with permission from Kramer, I. J.; Sargent, E. H. Colloidal Quantum Dot

Photovoltaics: A Path Forward. *ACS Nano* **2011**, *5*, 8506-8514. Copyright (2010) American Chemical Society.

Chapter 2, in full, is a reprint of the material as it appears in ACS Nano, Volume 3, 2010. Noh, Hyunwoo; Hung, Albert M.; Choi, Chulmin; Lee, Ju Hun; Kim, Jin-Yeol; Jin, Sungho; Cha, Jennifer N. The dissertation author was the primary investigator and author of this paper.

Chapter 3, in full, is a reprint of the material as it appears in ACS Nano, Volume 4, 2011. Noh, Hyunwoo; Choi, Chulmin; Hung, Albert M.; Jin, Sungho; Cha, Jennifer N. The dissertation author was the primary investigator and author of this paper.

Chapter 4, in full, is a reprint of the material as it appears in Small, Volume 7, 2011. Noh, Hyunwoo; Hung, Albert M.; Cha, Jennifer N. The dissertation author was the primary investigator and author of this paper.

Chapter 5, in full, is currently being prepared for submission for publication of the material. Noh, Hyunwoo; Nagpal, Prashant; Cha, Jennifer N. The dissertation author was the primary investigator and author of this material.

Hyunwoo Noh

Boulder, July 2013

VITA

2006	Bachelor of Engineering in Materials Science and Engineering, Korea University, Korea
2008	Master of Engineering in Advanced Materials Engineering, Korea University, Korea
2013	Doctor of Philosophy in Materials Science and Engineering, University of California, San Diego, USA

LIST OF PUBLICATIONS

[1] **Noh, H**.; Hung, A. M.; Choi, C.; Lee, J. H.; Kim, J. -Y.; Jin, S.; Cha, J. N. 50 nm DNA Nanoarrays Generated from Uniform Oligonucleotide Films. *ACS Nano* **2009**, *3*, 2376-2382.

[2] Cha, J. N.; Hung, A. M.; **Noh, H**. Biomolecular Architectures and Systems for Nanoscience Engineering. *Proc. of SPIE* **2010**, *7636*, 763710.

[3] **Noh, H**.; Choi, C.; Hung, A. M.; Jin, S.; Cha, J. N. Site-Specific Patterning of Highly Ordered Nanocrystal Superlattices through Biomolecular Surface Confinement. *ACS Nano* **2010**, *4*, 5076-5080.

[4] Hung, A. M.; **Noh, H.**; Cha, J. N. Recent Advances in DNA-based Directed Assembly on Surface. *Nanoscale*, **2010**, *2*, 2530-2537.

[5] Xu, P. F.; **Noh, H.**; Lee, J. H.; Cha, J. N. DNA Mediated Assembly of Single Walled Carbon Nanotubes:Role of DNA Linkers and Annealing. *Physical Chemistry Chemical Physics* **2011**, *13*, 10004-10008.

[6] **Noh, H.**; Hung, A. M.; Cha, J. N. Surface-Driven DNA Assembly of Binary Cubic 3D Nanocrystal Superlattices. *Small* **2011**, *7*, 3021-3025.

[7] Xu, P. F.; Hung, A. M.; **Noh, H.**; Cha, J. N. Switchable Nanodumbbell Probes for Analyte Detection. *Small* **2013**, *9*, 228-232.

[8] Xu, P. F*****.; **Noh, H.***; Lee, J.H; Domaille, D. W.; Nakatsuka, M. A.; Goodwin, A. P.; Cha, J. N. Imparting the Unique Properties of DNA into Complex Material Architecture and Function. *Materials Today* **2013**, *in press* (***** equal contribution)

[9] **Noh, H.**; Nagpal, P.; Cha, J. N. Scalable Assembly of 3D Excitonic Nanocrystal Assemblies by using DNA Interactions and DNA Mediated Charge Transport. *(manuscript in preparation)*

[10] Goodman, S.; Singh, V.; **Noh, H.**; Casamada, J.; Chatterjee, A.; Cha, J. N.; Nagpal, P. Hopping Transport between Nucleic Acid Sequences and Exciton Shelves for DNA-Quantum Dot Electronics. *(manuscript in preparation)*

ABSTRACT OF THE DISSERTATION

DNA Guided Self-Assembly of Nanocrystals for Optoelectronic Devices

by

Hyunwoo Noh

Doctor of Philosophy in Materials Science and Engineering

University of California, San Diego, 2013

Professor Jennifer N. Cha, Chair

While inherent properties of nanocrystals have been actively investigated within the last decade, control over positioning and ordering of nanomaterials at multiple length scales has been difficult to achieve. In the research shown here, DNA is used in conjunction with metal and semiconductor nanocrystals to facilitate their assembly at precise locations on a substrate with potential for programmable ordering. The inimitable ability of DNA to binding through stable, specific, and reversible molecular recognition has allowed the creation of nanocrystal assemblies through extraordinary control over spatial location and crystallization.

We first show an inexpensive printing method that enables repeated patterning of large area arrays of nanoscale materials by AFM and fluorescence microscopy. DNA strands were patterned with 50nm resolution by a soft-lithographic subtraction printing

process and DNA hybridization was used to direct the assembly of 10nm gold nanoparticles to create ordered two-dimensional nanoparticle arrays. This technique was further modified to demonstrate methods to generate patterned nanocrystal superlattices. Electron microscopy and fourier transformation analysis were used to investigate the role of chemical and geometrical confinement on interparticle DNA hybridization and particle packing and obtaining long-range order. Using similar strategies, we also demonstrate the generation of highly ordered 3-D body-centered-cubic (BCC) superlattices of gold nanocrystals at desired areas on a surface through specific DNA interactions. In this work, controlled film thicknesses from 20nm to 100nm could be easily obtained by varying initial gold nanoparticle concentrations and particles remained ordered in the z-direction as well.

These gold nanoparticle studies were then applied toward producing 3D thin film arrays of quantum dots (QDs) For this, successful aqueous phase transfer of CdTe QDs for DNA conjugation was first demonstrated. Next, the DNA conjugated CdTe QDs were assembled on TiO_2 films to fabricate ITO/TiO_2/DNA-CdTe/Au thin film devices which were then tested by current-voltage measurements. We demonstrate that producing close packed arrays as opposed to disordered ones significantly improves film formation with less defects. By tuning the QD size and film thicknesses, the correlation between V_{oc} and J_{sc} values was investigated to show the possibility of charge transport through DNA-QDs assembly for the application of optoelectronic devices.

CHAPTER 1: Introduction

1.1 Deoxyribonucleic Acid (DNA)

Double helix structure of DNA was first discovered by James Watson and Francis Crick.[1] DNA is composed of a family of purines and pyrimidines called four nucleotide bases, adenine (A), guanine (G), thymine (T), and cytosine (C) along highly negatively charged phosphate deoxyribose backbone. Its hybridization through hydrogen bonds between A-T and C-G produces a double helix consisting of anti-parallel complementary strands with 2nm width and 0.3nm base in general. It has three different conformations (A-DNA, B-DNA and Z-DNA) depending on hydration level, DNA sequence and the amount and direction of supercoiling. While A-DNA forms under a condition of high salt or dehydration B-DNA and Z-DNA are directly observed in Nature.[2] Once hybridized, the persistence length increases from ~1 nucleotide for single stranded DNA (ssDNA) to about 100 bases for double stranded DNA (dsDNA), and this rigidity allows self-assembled DNA structures to hold their shape upon assembly.

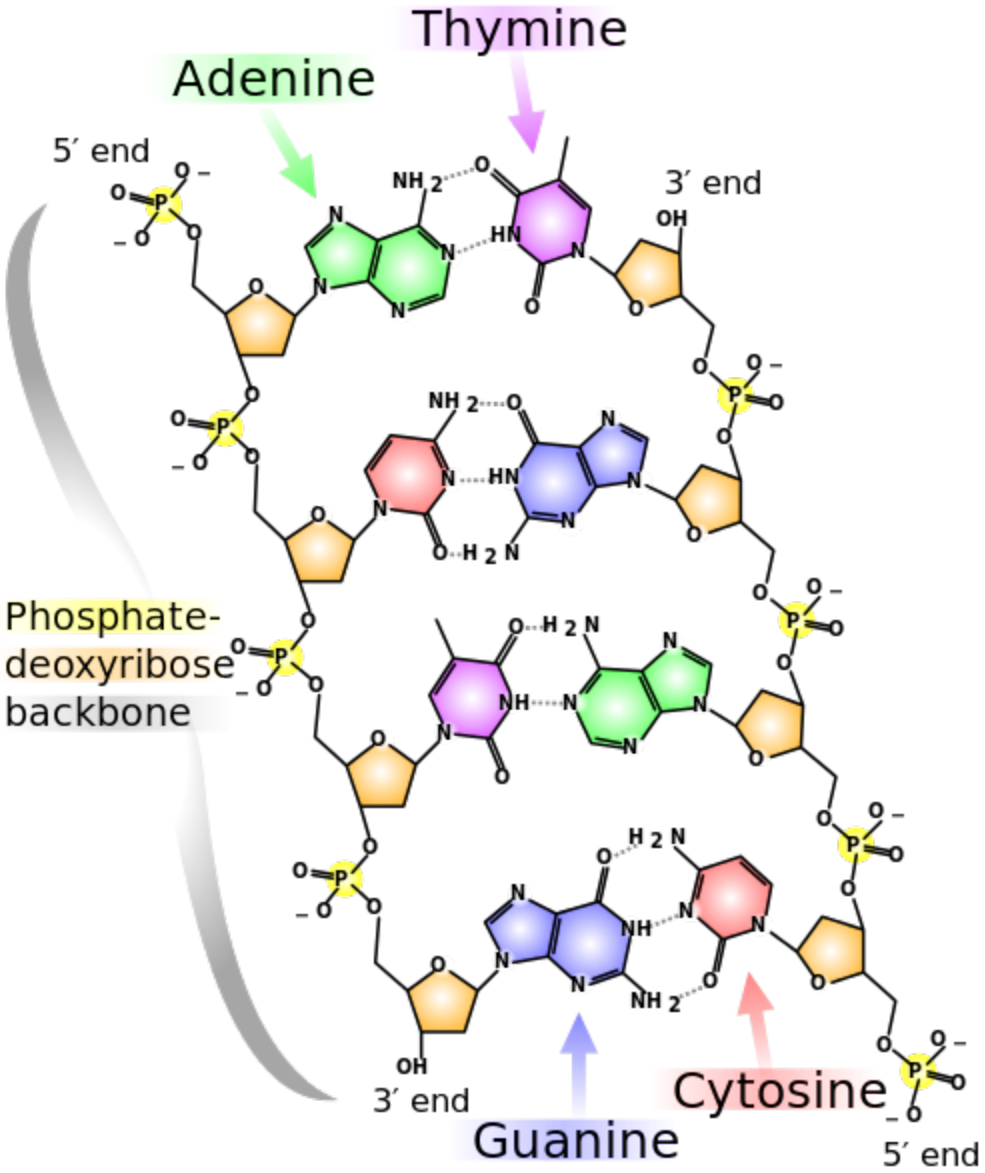

Fig. 1.1 Schematic of DNA structure[3]

Table 1.1 Summary of A-DNA, B-DNA and Z-DNA[4]

Geometry attribute:	**A-form**	**B-form**	**Z-form**
Helix sense	right-handed	right-handed	left-handed
Repeating unit	1 bp	1 bp	2 bp
Rotation/bp	33.6°	35.9°	60°/2
Mean bp/turn	11	10.5	12
Inclination of bp to axis	+19°	−1.2°	−9°
Rise/bp along axis	2.4 Å (0.24 nm)	3.4 Å (0.34 nm)	3.7 Å (0.37 nm)
Rise/turn of helix	24.6 Å (2.46 nm)	33.2 Å (3.32 nm)	45.6 Å (4.56 nm)
Diameter	23 Å (2.3 nm)	20 Å (2.0 nm)	18 Å (1.8 nm)

1.2 DNA-Mediated Assembly of Nanomaterials for Device Fabrication

The advent of nanotechnology has brought to existence a diverse set of nanomaterials possessing unique electronic, optical, or magnetic properties. One of the grand challenges associated with engineering functional materials or devices from such nanoscale objects has been how to integrate and assemble them into hierarchical arrays with minimal defects. However, these particles and surfaces are generally easily modified with oligonucleotides, which in turn allow the organization of nanomaterials into different packing densities and arrangements for a variety of applications, as demonstrated in initial groundbreaking work by Alivisatos and Mirkin.[5,6] By varying the length and sequence of the DNA on the nanoparticles, core-satellite structures[7] or discrete geometrical organizations[8, 9] have been formed in which the DNA controls not only the distance between particles[10] but also the angle of packing.[11] Particle distances have also been modified through dynamic hybridization schemes such as hairpin structures.[12] Beyond discrete nanoparticle clusters, Mirkin and Gang recently reported methods to create well-ordered bulk nanoparticle solids (Fig. 1.2a).[13,14] Specifically, tuning hybridization between two particles led to gold nanoparticle (AuNP) superlattices with either face-centered-cubic (FCC) or body-centered-cubic (BCC) orientation. Since their first demonstration, further studies have clarified the effect of particle size, hydrodynamic size, and length of DNA on assembly,[15] and similar techniques have been applied to create mixed-particle systems of AuNPs and quantum dots.[16] It is worth noting that this degree of tunability in nanoparticle ordering and packing cannot be easily achieved with synthetic polymers or small molecule systems,

nor is it trivial to obtain thermodynamically-stable nanoparticle superlattices through simple thermal annealing.

Anisotropic nanomaterials may also be organized with similar tools. The size and shape of metal nanostructures determine their plasmon behavior, and an understanding of the different facets on a given structure can allow face-selective DNA functionalization for engineering new optically active materials. For example, Mirkin and coworkers recently created a hexagonal close-packed superlattice of Au nanorods by using different DNA sequences and lengths (Fig. 1.2b),[17] and Mann and coworkers described a similar example in which nanorods were assembled in 2D along their long axes to maximize DNA overlap and hybridization.[18] DNA has also guided the assembly of various anisotropic nanoparticles such as nanoprisms and rhombic dodecahedra. In these cases, the inherent difference in surface energies in anisotropic colloidal particles allowed selective functionalization of the sides of the particles for building unique hybrid structures.[19,20] Furthermore, since DNA hybridization is thermally reversible, the plasmon responses of DNA-nanorod assemblies can be easily and controllably tuned through simple temperature changes.[21]

DNA-guided assembly directly on surfaces has also been shown as a promising method for the creation of nanoelectronic, nanophotonic, or optoelectronic solid-state devices, as such materials often require control over nanomaterial placement, organization, and orientation in both two and three dimensions. The overall strategy of these methods is to use complementary and/or orthogonal sequences in both surface-bound and particle-bound DNA to direct the assembly of particles both to a surface and to each other. DNA is deposited onto a surface through either physical interaction with a

hydrophilic surface (typically patterned from a hydrophobic resist) or covalent conjugation through an end group on the DNA. For example, 2D DNA origami has been deposited onto areas etched by either e-beam lithography or photolithography, followed by hybridization and deposition of DNA-AuNPs onto the etched surface.[22-24] Due to the mesoscale size regime of DNA origami, methods to merge top-down lithography with bottom-up self-assembled DNA have been developed to produce precise ordered arrays of 5nm AuNPs (Fig. 1.3c).[25,26] These DNA origami can also in principle be extended to organizing other nanomaterials on surfaces, including carbon nanotubes (CNTs)[27] or biomolecules (Fig. 1.3a, b).[28-30] Although CNTs are typically very difficult to disperse in water without the addition of surfactants[31] or chemical modification,[32] ssDNA can solubilize CNTs in aqueous media through π-π stacking of the DNA bases to the CNT sidewall.[33] Specific DNA oligonucleotides have also been shown to bind to specific CNT widths and chiralities,[34] empowering DNA for both CNT purification and assembly (Fig. 1.3c, d)[35,36]

In addition, cost-effective printing methods have been developed to produce patterned domains of large-area close packed nanoparticle films on substrates. For example, , nanoparticle superlattices with long range order could be obtained within DNA arrays patterned by traditional micro-contact printing or inking-subtraction-printing,[37] followed by thermal annealing into superlattices through hybridization between the DNA-AuNPs and the surface DNA.[38] Similar techniques have been applied to create 3D particle assemblies on substrates with surface strands used to promote interparticle hybrdization.[39] The ability to organize nanoparticle arrangements on surfaces through simple tuning of DNA hybridization exemplifies the power of using

a self-recognizing polymer such as DNA for controlling particle packing in both two and three dimensions. The typical approaches for engineering ordered thin films of nanoparticles on substrates to date have been to use electrostatic interactions,[40] spatial confinement,[41] or air-liquid interfaces.[42] Using DNA interactions to drive particle ordering provides a framework to assemble a diverse set of nanoparticle sizes and compositions, while avoiding barriers to manufacturing such as needing high nanoparticle concentrations or requiring slow evaporation. Furthermore, because DNA interactions can be programmed to include flexible, compressible sections, polydisperse nanoparticle batches may also be assembled into well-ordered arrangements.[15-17]

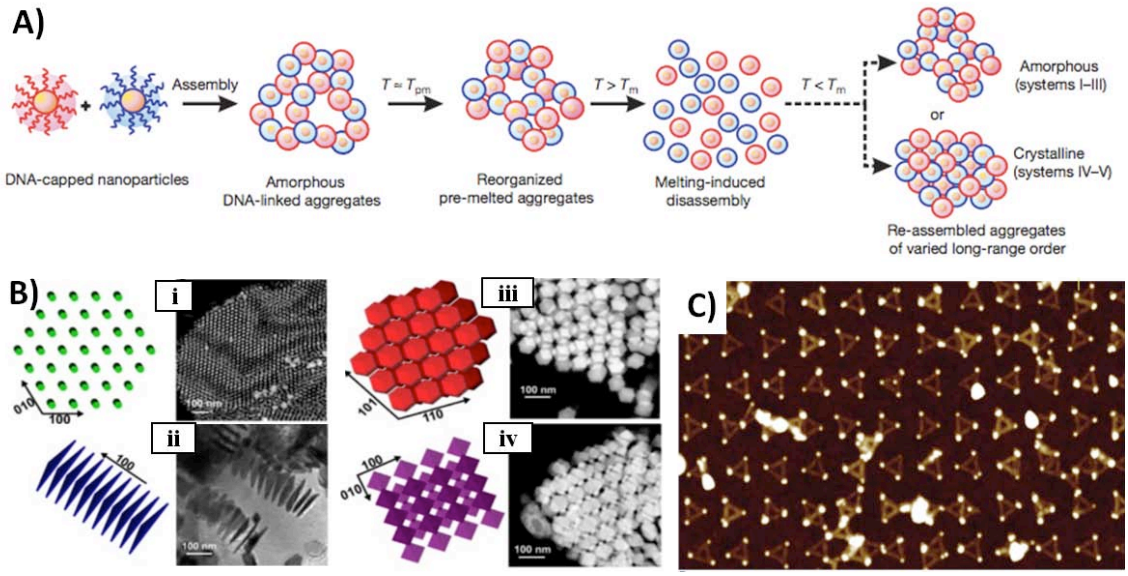

Fig. 1.2 (A) Amorphous and crystalline 3D gold nanoparticle arrays assembled through DNA interactions. Tpm and Tm encode for DNA pre-melting and melting temperatures, respectively.[14] (B) Schematic illustration and TEM image of superlattices with ordered i)nanorod (55nm length, 14nm width), ii) nanoprism (140nm edge length), iii) rhombic (64nm diameter) and iv) octahedra (83nm diameter) nanoparticles.[17] (C) DNA origami mediated assembly of gold nanoparticles on lithographically patterned surfaces.[25]

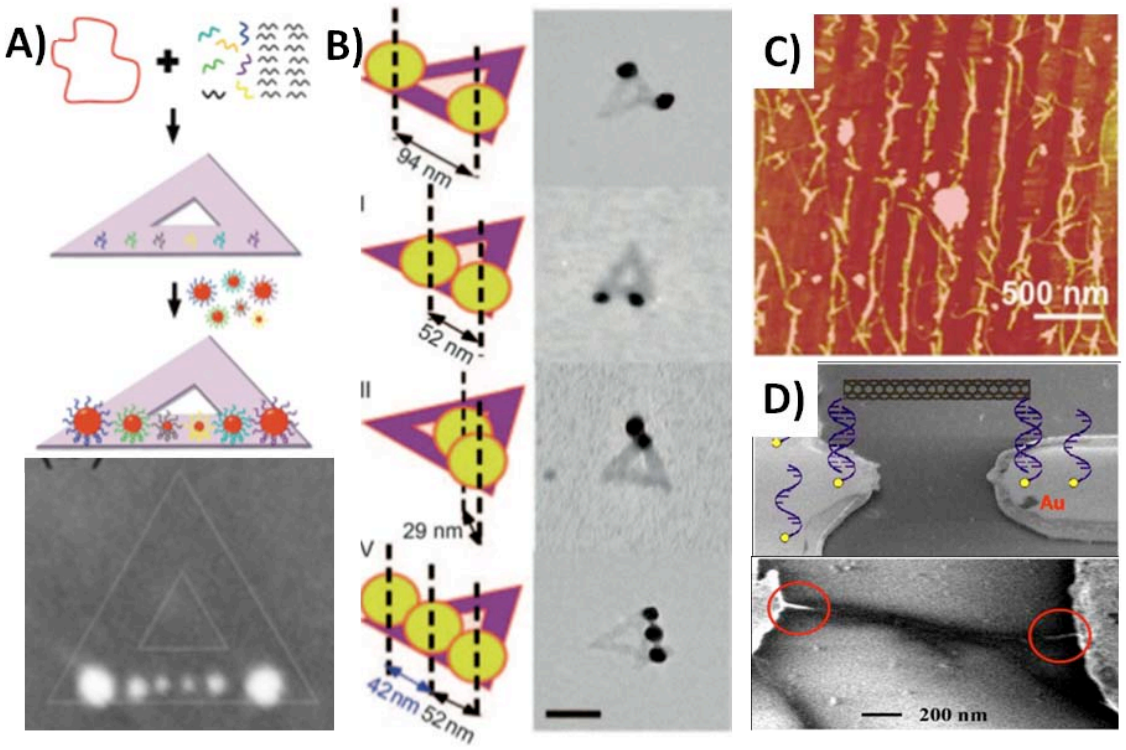

Fig. 1.3 DNA origami is used to pattern (a) gold nanoparticles of different sizes[29] and (b) silver nanoparticles in specified locations.[30] Carbon nanotubes aligned by DNA on (c) Si substrates and (d) across gold electrodes.[36]

1.3 Quantum Dot(QD) solar cells

Quantum dot (QD) solar cells are particularly advantageous in terms of performance and manufacturing. The first major advantage is that the optical property of QDs is able to be easily tuned by changing the size of the QD particles. As the size becomes smaller than the Bohr radius of the material, a quantum confinement effect will be observed. By minimizing the QD size to increase the band gap of the particles allows one to design suitable sizes of quantum dot to be used in devices for maximizing the absorption of the solar spectra for solar cells applications. The second benefit of QDs is that they can generate either multiple excitons (electron-hole pairs) or hot carriers,[43] where the absorption of one photon can create multiple excitons or excited electrons are separated without any loss as a phonon. These mechanisms increase the collection of carriers as well as open circuit voltage, resulting in improvement of device performance. Another attraction to the use of QDs is that they allow for facile and economic manufacturing processes. Solar cells made of quantum dots could be prepared by processes such as drop casting, dip coating and spin coating, which do not require extensive labor or high process costs, as opposed to expensive and complex microfabrication processes for the fabrication of Si solar cells. The QD material itself can also be produced with economically and with high throughput.

To take advantage of the intrinsic properties of the QDs and their facile fabrication process, there have been many efforts on achieving high efficient solar cells using QD components. There are several types of QDs solar cells such as single layer QD solar cells,[44-47] heterojunction QD solar cells and bulk heterojunction QD solar cells,[48-58] and quantum dot sensitized solar cell.[59-62] All these efforts are aimed at

improving light absorption and carrier separation for efficient collection of carriers to obtain the enhanced power conversion efficiency. To achieve the goal above, there has been an effort to study charge transport of quantum dot films.[63-65] In general, quantum dots are created using hydrocarbon capping ligands as a stabilizer but the alkyl chain ligands also act as an insulating barrier inhibiting carrier transport between QDs. An approach to alleviate the problem of carrier transport caused by the ligand focuses on a mechanism of carrier transport between quantum dots, generally known as tunneling or hopping. In this case, band-like transport of QD films can occur under the condition that the energy scale of the film disorder is smaller than the coupling energy, which means highly ordered arrays of QDs are needed to fulfill this condition. A couple of methods have been developed to solve this problem and are currently widely used; (1) a ligand exchange with short molecules[67] (2) sintering/burning of quantum dots to remove the ligands.[68] However, it has been stills challenging to build ordered arrays of QDs, people are looking towards various self-assembly methods to pattern the QDs due to the challenges of top-down placement of the nanometer-sized particles.

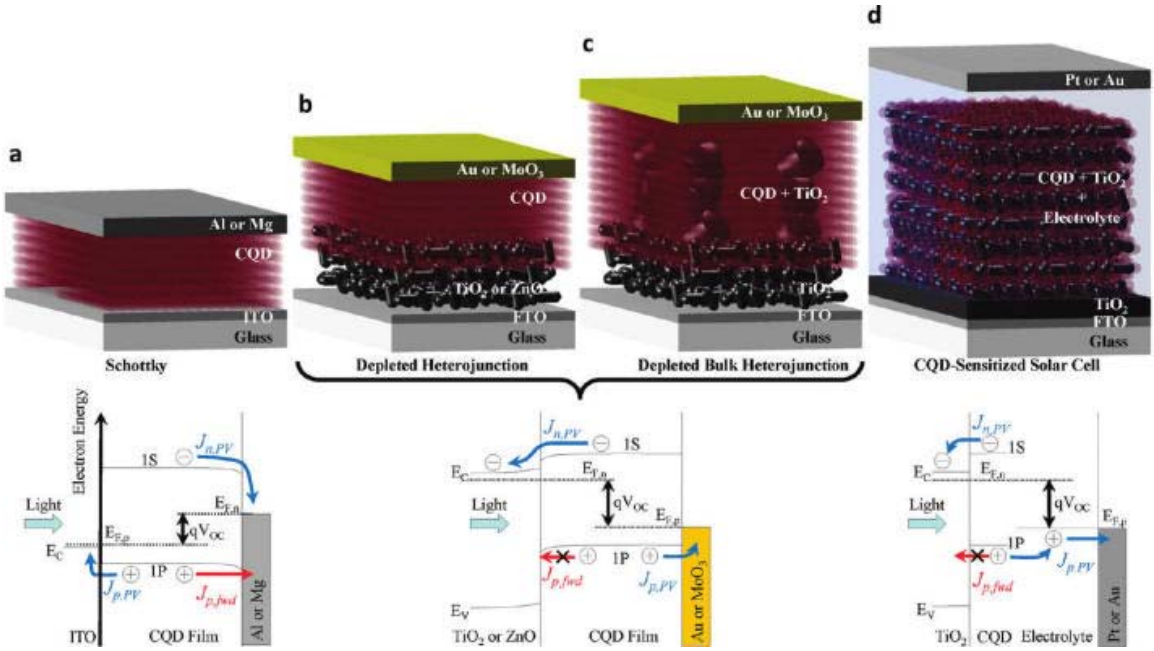

Fig. 1.4 Schematic of Quantum Dot(QD) based solar cells and its electron band diagrams. a) Single layer QD solar cell b) Depleted heterojunction QD solar cell c) Depleted bulk heterojunction solar cell d) QD sensitized solar cell.[66]

1.4 Overview of the dissertation

Chapter 2 describes a facile way to pattern DNA films which feature size is up to 50nm by subtraction printing. Selective adsorption of gold nanoparticles by means of DNA-DNA hybridization is demonstrated.

Chapter 3 further develops a method of confined DNA patterning by dual subtraction printing, which allows us to achieve long range order of hexagonally packed gold nanoparticles. Key factors such as physical and chemical confinement, an interaction between nanoparticles and humid annealing are discussed.

Chapter 4 describes the rational design of DNA sequence to build Body-Centered-Cubic array of gold nanoparticles on the substrate, in which smooth and uniformity of film is demonstrated with a facile thickness control.

Chapter 5 describes the expansion of an idea of gold nanoparticle-DNA assembly toward semiconducting nanoparticle(Quantum dot)-DNA assembly in order to build solar cells. A facile way to fabricate QD solar cells as well as charge transport between QD and DNA are discussed.

1.5 Acknowledgments

This chapter, in part, is a reprint of the material as it appears in Materials Today, 2013, in press. Xu, Phyllis F.[*]; Noh, Hyunwoo[*]; Lee, Ju Hun; Domaille, Dylan W.; Nakatsuka, Matthew A.; Goodwin, Andrew P.; Cha, Jennifer N. The dissertation author was the equally contributed primary investigator and author of this paper.

Fig. 1.4 is a reprinted with permission from Kramer, I. J.; Sargent, E. H. Colloidal Quantum Dot Photovoltaics: A Path Forward. *ACS Nano* **2011**, *5*, 8506-8514. Copyright (2011) American Chemical Society.

1.6 References

1. Watson, J.D.; Crick, F.H.C. A Structure for Deoxyribose Nucleic Acid. *Nature* **1953**, *171*, 737-738.

2. Ghosh, A; Bansal, M. A Glossary of DNA Structures from A to Z. *Acta Crystallogr D Biol Crystallogr* **2003**, *59*, 620–626.

3. http://en.wikipedia.org/wiki/DNA

4. http://en.wikipedia.org/wiki/A-DNA

5. Alivisatos, A. P.; Johnsson, K. P.; Peng, X.; Wilson, T. E.; Loweth, C. J.; Bruchez, M. P.; Schultz, P. G. Organization of 'Nanocrystal Molecules' Using DNA. *Nature* **1996**, *382*, 609-611.

6. Mirkin, C. A.; Letsinger, R. L.; Mucic, R. C.; Storhoff, J. J. A DNA-Based Method for Rationally Assembling Nanoparticles into Macroscopic Materials. *Nature* **1996**, *382*, 607-609.

7. Pal, S.; Sharma, J.; Yan, H.; Liu, Y. Stable Silver Nanoparticle–DNA Conjugates for Directed Self-Assembly of Core-Satellite Silver–Gold Nanoclusters. *Chem. Commun.* **2009**, *0*, 6059-6061.

8. Mastroianni, A. J.; Claridge, S. A.; Alivisatos, A. P. Pyramidal and Chiral Groupings of Gold Nanocrystals Assembled Using DNA Scaffolds. *J. Am. Chem. Soc.* **2009**, *131*, 8455-8459.

9. Fu, A.; Micheel, C. M.; Cha, J.; Chang, H.; Yang, H.; Alivisatos, A. P. Discrete Nanostructures of Quantum Dots/Au with DNA. *J. Am. Chem. Soc.* **2004**, *126*, 10832-10833.

10. Lee, J.; Wernette, D. P.; Yigit, M. V.; Liu, J.; Wang, Z.; Lu, Y. Site-Specific Control of Distances between Gold Nanoparticles Using Phosphorothioate Anchors on DNA and a Short Bifunctional Molecular Fastener. *Angew. Chem. Int. Ed.* **2007**, *46*, 9006-9010.

11. Wen, Y.; Chen, L.; Wang, W.; Xu, L.; Du, H.; Zhang, Z.; Zhang, X.; Song, Y. A Flexible DNA Modification Approach Towards Construction of Gold Nanoparticle Assemblies. *Chem. Commun.* **2012**, *48*, 3963-3965.

12. Xu, P.F.; Hung, A. M.; Noh, H.; Cha, J. N. Switchable Nanodumbbell Probes for Analyte Detection. *Small* **2013**, *9*, 228-232.

13. Park, S. Y.; Lytton-Jean, A. K. R.; Lee, B.; Weigand, S.; Schatz, G. C.; Mirkin, C.A. DNA-Programmable Nanoparticle Crystallization. *Nature* **2008**, *451*, 553-556.

14. Nykypanchuk, D.; Maye, M. M.; van der Lelie, D.; Gang, O. DNA-Guided Crystallization of Colloidal Nanoparticles. *Nature* **2008**, *451*, 549-552.

15. Macfarlane, R.; Lee, B.; Jones, M. R.; Harris, N.; Schatz, G. C.; Mirkin, C. A. Nanoparticle Superlattice Engineering with DNA. *Science* **2011**, *334*, 204-208.

16. Sun, D.; Gang, O. Binary Heterogeneous Superlattices Assembled from Quantum Dots and Gold Nanoparticles with DNA. *J. Am. Chem. Soc.* **2011**, *133*, 5252-5254.

17. Jones, M. R.; Macfarlane, R. J.; Lee, B.; Zhang, J.; Young, K. L.; Senesi, A. J.; Mirkin, C. A. DNA-Nanoparticle Superlattices Formed from Anisotropic Building Blocks. *Nat. Mater.* **2010**, *9*, 913-917.

18. Dujardin, E.; Hsin, L.-B.; Wang, C. R. C.; Mann, S. DNA-Driven Self-Assembly of Gold Nanorods. *Chem. Commun.* **2001**, 1264-1265.

19. Xu, L.; Kuang, H.; Xu, C.; Ma, W.; Wang, L.; Kotov, N. A. Regiospecific Plasmonic Assemblies for in Situ Raman Spectroscopy in Live Cells. *J. Am. Chem Soc.* **2012**, *134*, 1699-1709.

20. Millstone, J. E.; Georganopoulou, D. G.; Xu, X.; Wei, W.; Li, S.; Mirkin, C. A. DNA-Gold Triangular Nanoprism Conjugates. *Small* **2008**, *4*, 2176-2180.

21. Li, Z.; Zhu, Z.; Liu, W.; Zhou, Y.; Han, B.; Gao, Y.; Tang, Z. Reversible Plasmonic Circular Dichroism of Au Nanorod and DNA Assemblies. *J. Am. Chem. Soc.* **2012**, *134*, 3322-3325.

22. Sapsford, K. E.; Park, D.; Goldman, E. R.; Foos, E. E.; Trammell, S. A.; Lowy, D. A.; Ancona, M. G. Selective DNA-Mediated Assembly of Gold Nanoparticles on Electroded Substrates. *Langmuir* **2008**, *24*, 10245-10252.

23. Kannan, B.; Kulkarni, R. P.; Majumdar, A. DNA-Based Programmed Assembly of Gold Nanoparticles on Lithographic Patterns with Extraordinary Specificity. *Nano Lett.* **2004**, *4*, 1521-1524.

24. Lalander, C. H.; Zheng, Y.; Dhuey, S.; Cabrini, S.; Bach, U. DNA-Directed Self-Assembly of Gold Nanoparticles onto Nanopatterned Surfaces: Controlled Placement of Individual Nanoparticles into Regular Arrays. *ACS Nano* **2010**, *4*, 6153-6161.

25. Hung, A. M.; Micheel, C. M.; Bozano, L. D.; Osterbur, L. W.; Wallraff, G. M.; Cha, J. N. Large-Area Spatially Ordered Arrays of Gold Nanoparticles Directed by Lithographically Confined DNA Origami. *Nat. Nanotech.* **2010**, *5*, 121-126.

26. Kershner, R. J.; Bozano, L. D.; Micheel, C. M.; Hung, A. M.; Fornof, A. R.; Cha, J. N.; Rettner, C. T.; Bersani, M.; Frommer, J.; Rothemund, P. W. K.; Wallraff, G. M. Placement and Orientation of Individual DNA Shapes on Lithographically Patterned Surfaces. *Nat. Nanotech.* **2009**, *4*, 557-561

27. Maune, H.T., Han, S.-P.; Barish, R. D.; Bockrath, M.; Goddard, W. A. III; Rothemund, P. W. K.; Winfree, E. Self-Assembly of Carbon Nanotubes into Two-Dimensional Geometries using DNA Origami Templates. *Nat. Nanotech.* **2009**, *5*, 61-66.

28. Stephanopoulos, N.; Liu, M.; Tong, G. J.; Li, Z.; Liu, Y.; Yan, H.; Francis, M. B. Immobilization and One-Dimensional Arrangement of Virus Capsids with Nanoscale Precision Using DNA Origami. *Nano Lett.* **2010**, *10*, 2714-2720.

29. Ding, B.; Deng, Z.; Yan, H.; Cabrini, S.; Zuckermann, R. N.; Bokor, J. Gold Nanoparticle Self-Similar Chain Structure Organized by DNA Origami. *J. Am. Chem. Soc.* **2010**, *132*, 3248-3249.

30. Pal, S.; Deng, Z.; Ding, B.; Yan, H.; Liu, Y. DNA-Origami-Directed Self-Assembly of Discrete Silver-Nanoparticle Architectures. *Angew. Chem. Int. Ed.* **2010**, *49*, 2700-2704.

31. Arnold, M.S.; Green, A. A.; Hulvat, J. F.; Stupp, S. I; Hersam, M. C. Sorting Carbon Nanotubes by Electronic Structure Using Density Differentiation. *Nat. Nanotech.* **2006**, *1*, 60-65.

32. Liang, F.; Sadana, A. K.; Peera, A.; Chattopadhyay, J.; Gu, Z.; Hauge, R. H.; Billups, W. E. A Convenient Route to Functionalized Carbon Nanotubes. *Nano Lett.* **2004**, *4*, 1257-1260.

33. Zheng, M.; Jagota, A.; Semke, E. D.; Diner, B. A.; Mclean, R. S.; Lustig, S. R.; Richardson, R. E.; Tassi, N. G. DNA-Assisted Dispersion and Separation of Carbon Nanotubes. *Nat. Mater.* **2003**, *2*, 338-342.

34. Tu, X.; Manohar, S.; Jagota, A; Zheng, M. DNA Sequence Motifs for Structure Specific Recognition and Separation of Carbon Nanotubes. *Nature* **2009**, *460*, 250-253.

35. Xu, P.F.; Noh, H.; Lee, J. H.; Cha, J. N. DNA mediated assembly of single walled carbon nanotubes: role of DNA linkers and annealing. *Phys. Chem. Chem. Phys.* **2011**, *13*, 10004-10008.

36. Hazani, M.; Hennrich, F.; Kappes, M.; Naaman, R.; Peled, D.; Sidorov, V; Shvarts, D. DNA-Mediated Self-Assembly of Carbon Nanotube-Based Electronic Devices. *Chem. Phys. Lett.* **2004**, *391*, 389-392.

37. Noh, H.; Hung, A. M.; Choi, C.; Lee, J. H.; Kim, J.-Y.; Jin, S.; Cha, J. N. 50 nm DNA Nanoarrays Generated from Uniform Oligonucleotide Films. *ACS Nano* **2009**, *3*, 2376-2382.

38. Noh, H.; Choi, C; Hung, A. M.; Jin, S.; Cha, J.N. Site-Specific Patterning of Highly Ordered Nanocrystal Superlattices through Biomolecular Surface Confinement. *ACS Nano* **2010**, *4*, 5076-5080.

39. Noh, H.; Hung, A. M.; Cha, J. N. Surface-Driven DNA Assembly of Binary Cubic 3D Nanocrystal Superlattices. *Small* **2011**, *7*, 3021-3025.

40. Shevchenko, E. V.; Talapin, D. V.; Kotov, N. A.; O'Brien, S.; Murray, C. B. Structural Diversity in Binary Nanoparticle Superlattices. *Nature* **2006**, *439*, 55-59.

41. Cheng, W.; Park, N.; Walter, M.T.; Hartman, M.R.; Luo, D. Nanopatterning Self-Assembled Nanoparticle Superlattices by Moulding Microdroplets. *Nat. Nanotech.* **2008**, *3*, 682-690.

42. Dong A.; Chen, J.; Vora, P. M.; Kikkawa, J. M.; Murray, C. B. Binary Nanocrystal Superlattice Membranes Self-Assembled at the Liquid–Air Interface. *Nature* **2010**, *466*, 474-477.

43. Tisdale, W. A.; Williams, K. J.; Timp, B. A.; Norris, D. J.; Aydil, E. S.; Zhu, X.-Y. Hot-Electron Transfer from Semiconductor Nanocrystals. *Science* **2010**, *328*, 1543-1547.

44. Koleilat, G. I.; Levina, L.; Shukla, H.; Myrskog, S. H.; Hinds, S.; Pattantyus-Abraham, A. G.; Sargent, E. H. Efficient, Stable Infrared Photovoltaics Based on Solution-Cast Colloidal Quantum Dots. *ACS Nano* **2008**, *2*, 833-840.

45. Johnston, K. W.; Pattantyus-Abraham, A. G.; Clifford, J. P.; Myrskog, S. H.; MacNeil, D. D.; Levina, L.; Sargent, E. H. Schottky-Quantum Dot Photovoltaics for Efficient Infrared Power Conversion. *Appl. Phys. Lett.* **2008**, *92*, 151115.

46. Luther, J. M.; Law, M.; Beard, M. C.; Song, Q.; Reese, M. O.; Ellingson, R. J.; Nozik, A. J. Schottky Solar Cells Based on Colloidal Nanocrystal Films. *Nano Lett.* **2008**, *8*, 3488-3492.

47. Debnath, R.; Tang, J.; Barkhouse, D. A.; Wang, X.; Pattantyus-Abraham, A. G.; Brzozowski, L.; Levina, L.; Sargent, E. H. Ambient-Processed Colloidal Quantum

Dot Solar Cells via Individual Pre-Encapsulation of Nanoparticles. *J. Am. Chem. Soc.* **2010**, *132*, 5952-5953.

48. Leschkies, K. S.; Beatty, T. J.; Kang, M. S.; Norris, D. J.; Aydil, E. S. Solar Cells Based on Junctions between Colloidal PbSe Nanocrystals and Thin ZnO Films. *ACS Nano* **2009**, *3*, 3638-3648.

49. Luther, J. M.; Gao, J.; Lloyd, M. T.; Semonin, O. E.; Beard, M. C.; Nozik, A. J. Stability Assessment on a 3% Bilayer PbS/ZnO Quantum Dot Heterojunction Solar Cell. *Adv. Mater.* **2010**, *22*, 3704-3707.

50. Choi, J. J.; Lim, Y.-F.; Santiago-Berrios, M. B.; Oh, M.; Hyun, B.-R.; Sun, L.; Bartnik, A. C.; Goedhart, A.; Malliaras, G. G.; Abruna, H. D. et al. PbSe Nanocrystal Excitonic Solar Cells. *Nano Lett.* **2009**, *9*, 3749-3755.

51. Debnath, R.; Greiner, M .T.; Kramer, I. J.; Fischer, A.; Tang, J.; Barkhouse, D. A. R.; Wang, X.; Levina, L.; Lu, Z.-H.; Sargent, E. H. Depleted-Heterojunction Colloidal Quantum Dot Photovoltaics Employing Low-Cost Electrical Contacts. *Appl. Phys. Lett.* **2010,** *97*, 023109.

52. Gao, J.; Perkins, C. L.; Luther, J. M.; Hanna, M. C.; Chen, H.-Y.; Semonin, O. E.; Nozik, A. J.; Ellingson, R. J.; Beard, M. C. n-Type Transition Metal Oxide as a Hole Extraction Layer in PbS Quantum Dot Solar Cells. *Nano Lett*. **2011**, *11*, 3263-3266.

53. Pattantyus-Abraham, A. G.; Kramer, I. J.; Barkhouse, A. R.; Wang, X.; Konstantatos, G.; Debnath, R.; Levina, L.; Raabe, I. et al. Depleted-Heterojunction Colloidal Quantum Dot Solar Cells. *ACS Nano* **2010**, *4*, 3374-3380.

54. Liu, H.; Tang, J.; Kramer, I. J.; Debnath, R.; Koleilat, G. I.; Wang, X.; Fisher, A.; Li, R.; Brzozowski, L.; Levina, L. et al. Electron Acceptor Materials Engineering in Colloidal Quantum Dot Solar Cells. *Adv. Mater*. **2011**, *23*, 3832-3837.

55. Tang, J.; Kemp, K. W.; Hoogland, S.; Jeong, K. S.; Liu, H.; Levina, L.; urukawa, M. F.; Wang, X.;Debnath, R.; Cha, D. et al. Colloidal-Quantum-Dot Photovoltaics Using Atomic-Ligand Passivation. *Nat. Mater*. **2011**, *10*, 765-771.

56. Etgar, L.; Zhang, W.; Gabriel, S.; Hickey, S. G.; Nazeeruddin, Md. K.; Eychmüller, A.; Liu, B.; Grätzel, M., High Efficiency Quantum Dot Heterojunction Solar Cell Using Anatase (001) TiO2 Nanosheets. *Adv. Mater.* **2012**, *24*, 2202-2206.

57. Leschkies, K.S.; Jacobs, A. G.; Norris, D. J.; Aydil, E. S. Nanowire-Quantum-Dot Solar Cells and the Influence of Nanowire Length on the Charge Collection Efficiency. *Appl. Phys. Lett.* **2009**, *95*, 193103.

58. Barkhouse, D. A. R.; Debnath, R.; Kramer, I. J.; Zhitomirsky, D.; Pattantyus-Abraham, A. G.; Levina, L.; Etgar, L.; Grätzel, M.; Sargent, E.H. Depleted Bulk Heterojunction Colloidal Quantum Dot Photovoltaics. *Adv. Mater.* **2011**, *23*, 3134-3138.

59. Leschkies, K. S.; Divakar, R.; Basu, J.; Enache-Pommer, E.; Boercker, J. E.; Carter, C. B.; Kortshagen, U. R.; Norris, D. J.; Aydil, E. S. Photosensitization of ZnO Nanowires with CdSe Quantum Dots for Photovoltaic Devices. *Nano Lett.* **2007**, *7*, 1793-1798.

60. Giménez, S.; Mora-Sero, I.; Macor, L.; Guijarro, N.; Lana-Villarreal, T.; Gomez, R.; Diguna, L. J.; Shen, Q.; Toyoda, T.; Bisquert, J. Improving the Performance of Colloidal Quantum-Dot-Sensitized Solar Cells. *Nanotechnology* **2009**, *20*, 295204.

61. Kongkanand, A.; Tvrdy, K.; Takechi, K.; Kuno, M.; Kamat, P. V. Quantum Dot Solar Cells. Tuning Photoresponse through Size and Shape Control of CdSe−TiO2 Architecture. *J. Am. Chem. Soc.* **2008**, *130*, 4007-4015.

62. Pernik, D. R.; Tvrdy, K.; Radich, J. G.; Kamat, P. V. Tracking the Adsorption and Electron Injection Rates of CdSe Quantum Dots on TiO2: Linked versus Direct Attachment. *J. Phys. Chem. C.* **2011**, *115*, 13511-13519.

63. Guyot-Sionnest, P. Electrical Transport in Colloidal Quantum Dot Films. *J. Phys. Chem. Lett.* **2012**, *3*, 1169-1175.

64. Choi, J.-H.; Fafarman, A. T.; Oh, S. J.; Ko, D.-K.; Kim, D. K.; Diroll, B. T.;M uramoto, S.; Gillen, J. G.; Murray, C. B.; Kagan, C. R. Bandlike Transport in Strongly Coupled and Doped Quantum Dot Solids: A Route to High-Performance Thin-Film Electronics. *Nano Lett*. **2012**, *12*, 2631-2638.

65. Lee, J.-S.; Kovalenko, M. V.; Huang, J.; Chung, D. S.; Talapin, D. V. Band-Like Transport, High Electron Mobility and High Photoconductivity in All-Inorganic Nanocrystal Arrays. *Nat. Nanotech.* **2011**, *6*,348-352.

66. Kramer, I. J.; Sargent, E. H. Colloidal Quantum Dot Photovoltaics: A Path Forward. *ACS Nano* **2011**, *5*, 8506-8514.

67. Ip, A. H.; Thon, S. M.; Hoogland, S.; Voznyy, O.; Zhitomirsky, D.; Debnath, R.; Levina, L.; Rollny, L. R.; Carey, G. H.; Fischer, A.; et al. Hybrid Passivated Colloidal Quantum Dot Solids. *Nat. Nanotech.* **2012**, *7*, 577-582.

68. Jasieniak, J.; Macdonald, B. I.; Watkins, S. E.; Mulvaney, P. Solution-Processed Sintered Nanocrystal Solar Cells via Layer-by-Layer Assembly. *Nano Lett.* **2011**, *11*, 2856-2864.

CHAPTER 2: 50nm DNA nanoarrays generated from uniform oligonucleotide films

2.1 Introduction

In recent years, a wealth of nanoscale materials has demonstrated unique physical characteristics with the potential to yield enormous societal benefits, particularly toward health and energy.[1-17] However, challenges in fabricating devices from these materials over large areas, reproducibly, cheaply, and with high fidelity have hindered their widespread application. This is due primarily to the difficulties in parallel manipulation of large quantities of individual components whose dimensions are well below 10 nm and organizing them into configurations that are amenable to device and circuit wiring. Conventional patterning approaches based on lithography have to date been limited to defining relatively large-area features that result in the deposition of poorly organized ensembles of these nanostructures, thus compromising their performance.

In light of some of these challenges, self-assembling biological systems such as DNA and protein arrays have been investigated to address sub-20 nm scale materials.[18-31] The beauty of biological templates is that these systems provide immediate access to the sub-10 nm regime, and biomolecular recognition can be used to accurately position particular sets of nanoscale objects at will. For example, DNA- and protein-based self-assembled arrays have been used to build discrete assemblies of gold and semiconductor nanocrystals into twodimensional patterns.[21-24,27-29] Despite these single demonstrations, however, production of highly parallel arrays of nanoscale materials over

very large areas has not yet been shown. In fact, methods to generate large-area assemblies of nanoparticles have only recently been demonstrated with the discovery and implementation of finite 100 nm DNA structures, known as DNA origami.[32] However, in all of these studies, the DNA scaffolds had to be assembled on substrates patterned by electron-beam lithography, which is highly time-consuming and expensive (unpublished data).

In the aforementioned studies, the initial primary challenge was to accurately place and direct the assembly of the DNA strands and structures themselves on surfaces.One of the best known and least expensive methods to fabricate patterned DNA arrays is microcontact printing (μCP), but the inherent difficulties of generating poly(dimethylsiloxane) (PDMS) stamps with submicrometer dimensions have hindered attempts to pattern DNA below 500 nm. More recently, Wang and co-workers used poly(methylmethacrylate) (PMMA) stamps that were prepared first by nanoimprint lithography (NIL) to generate 250 nm lines of covalently attached single-stranded DNA (ssDNA) on silicon.[33] Stellacci and Crooks also independently developed a replica based stamping approach starting from patterned ssDNA covalently attached on surfaces to generate daughter patterns of ssDNA on other substrates.[34,35] Obtaining DNA patterns with submicrometer dimensions has yet to be achieved using a simple stamping approach that obviates repeated use of lithography tooling such as NIL or photolithography or the need for chemical attachment of DNA to surfaces.

Recently, Delamarche and co-workers developed a facile “subtraction printing” method to fabricate large area antibody arrays with 100 nm resolution.[36] While proteins have directed the assembly of nanocrystals, issues of protein stamping and

stability make them difficult and expensive to use for nanoscale assembly. Since DNA can be further used to direct the assembly of nanoscale materials, we investigated this technique to create arrays of linear ssDNA of varying dimensions.

2.2 Materials and Methods

2.2.1 PDMS preparation

PDMS substrates (Sylgard 184, Dow Corning) were prepared by mixing and degassing a mixture of base and curing agent (ratio 10:1). PDMS liquid was poured into a petri dish and then thermally cured at 80 °C in an oven for 1 h.

2.2.2 Silicon Masters

The silicon masters were fabricated on (100) silicon wafers patterned with 193 nm deep ultraviolet (DUV) lithography and a reactive-ion-etch (RIE) process with an oxide hardmask. Approximately 100 nm thick SiO2 was deposited on 300 mm diameter silicon wafers in an Applied Materials 5000 plasma enhanced chemical vapor deposition (PE-CVD) system using tetraethoxysilane (TEOS) chemistry. A UV-sensitive high-resolution photoresist was then spin-coated on the silicon wafers. An antireflective (AR) coating was applied on top of the resist to eliminate standing waves in the photoresist. The DUV lithography was performed on an ASML/SVGL Micrascan 193 nm step-and-scan lithography system. The resist was developed, and the fine lithographic features were transferred with high fidelity by RIE etching first into the oxide layer to create the hard-mask and then into the silicon substrate. The SiO2 was etched with fluorine based chemistry in an Applied Materials Centura 5200 etcher, and the silicon was etched with chlorine-based chemistry in a LAM Rainbow 9400PTX etcher.

2.2.3 Silicon Masters with Sub-50 nm Dimensions

Original line patterns (120 nm) generated by DUV lithography were placed in a conventional resistive heating furnace and oxidized in pure O2 (99%) for 3 h at 1000 °C, with optional chemical etching of the oxide layer to form the pillar pattern with sub-50 nm width for nanoimprint. The Si template was then replicated by imprinting onto a poly(methylmethacrylate) (PMMA)-coated silicon wafer using an ANT-2 nanoimprinter. After transferring the pattern into the substrate, PMMA was used as an etching mask to faithfully transfer the patterns into Si wafer by a SF6/C4F8 mixture RIE, achieving a sub-50 nm wide line hole.

2.2.4 DNA Patterning

Si master and planar Si substrates were cleaned with acetone, ethanol, and DI water successively using a sonication bath. PDMS substrates were treated with ethanol and DI water successively using a sonication bath. After cleaning, both the silicon and PDMS substrates were treated with a UVO cleaner (Jelight, model 42) for 1 h under 3 scfh oxygen gas. UVO-cleaned PDMS substrates were inked with 1 µL of 20 µM amine-modified polyadenine and incubated in a Petri dish lined with wet Kimwipes for 45 min. The DNA-inked PDMS was then briefly treated with nitrogen gas for 5-10 s. Both the subtraction and printing steps were done using 50 g weights and using 30 s transfer times.

2.2.5 Gold Nanoparticle Conjugation

Phosphine-stabilized 10 nm gold nanocrystals (Ted Pella) were reacted with 5’-thiolated polythymine (T15) using ratios of 200:1 DNA to gold. After a minimum of 1 h,

excess DNA was removed by microcentrifuge filtration and gel electrophoresis was run to confirm DNA to gold conjugation. T15-modified gold nanocrystal solutions were reacted at room temperature for 5 min with the patterned A15. After adsorption of the gold nanocrystal solutions, all of the substrates were quickly immersed in a bath (1x TAE buffer) of 125 mM $MgCl_2$ for 2 s to wash away excess gold nanocrystals. Next, the samples were introduced to a solution of 50% ethanol in water (v/v) for ~2 s and then immersed in 90% ethanol to wash away excess salts and dehydrate the DNA.

2.2.6 Characterization

SEM images were obtained with Phillips XL30 ESEM. All images in this paper were taken with a secondary electron mode. The accelerating voltage was 20 kV. Tapping mode AFM images were obtained using Digital Instrument MultiMode Nanoscope IV with an “E” scanner and using Ultrasharp AFM tips

2.3 Results and Discussion

2.3.1 Illustration of DNA subtraction printing

The general scheme of using the subtraction printing method for obtaining clean patterns of ssDNA on silicon and native oxide is shown in Fig. 2.1. In subtraction printing, material is transferred from flat PDMS to a patterned silicon master only where there is conformal contact between the DNA film and the silicon surface, but not where there are etched holes or trenches in the silicon substrate. This leaves behind patterned DNA arrays on the flat PDMS that are subsequently transferred ("printed") by contact with a planar silicon or oxide surface. While this had been clearly demonstrated with antibodies in the earlier work, the basic chemical and physical differences between that of DNA and proteins required significant optimization for successful inking of DNA on PDMS and transfer to silicon.

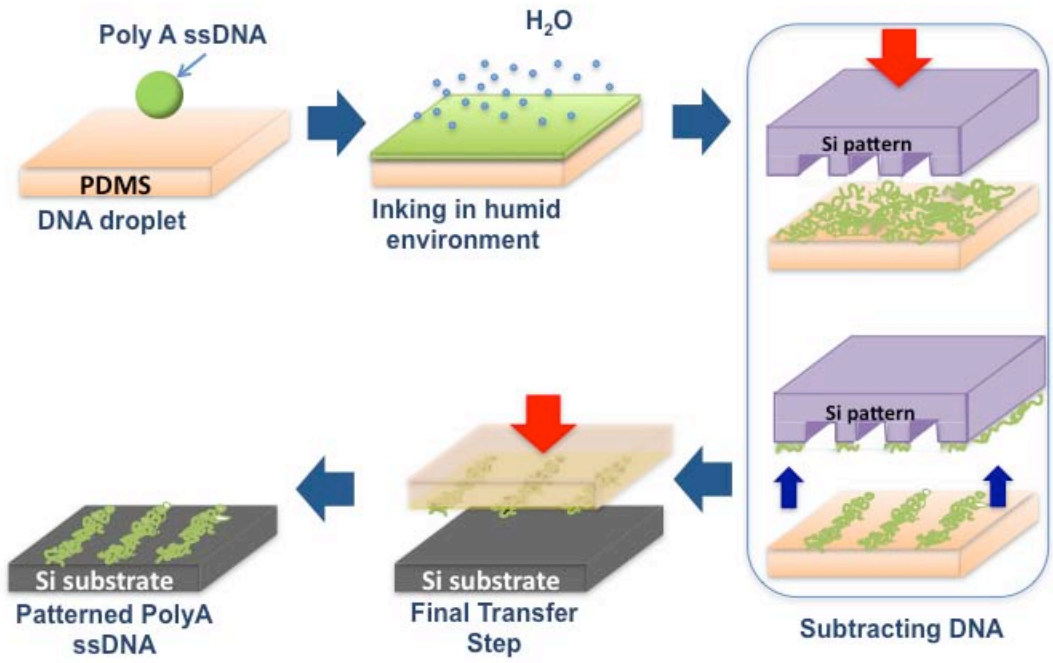

Fig. 2.1 Schematic depicting method of DNA adsorption to planar PDMS and subtraction printing to generate patterns of ssDNA on silicon. Solutions of ssDNA were first adsorbed and slowly evaporated on UV/ozone-treated planar PDMS substrates. After drying in a humidified environment for ~45min, the DNA films were brought into conformal contact with UV/ozone-treated lithographically patterned silicon masters. After subtraction printing, patterned ssDNA domains remained behind on the planar PDMS, which were then transferred to flat silicon substrates.

2.3.2 Criteria of DNA subtraction printing

One of the predominant criteria to obtain well-defined patterns of DNA or proteins through subtraction-based PDMS stamping is the optimization of adhesion between the biomolecules and the PDMS surface relative to the receiving surface.[37,38] Because the PDMS surface is much more hydrophobic than cleaned oxide or glass substrates, it can sometimes be difficult to obtain conformal wetting and adhesion of charged, hydrophilic species, like DNA, to the PDMS substrate. For both μCP and subtraction printing, a certain amount of adherence between DNA and PDMS is needed to avoid dewetting or delamination. For subtraction printing, sufficient adhesion between the DNA and the silicon surface is absolutely necessary because the process requires complete transfer of DNA from the PDMS upon contact, whereas partial transfer can sometimes be sufficient for μCP. Another major challenge with printing hydrophilic species is controlling the amount of water in the system in order to prevent excess flow of the biomolecules while still allowing for material transfer.

Due to the highly charged nature of both single- and double-stranded DNA and high levels of hydration, the issue of flow proved to be a significant challenge toward obtaining proper subtraction and printing of DNA films on PDMS even after removal of excess solvent by spin coating or nitrogen drying. In initial studies, a standard published procedure for biomolecule inking on PDMS was used where DNA solutions were first incubated on the PDMS substrates for varied amounts of time followed by nitrogen blow drying for a few seconds. The DNA solutions used in these experiments varied in magnesium concentrations ranging from 0 to 125 mM $MgCl_2$, and both untreated and UV/ozone-treated PDMS substrates were tested. However, in all cases, DNA solution

inking on PDMS followed by nitrogen drying or spin-coating yielded both poor pattern fidelity (Fig. 2.2) as well as the negative tone of the expected patterns. This was the case regardless of DNA concentration, magnesium concentration, inking time, pretreatment of the silicon substrates with magnesium solutions, surface oxidation of PDMS by UV/ozone, or spin-coating speeds. We hypothesize that the large hydration sphere around the DNA strands increases DNA mobility, causing the adsorbed DNA strands to act as a fluid and essentially flow into the etched domains of the silicon substrate, leaving behind any excess DNA on PDMS as a DNA film with micrometer sized holes. In contrast, when DNA solutions were completely dried on the PDMS stamps, no DNA was observed to transfer from the PDMS surface to either the patterned or planar silicon substrates. In light of both of these results, it became clear that, although excess solvent must be removed from the adsorbed DNA film, the DNA strands also needed to remain partially hydrated in order for effective transfer from PDMS to silicon to occur.

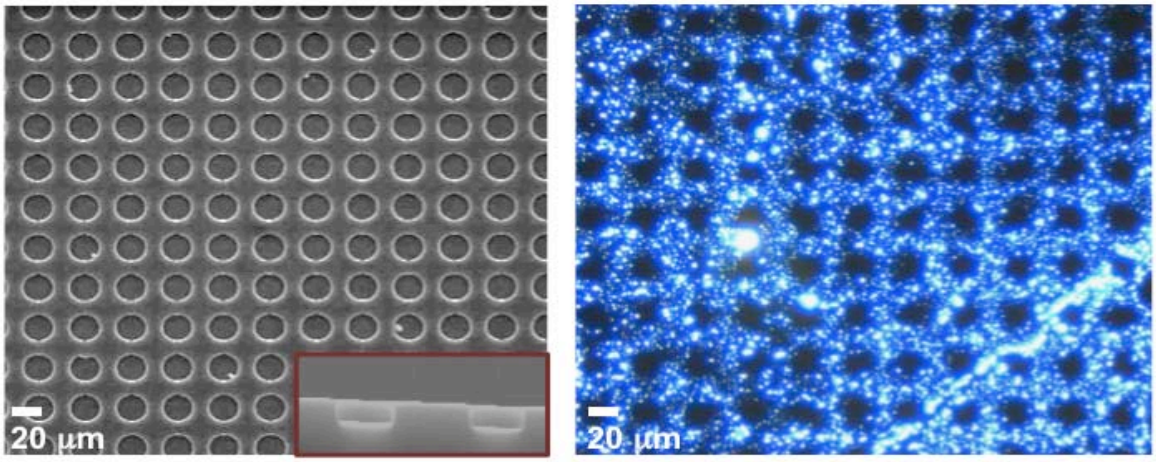

Fig. 2.2 (A) SEM image of 20µm holes etched into silicon (B) Fluorescence image of DNA patterns generated using 20µm silicon master when DNA was inked onto the PDMS by nitrogen blow drying DNA solutions pre-adsorbed onto the PDMS substrates.

2.3.3 Generation of micron sized DNA dot patterns

As a means to both address issues of DNA flow as well as effective transfer from PDMS to silicon, DNA solutions of varying concentrations were left to slowly evaporate on the flat PDMS surfaces in a humidified environment. The reason for this setup was to reproducibly control the evaporation speed of the DNA solutions on PDMS. A critical component of the subtraction printing process required DNA films that contained no visible excess water but were hydrated enough to allow for effective transfer, and these were most reproducibly obtained by slow evaporation of the DNA solutions on PDMS in Petri dishes lined with Kimwipes. A sample procedure is as follows: 20 pmol (1 µL) of ssDNA was spread onto 3 mm x 4 mm PDMS substrates and left for 45 min in a humidified chamber built from Petri dishes lined with wet Kimwipes (Fig. 2.1). Immediately after solvent evaporation (45 min), all of the samples were treated briefly with a nitrogen flow for 5-10 s and brought into conformal contact with UV/ozone-treated lithographically patterned and etched silicon substrates. Any DNA patterns generated by subtraction printing and left on the flat PDMS substrates were next brought into a second conformal contact with planar, UV/ozone-treated silicon substrates (Fig. 1). As shown in Fig. 3, silicon masters with 5 and 1 µm holes could be used to generate 5 and 1 µm dot patterns of single-stranded DNA (ssDNA), polyadenine, A_{15}, on flat silicon.

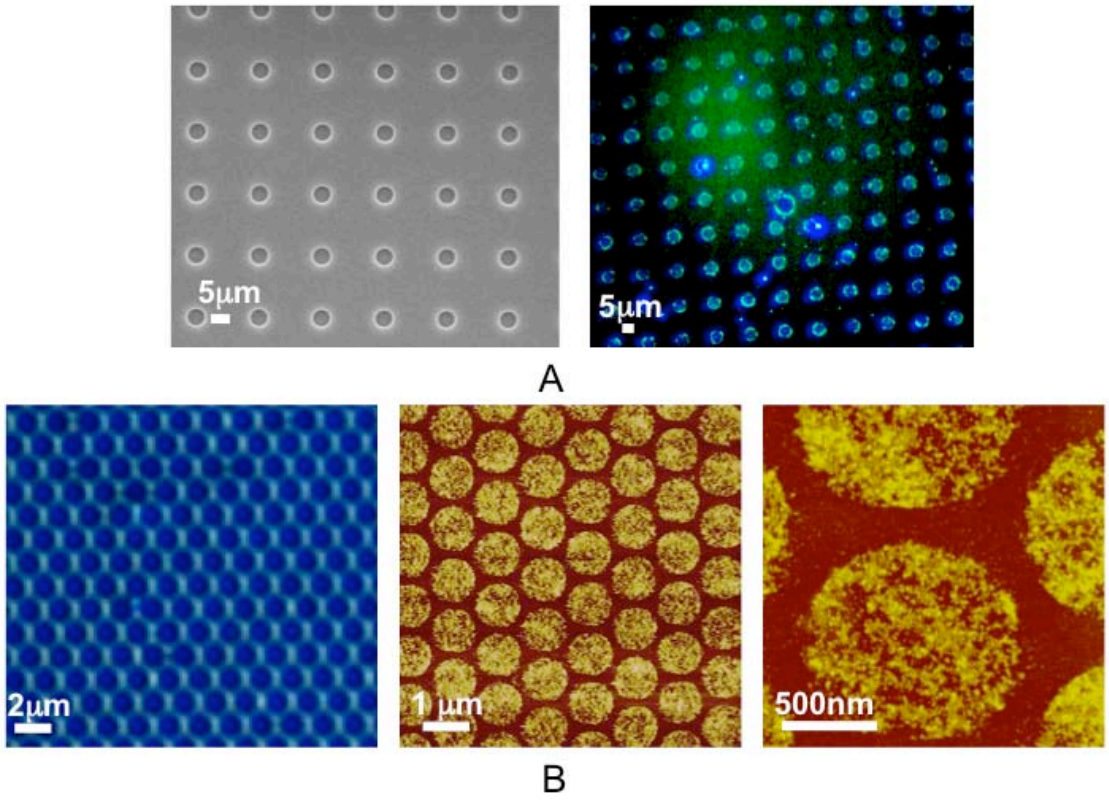

Fig. 2.3 (A) Etched holes (5 µm) in silicon and dot patterns (5 µm) of fluorescently tagged polyadenine (A_{15}). (B) Optical micrograph of 1 µm holes etched in silicon and AFM height images of 1 µm dot patterns of polyadenine obtained after subtraction printing from the silicon master.

2.3.4 Generation of nanometer sized DNA dot, line and cross patterns

Next, sub-1 μm silicon masters generated by deep UV lithography (DUV) were used to measure the scalability of the patterns that could be generated. By using the exact same patterning steps as for the larger micrometer-size patterns, ssDNA domains as small as 100 nm were repeatedly patterned on silicon with excellent fidelity. Both ssDNA dots and lines as small as 95 nm were also generated (Figure 4), illustrating effective pattern transfer regardless of shape. Even smaller features were obtained by placing silicon line patterns made by DUV lithography in a conventional resistive heating furnace to oxidize in O_2 (99%) for 3 h at 1000 °C, then etched to form sub-50 nm lines. These were then replicated by NIL into PMMA resists, which were used as an etching mask to faithfully transfer the patterns into Si wafer by a SF_6/C_4F_8 mixture RIE, achieving 40 nm wide trenches in silicon. As shown in Figure 5a, these silicon masters could be used to obtain 40-50 nm lines of ssDNA with ease. Finally, the ease and mildness of the subtraction printing process prevents the removal or degradation of the previously deposited ssDNA, allowing for multiple patterning of different ssDNA sequences into complex patterns. Specifically, grid-like, 100 nm line patterns of ssDNA were produced by performing two sequential printing steps at right angles to one another (Figure 5b).

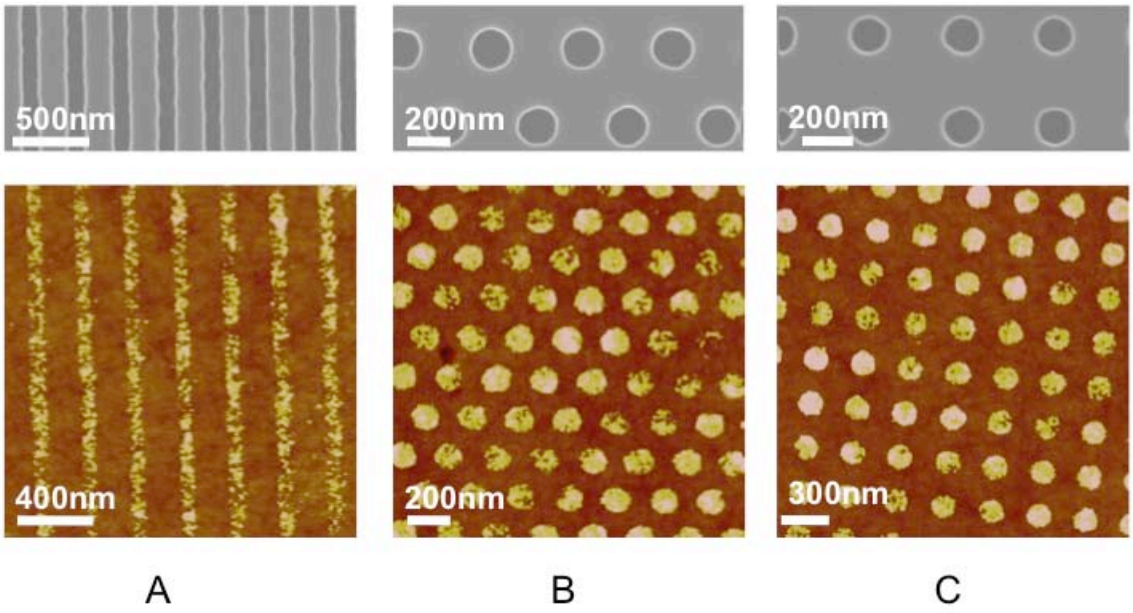

Fig. 2.4 (A) Etched lines (~100nm) in silicon and lines of ssDNA (95nm) generated after subtraction printing of DNA films with the 100nm silicon patterns. (B) Etched holes (180 nm) in silicon and dot patterns (180nm) of ssDNA. (C) Etched holes (160nm, square array) in silicon and dot patterns (160-170 nm, square array) of ssDNA generated.

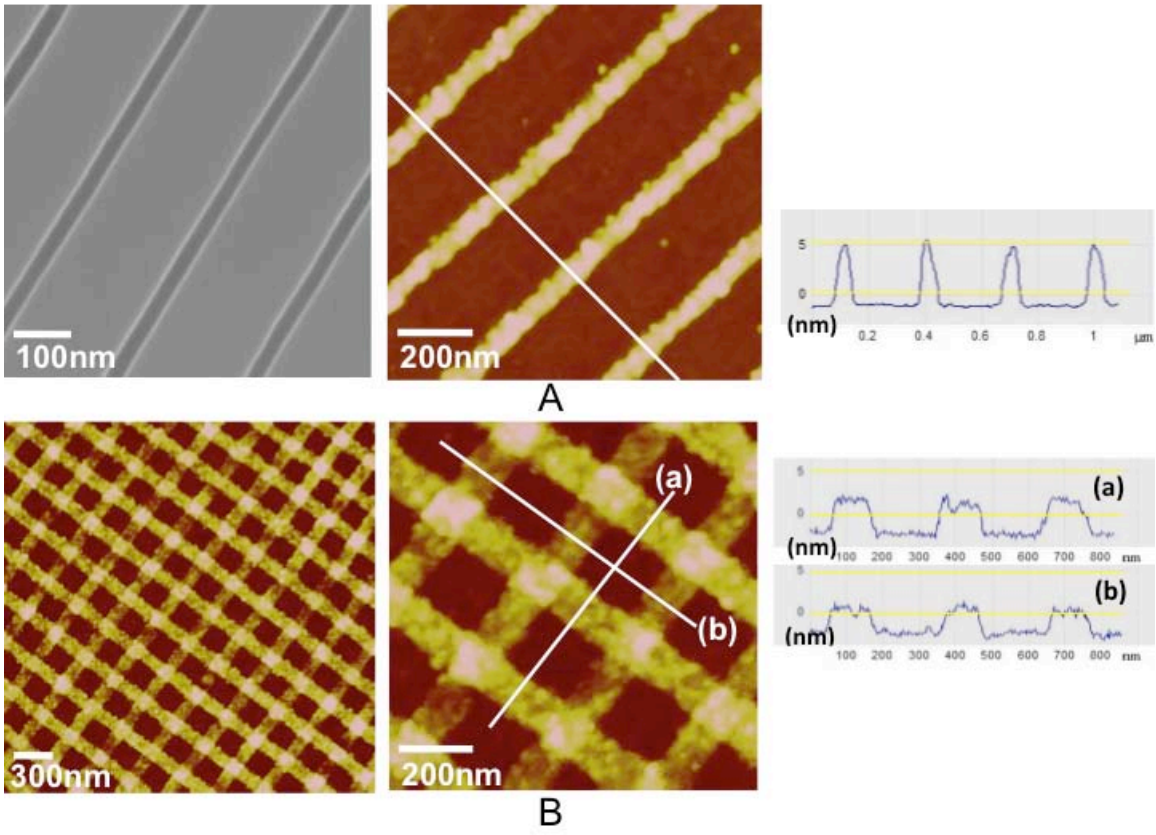

Fig. 2.5 (A, Left) Large-area AFM image of 50nm DNA lines obtained after subtraction printing. (Right) AFM images of 50nm DNA lines obtained after subtraction printing and height profile analysis. (B, Left) AFM images of 100nm crossed lines of ssDNA. (Right) Higher magnification AFM image of 100nm crossed lines of ssDNA and height profile analysis.

2.3.5 A role of $MgCl_2$ on physisorption of DNA on Si substrate

While there was some variability of DNA film thickness across the PDMS substrate, this did not appear to cause visible differences in the overall fidelity of the DNA patterns obtained on the receiving silicon surface. As determined by AFM height measurements, each domain was approximately 5 nm in height, correlating to an approximate film thickness of 1-2 strands of A_{15} DNA oligonucleotides. If it is assumed that a 15mer ssDNA is ~5 nm when fully extended, then one can assume that at least a single monolayer of ssDNA is patterned. However, since ssDNA is known to often coil and form condensed and globular structures,[39] it is more likely that multiple layers of ssDNA are patterned on the silicon surface after printing. Regardless, any ssDNA not directly adsorbed to the silicon surface would be washed away in either water or buffer, leaving behind only a monolayer of ssDNA on the substrate. Indeed, since no covalent chemistry was employed in these studies to directly conjugate the DNA to the silicon surface, much of the adsorbed and patterned ssDNA domains were observed to completely wash away with repeated water rinses. However, high magnesium buffer (125 mM $MgCl_2$) was found to prevent the complete disassociation of the ssDNA from the silicon surface.[40] This use of magnesium became a critical aspect when using the patterned DNA for directing nanoparticle assembly. In order to generalize this process for nanomaterials sensitive to excess magnesium, methods to covalently conjugate the ssDNA to silicon after transfer from PDMS are currently being investigated.

2.3.6 Direct assembly of 10nm AuNPs on DNA patterns

The ability to generate 50 nm features of ssDNA over macroscopic areas repeatedly and with minimal lithography or complex chemistry provides a means to direct the assembly of nanoscale materials at low cost and with a limited number of fabrication steps. The assembly of gold nanocrystals onto lines of printed ssDNA through DNA hybridization is demonstrated here. Specifically, 10 nm gold nanocrystals modified with polythymine (T_{15}) were reacted at room temperature in magnesium buffer for 5 min with 50 nm patterned lines of A_{15}. After adsorption of the gold nanocrystal solutions, the substrate was quickly immersed in a fresh bath of Tris-acetate-EDTA (TAE) buffer with 125mM $MgCl_2$ to wash away excess, unbound gold nanocrystals. Next, the samples were introduced to solutions of 50% ethanol (v/v) and 50% water to wash away excess magnesium and finally immersed in 90% ethanol for 20 min to remove excess water and effectively dry the nanocrystals to the patterned DNA lines. As shown in Figure 6, the patterned ssDNA remained on the surface after introduction of new solutions of T_{15} conjugated 10 nm gold nanoparticles. All of the gold nanocrystals appeared to hybridize to the A_{15} sites in a matter of minutes, and extended incubation did not appear to cause a substantial difference in the number of nanoparticles bound. Furthermore, when ssDNA lines were annealed at room temperature with solutions of DNA conjugated gold nanocrystals, two-dimensional, close packed arrays of gold nanoparticles were obtained with observed hierarchical ordering of the gold colloids themselves (Figure 6b,c). Although the printed ssDNA lines were measured to be between 50 and 60 nm in width, the assembled gold nanocrystal lines varied in widths from 60 to ~100 nm. The differences in the widths of the printed ssDNA lines from the nanocrystal line patterns are

presumed to occur due to nanocrystal hybridization that can occur at the edges of the ssDNA domains. When 100 nm crossed line patterns of A_{15} were exposed to the T_{15}-conjugated 10 nm gold nanocrystals, continuous arrays of nanoparticles were obtained that clearly followed the DNA crossed line patterns (Figure 6d). The ability to obtain long-range order of nanocolloids by confining the particles to sub-100 nm domains can clearly be applied toward fabrication of useful photonic, electronic, and magnetic devices and will be of future study.

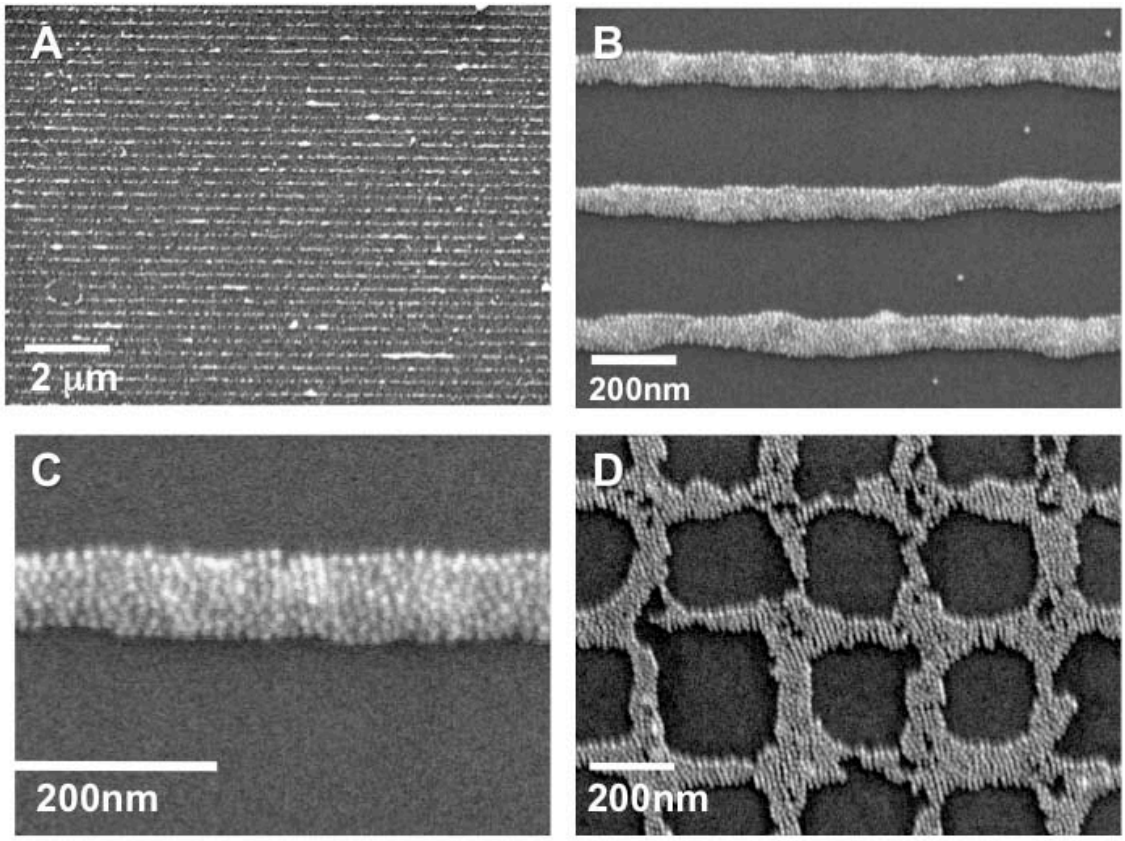

Fig. 2.6 (A) Thymine (T_{15}) conjugated 10nm gold nanocrystals annealed to ~50-60nm polyadenine (A_{15}) patterned lines on silicon. (B,C) Higher magnification image of gold nanocrystal assemblies showing two-dimensional nanoparticle packing within the 60-100nm nanocrystal line patterns. (D) Gold nanocrystal assemblies on 100nm crossed lines of polyadenine (A_{15}).

2.4 Conclusion

We have demonstrated here a facile method to produce submicrometer features of ssDNA that allow the arrangement of a wide variety of nanoscopic components over macroscopic areas. The strengths of this approach are its versatility, ease of fabrication, and minimization of lithographic tooling and processes. Furthermore, the resulting nanometer scale chemical patterns allow not only the directed placement of nanoscale materials but also the investigation of the role of chemical confinement in creating complex assembled arrays. Finally, mild conditions used in the stamping process will facilitate the fabrication of threedimensional nanoscale assemblies routinely and predictably over large areas, a feat that has been difficult to achieve with current technologies.

2.5 Acknowledgments

This chapter, in full, is a reprint of the material as it appears in ACS Nano, Volume 3, 2009. Noh, Hyunwoo; Hung, Albert M.; Choi, Chulmin; Lee, Ju Hun; Kim, Jin-Yeol; Jin, Sungho; Cha, Jennifer N.. The dissertation author was the primary investigator and author of this paper.

2.6 References

1. Lu, W.; Lieber, C.M. Nanoelectronics from the Bottom up. *Nature Materials* **2007,** *6,* 841-850.

2. Huang, Y.; Duan, X.; Wei, Q.; Lieber, C.M. Directed Assembly of One-Dimensional Nanostructures into Functional Networks. *Science* **2001,** *291,* 630-633.

3. Rueckes, T.; Kim, K.; Joselevich, E.; Tseng, G.Y.; Cheung, C.-L.; Lieber, C.M. Carbon Nanotube-Based Nonvolatile Random Access Memory for Molecular Computing. *Science* **2000,** *289,* 94-97.

4. McEuen, P. L.; Fuhrer, M.S.; Park, H. Single-Walled Carbon Nanotube Electronics. *IEEE Trans. Nanotechnology* **2002,** *2,* 78-85

5. Lieber, C.M. Nanoscale Science and Technology: Building a Big Future from Small Things. *Mater. Res. Soc. Bull.* **2003,** *28,* 486-491.

6. Cheng, M. M.-C.; Cuda, G.; Bunimovich, Y.L.; Gaspari, M.; Heath, J.R.; Hill, H.D.; Mirkin, C.A.; Nijdam, A.J.; Terracchiano, R.; Thundat, T.; Ferrari, M. Nanotechnologies for Biomolecular Detection and Medical Diagnostics. *Curr. Opin. Chem. Biol.* **2006,** *10,* 11-19.

7. Taton, T.A.; Mirkin, C.A.; Letsinger, R.L. Scanometric DNA Array Detection with Nanoparticle Probes. *Science* **2000,** *289,* 1757-1760.

8. Cui, Y.; Wei, Q.; Park, H.; Lieber, C.M. Nanowire Nanosensors for Highly Sensitive and Selective Detection of Biological and Chemical Species. *Science* **2001,** *293,* 1289-1292.

9. McAlpine, M.C.; Ahmad, H.; Wang, D.; Heath, J.R. Highly Ordered Nanowire Arrays on Plastic Substrates for Ultrasensitive Flexible Chemical Sensors. *Nat. Mater.* **2007,** *6,* 379-384.

10. Xu, J.M. Plastic Electronics and Future Trends in Microelectronics. *Synth. Met.* **2000,** *115,* 1-3.

11. Ferrari, M. Cancer Nanotechnology: Opportunities and Challenges. *Nature Rev. Cancer* **2005,** *5,* 161-171.

12. Thundat, T.; Majumdar, A. Microcantilevers for Physical, Chemical, and Biological Sensing. *Sensors Sensing Biol. Eng.* **2003,** 338-355.

13. Chaudhary, S.; Lu, H.; Müller, A.M.; Bardeen, C.J.; Ozkan, M. Hierarchical Placement and Associated Optoelectronic Impact of Carbon Nanotubes in Polymer-Fullerene Solar Cells. *Nanoletters* **2007,** *7,* 1973-1979.

14. Beek, W.J.E.; Wienk, M.M.; Janssen, R.A.J. Efficient Hybrid Solar Cells from Zinc Oxide Nanoparticles and a Conjugated Polymer. *Adv. Mater.* **2004,** *16,* 1009-1013.

15. Huynh, W.U.; Dittmer, J.J.; Alivisatos, A.P. Hybrid Nanorod-Polymer Solar Cells. *Science* **2002,** *295,* 2425-2427.

16. Gur, I.; Fromer, N.A.; Geier, M.L.; Alivisatos, A.P. Air-Stable All-Inorganic Nanocrystal Solar Cells Processed from Solution. *Science* **2005,** *310,* 462-465.

17. Law, M.; Greene, L.E.; Johnson, J.C.; Saykally, R.J.; Yang, P. Nanowire Dye-Sensitized Solar Cells. *Nature Materials* **2005,** *4,* 455-459.

18. Seeman, N.C.; Belcher, A.M. Emulating Biology: Building Nanostructures from the Bottom up. *Proc. Natl. Acad. Sci.* **2002,** *99,* 6451-6455.

19. Claridge, S.A.; Liang, H.W.; Basu, S.R.; Fréchet, J.M.J.; Alivisatos, A.P. Isolation of Discrete Nanoparticle−DNA Conjugates for Plasmonic Applications . *Nanoletters* **2008,** *8,* 1202-1206.

20. Fu, A.H.; Micheel, C.M.; Cha, J.; Chang, H.; Yang, H.; Alivisatos, A.P. Discrete Nanostructures of Quantum Dots/Au with DNA. *J. Am. Chem. Soc.* **2004,** *126,* 10832-10833.

21. Le, J.D.; Pinto, Y.; Seeman, N.C.; Musier-Forsyth, K.; Taton, T.A.; Kiehl, R.A. DNA-Templated Self-Assembly of Metallic Nanocomponent Arrays on a Surface. *Nanoletters* **2004,** *4,* 2343-2347.

22. Deng, Z.; Tian, Y.; Lee, S.-H.; Ribbe, A.E.; Mao, C. DNA-Encoded Self-Assembly of Gold Nanoparticles into One-Dimensional Arrays. *Angew. Chem. Int. Ed.* **2005,** *44,* 3582-3585.

23. Zhang, J.; Liu, Y.; Ke, Y.; Yan, H. Periodic Square-Like Gold Nanoparticle Arrays Templated by Self-Assembled 2D DNA Nanogrids on a Surface. *Nanoletters* **2006,** *6,* 248-251

24. Alivisatos, A.P.; Johnsson, K.P.; Peng, X.; Wilson, T.E.; Loweth, C.J.; Bruchez, M.P.; Schultz. P.G. Organization of 'Nanocrystal Molecules' Using DNA. *Nature* **1996,** *382,* 609-611.

25. Aldaye, F.A.; Palmer, A.L.; Sleiman, H.F. Assembling Materials with DNA as the Guide. *Science* **2008,** *321,* 1795-1799.

26. Seeman, N.C. DNA in a Material World. *Nature* **2003,** *421,* 427-431.

27. Yan, H.; Park, S.H.; Finkelstein, G.; Reif, J.H.; LaBean, T.H. DNA-Templated Self-Assembly of Protein Arrays and Highly Conductive Nanowires. *Science* **2003,** *301,* 1882-1884.

28. McMillan, R.A.; Paavola, C.D.; Howard, J.; Chan, S.L.; Zaluzec, N.J.; Trent, J.D. Ordered Nanoparticle Arrays Formed on Engineered Chaperonin Protein Templates. *Nat. Mater.* **2002,** *1*, 247-252.

29. Dieluweit, S.; Pum, D.; Sleytr, U.B.; Kautek, W. Monodisperse Gold Nanoparticles Formed on Bacterial Crystalline Surface Layers (S-layers) by Electroless Deposition. *Mater. Sci. Eng. C* **2005,** *25*, 727-732.

30. Mao, C.; Solis, D.J.; Reiss, B.D.; Kottman, S.T.; Sweeney, R.Y.; Hayhurst, A.; Georgiou, G.; Iverson, B.; Belcher, A.M. Virus-Based Toolkit for the Directed Synthesis of Magnetic and Semiconducting Nanowires. *Science* **2004,** *303,* 213-217.

31. Lee, S.-W.; Mao, C.; Flynn, C.E.; Belcher, A.M. Ordering of Quantum Dots Using Genetically Engineered Viruses. *Science* **2002,** *296,* 892-895.

32. Rothemund, P.W.K. Folding DNA to Create Nanoscale Shapes and Patterns. *Nature* **2006,** *440,* 297-302.

33. Wang, Y.; Goh, S.H.; Bi, X.; Yang, K.-L. Replication of DNA Submicron Patterns by combining Nanoimprint Lithography and Contact Printing. *J. Colloid and Interface Science* **2009,** *333*, 188-194.

34. Yu, A.A.; Savas, T.A.; Taylor, G.S.; Guiseppe-Elie, A.; Smith, H.I.; Stellacci, F. Supramolecular Nanostamping: Using DNA as Movable Type. *Nanoletters* **2005,** *5*, 1061-1064.

35. Lin, H.; Kim, J.; Sun, L.; Crooks, R.M. Replication of DNA Microarrays from Zip Code Masters. *J. Am. Chem. Soc.* **2006,** *128,* 3268-3272.

36. Coyer, S.R.; García, A.J.; Delamarche, E. Facile Preparation of Complex Protein Architectures with Sub-100-nm Resolution on Surfaces. *Angew. Chem. Int. Ed.* **2007,** *46,* 6837-6840.

37. Lange, S.A.; Benes, V.; Kern, D.P.; Hörber, J.K.H.; Bernard, A. Microcontact Printing of DNA Molecules. *Anal. Chem.* **2004,** *76*, 1641-1647

38. Guan, J.; Lee, L.J. Generating, Highly Ordered DNA Nanostrand Arrays. *Proc. Natl. Acad. Sci.* **2005,** *102,* 18321-18325.

39. Washizu, M.; Kimura, Y.; Kobayashi, T.; Kurosawa, O.; Matsumoto, S.; Mamine, T. Stretching DNA as a Template for Molecular Construction. *AIP Conf. Proc*, **2004**, *725,* 67-76.

40. Pastre, D.; Hamon, L.; Landousy, F.; Sorel, I.; David, M. O.; Zozime, A.; Le Cam, E.; Pietrement, O. Anionic Polyelectrolyte Adsorption on Mica Mediated by Multivalent Cations: A Solution to DNA Imaging by Atomic Force Microscopy under High Ionic Strengths. *Langmuir*, **2006**, *22,* 6651-6660.

CHAPTER 3: Site-specific patterning of highly ordered nanocrystal superlattices through biomolecular surface confinement

3.1 Introduction

The ability to direct the assembly of single or multicomponent nanoparticles into meso- or macroscale single two- and three-dimensional crystals of any desired configuration, orientation, and geometry is currently of significant interest for high-powered applications in both energy and health.[1-14] While the properties of nanomaterials of varying composition, size, and morphology can be tuned easily, it has remained a daunting task to hierarchically assemble nanocrystals with perfect or near-perfect long-range order in both two and three dimensions at predefined sites on a substrate.[15,16] Methods to engineer patterned 2-D nanocrystal superlattices of arbitrary feature size, pitch, and density have remained elusive because highly ordered close-packed nanocrystal arrays are typically obtained by kinetically driven evaporation processes, which produce local order but limited long-range positional order.[5,17-19] To arrange organic and inorganic materials into programmed assemblies with precision and order, nature both sequesters the raw materials into confined spaces and encourages their association through highly specific noncovalent interactions between biomolecules. We demonstrate here that similar strategies can be employed by confining nanoparticles to geometrically defined 2-D DNA sites on a surface and using biomolecular associative interparticle interactions to generate thermodynamically stable arrays of hexagonally packed nanocrystals with significant long-range order observed over 1-2 μm. We

furthermore show that chemically immiscible boundaries at the edges of each nanocrystal array strongly influence particle packing and ordering; as the 2-D DNA features decrease in size from 3 μm to 200 nm, 60° parallelogram DNA patterns promoted long-range order of hexagonally packed particles but square DNA arrays generated largely disordered arrangements. In this report, we also demonstrate that obtaining long-range order within a nanocrystal superlattice requires both interparticle DNA hybridization and solvent-less thermal annealing above the melting temperatures (T_m) of the DNA strands.

3.2 Materials and Methods

3.2.1 Silicon patterns

Silicon line patterns of 200nm and 400nm dimensions were fabricated as published [23] The micron sized Si templates were obtained from a photolithographically patterned (100) silicon wafer (Ultrasil Corp.) and a reactive-ion-etch (RIE) A positive photoresist was first spin-coated on the silicon wafer followed by exposure using a a Karl Suss MA6 Mask Aligner system to create the patterned lines. After exposure and development, a 2 μm thick mask was used to transfer the line patterns into silicon by RIE using a SF_6/C_4F_8 mixture gas.

3.2.2 DNA patterning

All silicon substrates were cleaned by sonication in acetone, ethanol and DI water successively. PDMS substrates were cleaned by sonication in ethanol and DI water. Both PDMS and Si substrates were next rendered hydrophilic by UVO (Jelight, model 42) treatment with 3 SCFH oxygen gas. UVO treated PDMS substrates were inked with 1ul of 20uM polyadenine(A_{15})(Integratred DNA Technologies) and incubated in a humid chamber for 30 minutes. The DNA inked PDMS substrates were then briefly blown dry with nitrogen. Each subtraction printing step was performed by loading a 50g weight on top of the PDMS bringing it into contact with the silicon master for 30 seconds. DNA patterned Si substrates were next vapor treated with hexyltrimethoxysilane(Gelest Inc.) in a 45^oC oven.

3.2.3 Conjugation of AuNPs-DNA

10nm gold nanoparticles (Ted Pella) first reacted with bis-(p-sulphonatophenyl)phenylphosphine dihydrate dipotassium salt (Strem Chemicals) and concentrated according to ref. [24]. The phosphine stabilized nanoparticles were then mixed with 5' thiolated polythymine(T_{15}) using 200:1 molar ratios of DNA to gold and incubated for at least 12 hours. Excess salts and DNA were removed by washing particle solutions out three times using a 30kDa MWCO centrifuge filter. (NANOSEP, Pall corp.) Nanoparticles were resuspended in DI water and kept stored in a refrigerator at 4-8^{o}C.

3.2.4 AuNPs hybridization

6ul of DNA conjugated gold nanoparticles solution with $MgCl_2$ was dropped onto a DNA patterned Si substrate and absorbed for 5min. To remove excess AuNPs and salts, the substrates were next briefly dipped in the solutions of 125mM Mg in 1xTAE buffer followed by a 5sec 50% ethanol rinse and a 30min immersion in 90% ethanol. Thermal annealing of the gold nanoparticle arrays was done by heating the substrates at 60^{0}C in a humid environment for 4-5hrs.

3.3 Results and Discussion

3.3.1 Physical and chemical confinement of DNA coated gold nanoparticles

To confine particles specifically to geometrically defined sites on a substrate, arrays of micro- and mesoscale features of DNA, oligonucleotides were first prepared on silicon oxide using a modified version of a previously developed subtraction printing process (Fig. 3.1).[20] By subtraction printing twice on two separate silicon masters, 2-D DNA patterns could be generated that encode sharp edges and corners with sub-200 nm resolution, which are typically difficult to obtain by conventional photolithography or e-beam lithography. In order to minimize the thickness of the DNA arrays, all of the polydimethylsiloxane (PDMS) substrates were inked with 20 pmol of polyadenine (A_{15}) to produce DNA features 4-5 nm in height, corresponding to about 1-2 layers of A_{15}. Next, as a means to confine nanoparticles to the DNA arrays and discourage their association outside of the patterned domain, the remaining exposed silicon surfaces were covalently modified with hexyltrimethoxysilane (HTS) by vapor phase silylation for 15 h at 45 °C.[21,22] Contact angle and ellipsometry measurements of bare silicon substrates exposed to HTS after 15 h confirmed sufficient surface treatment to generate a highly hydrophobic surface. Through ellipsometry and AFM scratch measurements, the film thickness was determined to be between 0.769 and 0.8 nm and showed a water contact angle of 78.2°.

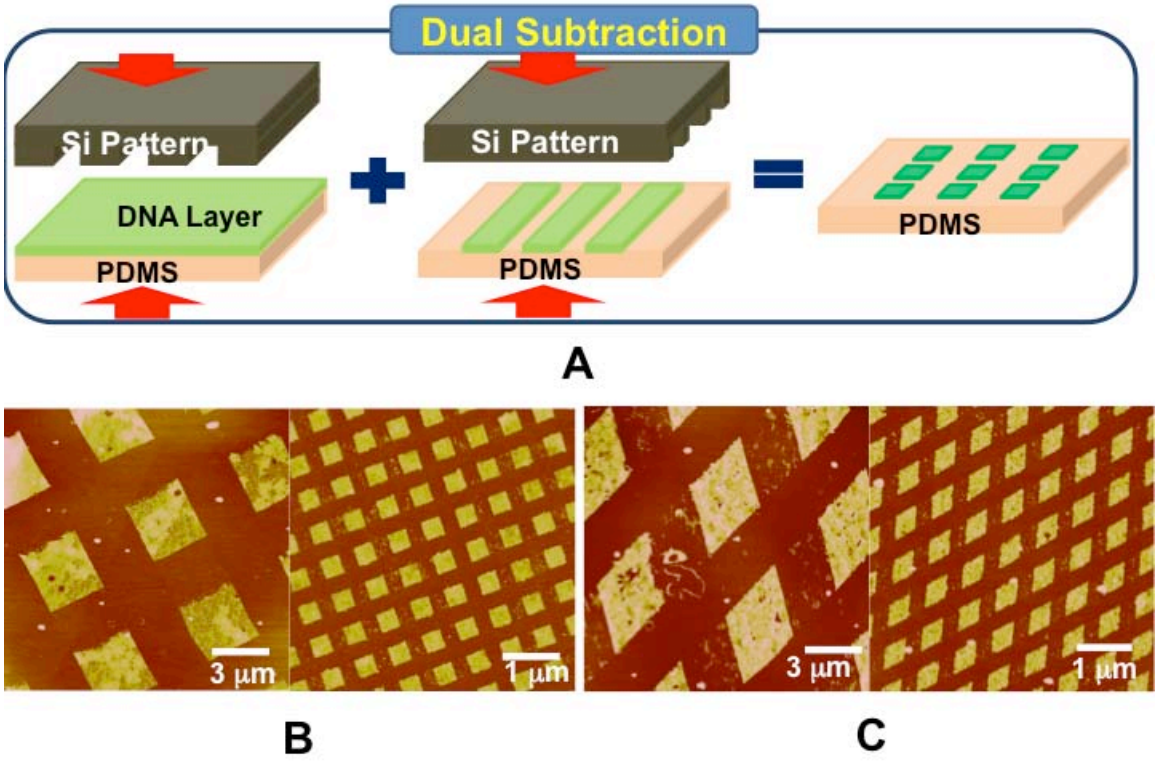

Figure 3.1 (A) Schematic of double subtraction method used to generate 2-D features of DNA on PDMS. (B) AFM images of 3μm and 400nm squares generated by double subtraction and printing. (C) AFM images of 3μm and 400nm parallelograms generated by double subtraction and printing.

3.3.2 The role of thermal annealing on AuNPs ordering

After HTS surface treatment, 100 nM solutions of polythymine (T_{15})-conjugated 10 nm gold nanocrystals were adsorbed onto the printed polyadenine (A_{15}) substrates, followed by ethanol rinsing to remove excess gold and salts. After these steps, since the gold solutions had only been in contact with the substrate for 5 min, the assembled particles were largely disordered with respect to each other, and neither local nor long range order was seen (Fig. 3.2). To allow the nanoparticles to reach their equilibrium state, the samples were next subjected to thermal annealing in a humid environment at 60 °C-above the T_m of the DNA-for 4-5 h. Annealing in this manner promoted particle mobility while minimizing the risk of particle removal due to the presence of bulk solvent.

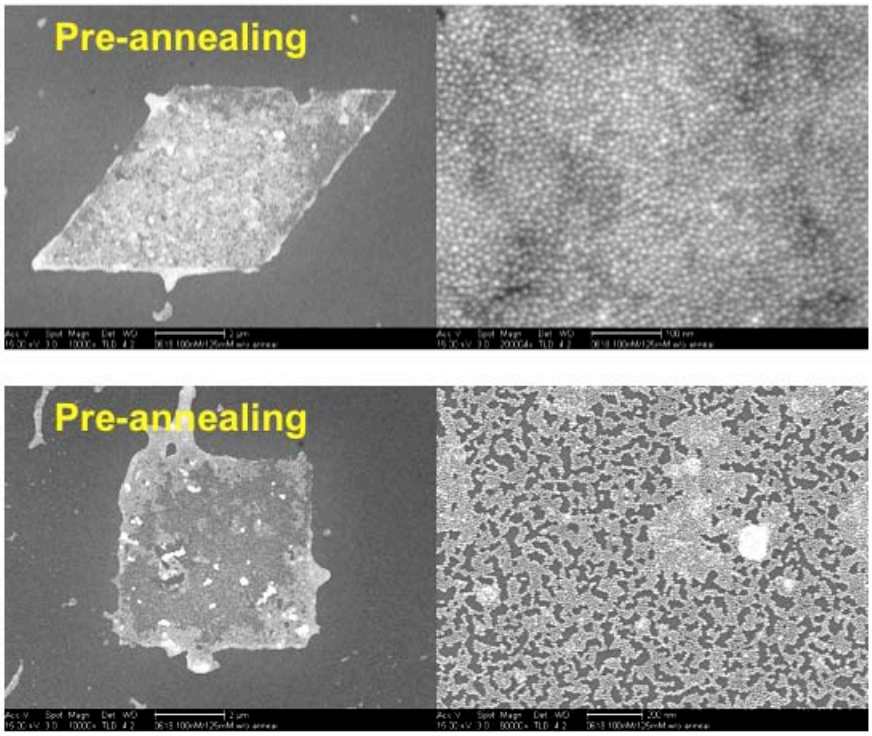

Fig. 3.2 Low and high magnification SEM images of nanocrystal superlattices obtained immediately after adsorbing T15-conjugated gold to 3µm parallelogram and 3µm square patterns of A15. No annealing step was performed.

3.3.3 Long range order of gold nanoparticle on DNA patterns

As shown in Fig. 3.3a, after thermal annealing in saturated water vapor for 5 h, extremely well-ordered arrays of hexagonally packed nanoparticle superlattices were observed within each patterned parallelogram array. As will be discussed later, nanocrystal hexagonal packing was most likely due to some of the surface bound A_{15} strands acting as bridging linkers between T_{15} strands on neighboring particles. While the nanocrystal packing within 3 μm square DNA features also showed a fair amount of order, in general, many more grain boundaries were observed, and the edges of the square gold nanocrystal arrays were not well-defined or as sharp as those observed with the parallelogram patterns (Fig. 3.3b). By imaging a roughly 1.5 μm area within a single parallelogram nanoparticle array, the gold nanoparticles were found to tightly pack into a well-ordered 2-D hexagonal superlattice. Fourier transforms (FT) of selected areas within the 1.5 μm domain show that the rotation of the superlattice over this image area varied by no more than ±7° (relative to area IV), confirming strong long-range positional order (Figure 3.4).

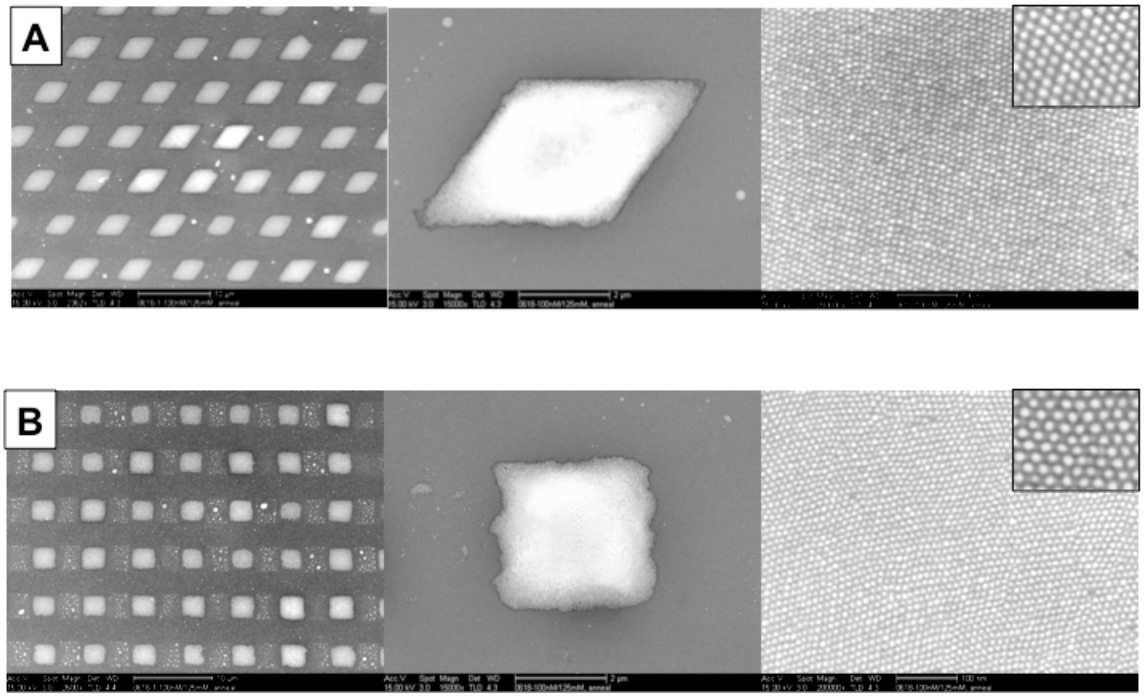

Fig. 3.3 Low- and high- magnification SEM images of nanocrystal superlattices obtained after adsorbing and annealing T_{15}-conjugated gold to (A) 3μm parallelogram and (B) 3μm square patterns of A_{15}.

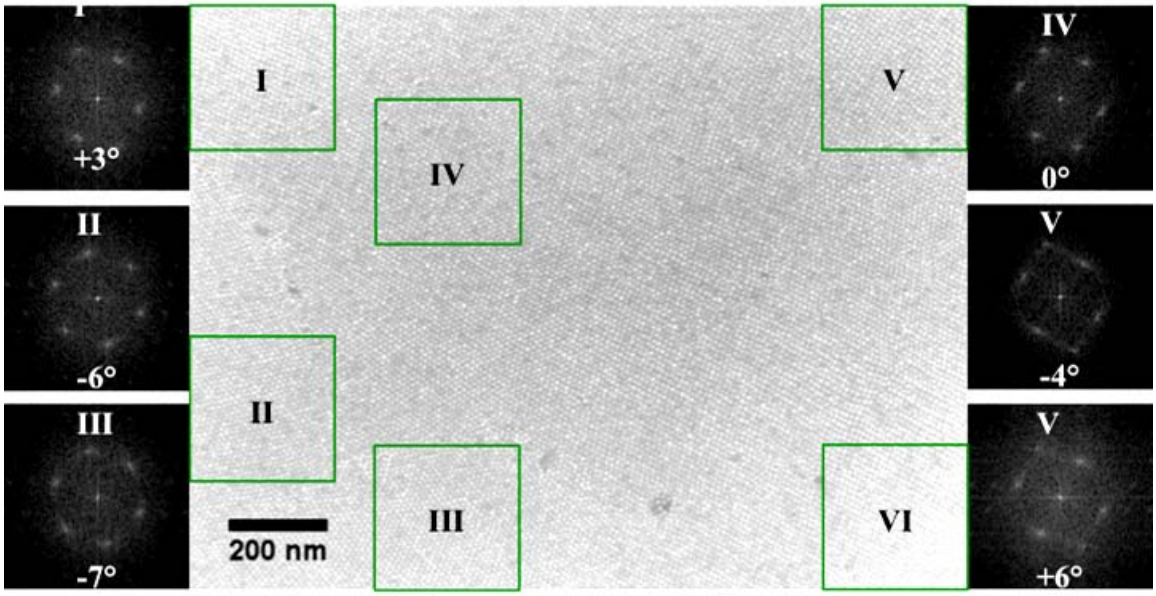

Fig. 3.4 SEM image of a 1.5 m area within a single parallelogram nanocrystal array. The gold nanoparticles are tightly packed in a 2-D hexagonal superlattice. Fourier transforms of selected areas shows that the rotation of the superlattice over this image area varies by no more than ±7°. (relative to area IV)

3.3.4 The role of the boundaries of DNA patterns on AuNPs packing

While it appears that the combination of interparticle DNA hybridization and thermal annealing allowed for the formation of highly ordered superlattice nanocrystal arrays, the role that particle confinement and the hydrophobic boundaries surrounding each DNA pattern play on nanocrystal packing and ordering remains less clear. When large micrometer sized features of DNA are used for the assembly process, it is difficult to discern the roles of the boundaries since any effect they may have on particle packing and ordering is mitigated at locations far from the edge. However, as the DNA patterns decrease in size, the boundary edges and corners should begin to have a dominating effect if there is in fact strong chemical confinement. These forces might even be strong enough to prevent the energetically favored nanocrystal hexagonal packing seen thus far such that while long-range order might be obtained on smaller parallelogram DNA patterns, mainly disordered arrays of particles would be seen on the DNA squares.

In order to test the effect of strong geometric chemical confinement on nanocrystal ordering, ~200 nm mesoscale parallelogram and square features of A_{15} were first patterned on silicon as described above. Next, as with the micrometer DNA features, T_{15}-conjugated gold nanocrystals were added followed by ethanol rinsing to remove excess salts and nanocrystals. All of the gold arrays were subsequently subjected to thermal annealing at 60 °C for 5 h. As is shown clearly in Fig. 3.5a, the sequestration of gold nanocrystals to the roughly 200 nm parallelogram features of DNA within the HTS monolayer was enough to drive both local hexagonal packing of 10 nm gold nanocrystals as well as good long-range positional order. Fourier transform analysis of an image of an individual ~200 nm parallelogram nanoparticle array in its entirety yielded six diffuse

spots, quantitatively demonstrating partial orientation order within the 200 nm superlattice. In contrast, T_{15}-conjugated gold nanocrystals patterned on the 200 nm square A_{15} domains showed completely disordered arrangements (Fig. 3.5b).

Because the DNA sequences, nanoparticle concentrations, annealing temperatures, and times were all held exactly the same, the only reason disorder would be observed within the square arrays and not the parallelograms is that the edge and corner boundaries of the mesoscale DNA patterns place a significant constraint to prevent any particle migration or association with the neighboring hydrophobic HTS areas. Although it should be noted that the overall edge roughness and corner sharpness of the 200 nm square and parallelogram nanoparticle arrays are weak, highly ordered packing is still not observed even in larger 400 nm square arrays where edge roughness and corner rounding should be less influential (Fig. 3.6). This is most likely because, even with a perfectly shaped 90° corner, the sides of a square would favor two competing hexagonally close-packed (hcp) orientations rotated 30° with respect to each other. While with very large squares, this would result in multiple grains and grain boundaries in smaller squares, and these grain boundary defects will most likely occupy the majority of the packed nanoparticle area. Therefore, despite the strong tendency of the particles to pack into hcp arrays as observed within the parallelogram features, the boundaries of the square DNA domains drove disorder toward the energetically unfavorable non-hcp orientations. The clear difference in packing and ordering observed between the two different patterned DNA geometries demonstrates the strong confinement effect the chemically immiscible boundaries have on particle sequestration and orientation and their importance toward obtaining long-range order within close-packed nanocrystal arrays.

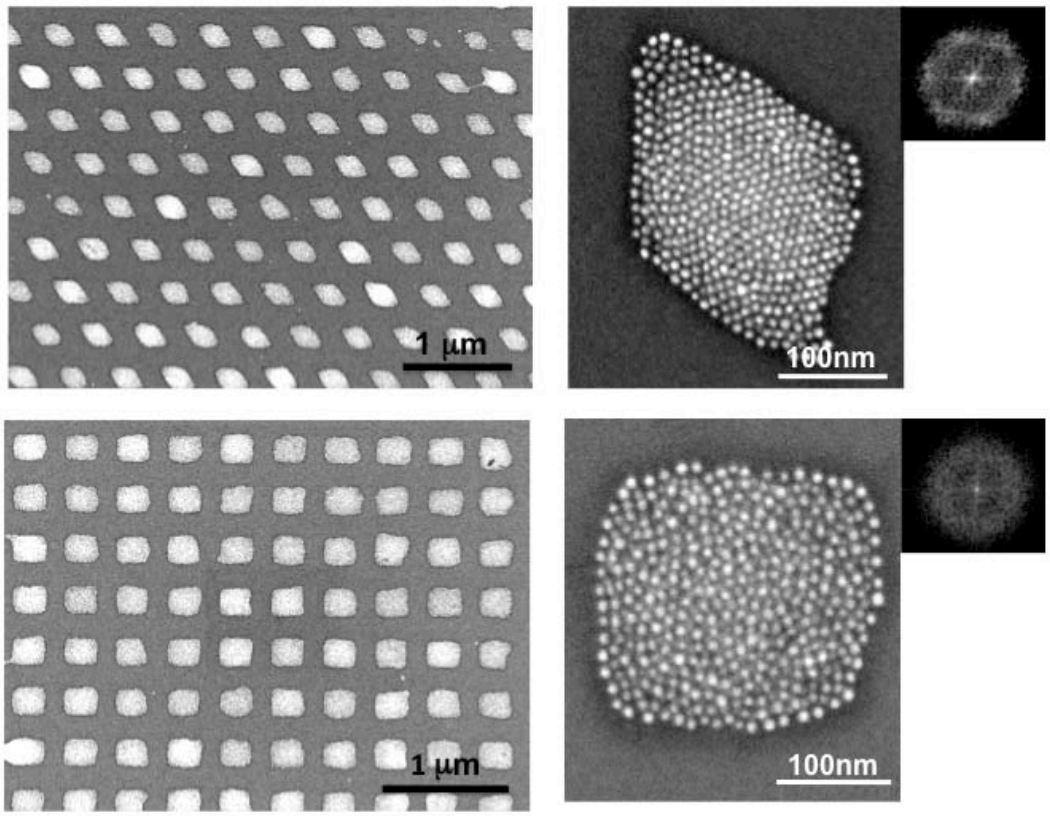

Fig. 3.5 Low and high magnification SEM images of nanocrystal superlattices obtained after adsorbing and annealing T15-conjugated gold to (A) 200nm parallelogram and (B) 200nm square patterns of A15. Insets show FTs of a ~200nm parallelogram and 200nm square nanocrystal array, each in its entirety.

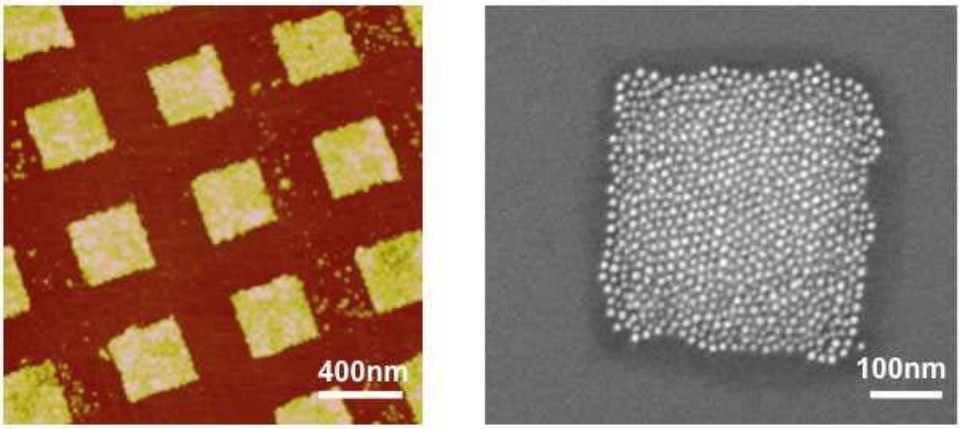

Fig. 3.6 AFM images of subtraction-printed 400nm DNA squares. (Right) SEM image of a nanocrystal array obtained after adsorbing T15-conjugated gold to the 400nm square patterns of A15 followed by thermal annealing.

3.3.5 The role of interparticle interaction by DNA-DNA hybridization

In order to demonstrate that the observed hexagonal packing of the nanoparticles was due to interparticle hybridization mediated by the A_{15} strands, T_{10}-AAGACGAATATTTAACAA (DNA-1) conjugated 10 nm gold was adsorbed to 3 μm parallelogram arrays of the DNA oligonucleotide A_{10}-TTCTGCTTATAAATTGTT (cDNA-1). Because, in this case, a strand of DNA on the surface can only hybridize to one strand on any given particle, no DNA-assisted inteparticle bridging can occur. Using the exact same assembly conditions as the T_{15} and A_{15} systems, nanocrystal arrays from the DNA-1 and cDNA-1 sequences appeared to be largely disordered with very limited local order (Fig. 3.7). Because very minimal hexagonal packing was seen in this case, it is clear that hexagonal ordering was not caused by the physical entrapment of gold nancrystals to a given domain but rather that the crystallographic orientation was thermodynamically driven, with multiple A_{15} strands acting as DNA linkers to drive interparticle association. These interactions would be caused either by substrate-bound DNA or desorbed DNA hybridizing to two separate strands on neighboring gold nanoparticles. When a strand of DNA on the surface can only hybridize to a single strand on an individual particle, there is no interparticle attractive force to drive assembly, resulting largely in disordered arrangements.

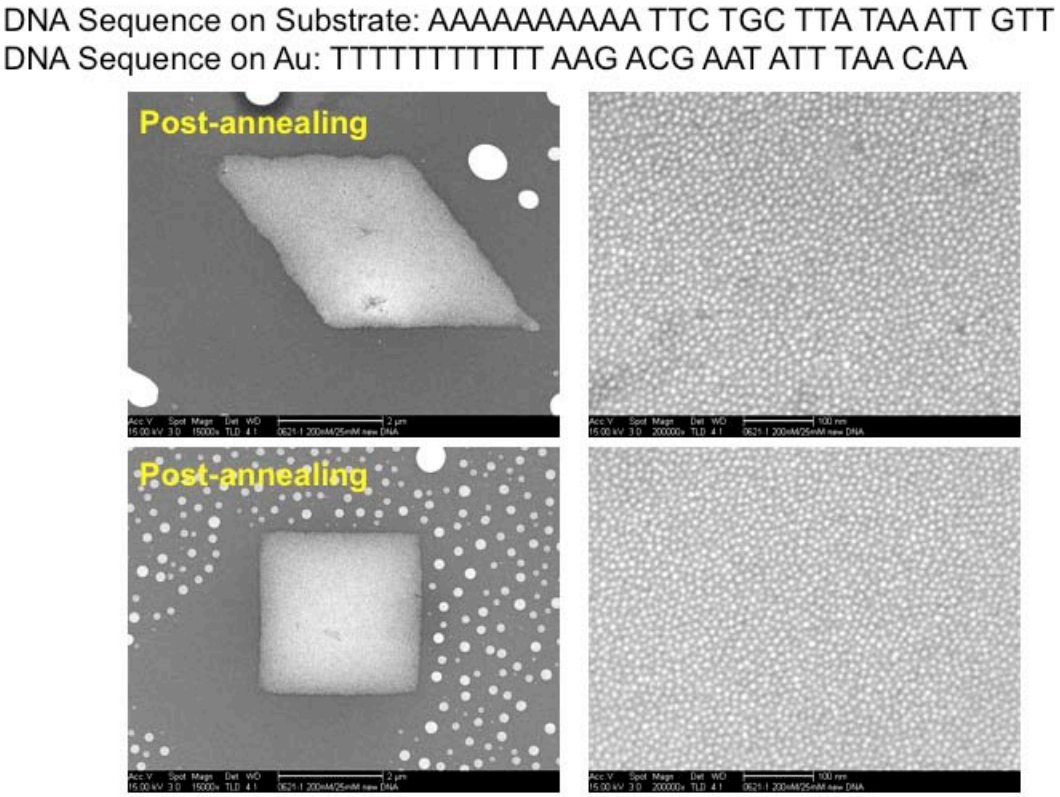

Fig. 3.7 Low and high magnification SEM images of nanocrystal superlattices obtained after adsorbing T10-AAGACGAATATTTAACAA conjugated 10nm gold to 3mm parallelogram and square arrays of the DNA oligonucleotide A10-TTCTGCTTATAAATTGTT followed by thermal annealing. Higher magnification images of the nanocrystal arrays showed mostly disordered arrangements.

3.4 Conclusion

We demonstrate here that, by combining particle sequestration and confinement with interparticle attractive forces with thermal annealing, it is possible to obtain thermodynamically stable, well-defined nanoparticle superlattices that show long-range positional order at specific, predetermined sites on a substrate. We furthermore show that strong confinement effects can be induced simply by having chemically immiscible boundaries at the edges of each nanocrystal array and that these can strongly influence particle packing and ordering. The work shown thus far demonstrates the first lessons toward obtaining highly ordered 2- and 3-D nanoparticle structures in a deterministic and controllable fashion and these will be applied in future studies toward engineering more complex nanocrystal arrangements that show different crystallographic orientations or are composed of multiple types of nanocrystal materials.

3.5 Acknowledgments

This chapter, in full, is a reprint of the material as it appears in ACS Nano, Volume 4, 2011. Noh, Hyunwoo; Choi, Chulmin; Hung, Albert M.; Jin, Sungho; Cha, Jennifer N.. The dissertation author was the primary investigator and author of this paper.

3.6 References

1. Murray, C.B.; Kagan, C.R.; Bawendi, M.G. Self-Organization of CdSe Nanocrystallines into 3-Dimensional Quantum-Dot Superlattices. *Science* **1995**, *270*, 1335-1338.

2. Zhao, Y.; Thorkelsson, K.; Mastroianni, A.J.; Schilling, T.; Luther, J.M.; Rancatore,B.J.; Matsunaga, K.; Jinnai, H.; Wu, Y.; Poulsen, D.; Fréchet. J.M.J.; Alivisatos, A.P.; Xu, Ting. Small-Molecule-Directed Nanoparticle Assembly towards Stimuli-Responsive Nanocomposites. *Nat. Mater.* **2009**, *8*, 979-985.

3. Rosi, N.L.; Mirkin, C.A. Nanostructures in Biodiagnostics. *Chem. Rev.* **2005**, *105*, 1547-1562.

4. Perrault, S.D.; Chan, W.C.W. *In Vivo* Assembly of Nanoparticle Components to Improve Targeted Cancer Imaging. *Proc. Natl. Acad. Sci.USA* **2010**, *107*, 11194-11199.

5. Cheng, W.; Campolongo, M.J.; Cha, J.J.; Tan, S.J.; Umbach, C.C.; Muller, D.A.; Luo, D. Free Standing Nanoparticle Superrlattice Sheets Controlled by DNA. *Nat. Mater.* **2009**, *8*, 519-525.

6. Gur, I.; Fromer, N.A.; Geier, M.L.; Alivisatos, A.P. Air-Stable All-Inorganic Nanocrystal Solar Cells Processed from Solution. *Science* **2005,** *310*, 462-465.

7. Velev, O.D.; Gupta, S. Materials Fabricated by Micro- and Nanoparticle Assembly: The Challenging Path from Science to Engineering. *Adv. Mater.* **2009**, *21*, 1897-1905.

8. Cheng, M. M.-C.; Cuda, G.; Bunimovich, Y.L.; Gaspari, M.; Heath, J.R.; Hill, H.D.; Mirkin, C.A.; Nijdam, A.J.; Terracchiano, R.; Thundat, T.; Ferrari, M. Nanotechnologies for Biomolecular Detection and Medical Diagnostics. *Curr. Opin. Chem. Biol.* **2006,** *10*, 11-19.

9. Tang, Z.; Zhang, Z.; Wang, Y.; Glotzer, S.C.; Kotov, N.A. Self-Assembly of CdTe Nanocrystals into Free-Floating Sheets. *Science* **2006**, *314*, 274-278.

10. Ryeenga, M.; McLellan, J.M.; Xia, Y. Controlling the Assembly of Silver Nanocubes through Selective Functionalization of Their Faces. *Adv. Mater.* **2008**, *20*, 2416-2420.

11. Taton, T.A.; Mirkin, C.A.; Letsinger, R.L. Scanometric DNA Array Detection with Nanoparticle Probes. *Science* **2000,** *289*, 1757-1760.

12. Park, S.Y.; Lytton-Jean, A.K.R.; Lee, B.; Weigand, S.; Schatz, G.C.; Mirkin, C.A. DNA-Programmable Nanoparticle Crystallization. *Nature* **2008**, *451*, 553-556.

13. Nykypanchuk, D.; Maye, M.M.; van der Lelie, D.; Gang, O. DNA-Guided Crystallization of Colloidal Nanoparticles. *Nature* **2008**, *451*, 549-552.

14. Ferrari, M. Cancer Nanotechnology: Opportunities and Challenges. *Nature Rev. Cancer* **2005,** *5*, 161-171.

15. Kannan, B.; Kulkarni, R.P.; Majumdar, A. DNA-Based Assembly of Gold Nanoparticles on Lithographic Patterns with Extraordinary Specificity. *Nano Lett.* **2004**, *4*, 1521-1524.

16. Cui, Y.; Björk, M.T.; Liddle, J.A.; Sönnichsen, C.; Boussert, B.; Alivisatos, A.P. Integration of Colloidal Nanocrystals into Lithographically Patterned Devices. *Nano Lett.* **2004**, *4*, 1093-1098.

17. Cheng, W.; Park, N.; Walter, M.T.; Hartman, M.R.; Luo, D. Nanopatterning Self-Assembled Nanoparticle Superlattices by Moulding Microdroplets. *Nat. Nanotech.* **2008**, *3*, 682-690.

18. Mueggenburg, K.E.; Lin, X.-M.; Goldsmith, R.H.; Jaeger, H.M. Elastic Membranes of Close-Packed Nanoparticle Arrays. *Nat. Mater.* **2007**, *6*, 656-660.

19. Shevchenko, E.V.; Talapin, D.V.; Kotov, N.A.; O'Brien, S.; Murray, C.B. Structural Diversity in Binary Nanoparticle Superlattices. *Nature* **2006**, *439*, 55-59.

20. Noh, H.; Hung, A.M.; Choi, C.; Lee, J.H.; Kim, J.-Y.; Jin, S.; Cha, J.N. 50nm DNA Nanoarrays Generated from Uniform Oligonucleotide Films. *ACS Nano* **2009**, *3*, 2376-2382.

21. Kershner, R.J.; Bozano, L.D.; Micheel, C.M.; Hung, A.M.; Fornof, A.R.; Cha, J.N.; Rettner, C.T.; Bersani, M.; Frommer, J; Rothemund, P.W.K.; Wallraff, G.M. Placement and Orientation of Individual DNA Shapes on Lithographically Patterned Surfaces. *Nat. Nanotech.* **2009**, *4*, 557-561.

22. Hung, A.M.; Micheel, C.M.; Bozano, L.D.; Osterbur, L.W.; Wallraff, G.M.; Cha, J.N. Large-Area Spatially Ordered Arrays of Gold Nanoparticles Directed by Lithographically Confined DNA Origami. *Nat.Nanotech.* **2010**, *5*, 121-126.

23. Park, J.; Chen, L.-H.; Hong, D.; Choi, C.; Loya, M.; Brammer, K.; Bandaru, P.; Jin, S. Geometry Transformation and Alterations of Periodically Patterned Si Nanotemplates by Dry Oxidation. *Nanotechnology* **2009**, *20*, 015303.

24. Loweth, C.J.; Caldwell, W.B.; Peng, X.; Alivisatos, A.P.; Schultz, P.G. DNA-Based Assembly of Gold Nanocrystals. *Angew. Chem. Int. Ed.* **1999**, *38*, 1808-1812.

CHAPTER 4: Surface-driven DNA assembly of binary cubic 3D nanocrystal superlattices

4.1 Introduction

Meso- and macroscale three-dimensional nanocrystal assemblies of arbitrary configuration and crystallographic orientation are highly desired for new solid-state optoelectronic and electromagnetic materials. However, the nanoscale precision and control required to engineer such devices in three dimensions over macroscopic areas site specifically has yet to be achieved. Natural systems arrange bulk organic and inorganic materials into precisely ordered, programmed assemblies by sequestering raw materials into confined spaces and associating them through highly specific non-covalent interactions between biomolecules. Using similar strategies, we demonstrate here the generation of highly ordered 3-D body-centered-cubic (BCC) superlattices of differently modified gold nanocrystals at desired areas on a surface through specific DNA interactions. Through the combination of surface-bound printed DNA designed to capture the nanoparticles and two distinct DNA oligonucleotide sequences designed to arrange the particles in the confined space, 3-D BCC arrangements of nanoparticles were obtained through simple incubation of the surface with gold nanoparticles and subsequent thermal annealing. Furthermore, controlled film thicknesses from 20nm to 100nm were easily obtained through variation of initial gold nanoparticle concentration, and particles remained ordered in the z-direction as well.

For a number of applications, it is critical to obtain 3-D nanocrystal superlattices at predefined locations on a substrate.[1,2] For example, vertically ordered stacked arrays of alternating layers of magnetic and metal nanocrystals with sub-20nm resolution would have an enormous impact on ultra-high density recording media and data storage, while binary semiconductor/metal nanostructures may lead to novel high-efficiency photoemitters. Predominantly hexagonal close packed particle arrays have been obtained through slow solvent evaporation at low pressure.[3-7] Recently, Akey, et al[8] used slow drying and microfluidic flow to achieve a thick three-dimensional quantum dot superlattice on substrates patterned by electron-beam lithography. In addition, several types of binary superlattices have been achieved through precise control over nanoparticle size and surface charge density.[9,10] However, these methods require highly monodisperse nanoparticle samples and complicated fabrication processes that has limited their potential for manufacturability. Alternative approaches using DNA have been demonstrated recently by Park et al[11] and Nykypanchuk et al[12], who showed that bulk gold nanocrystal solids of both BCC and FCC orientation could be obtained by tuning interparticle DNA interactions in solution. DNA has also been used to direct the assembly of metal nanocrystals site specifically on a substrate using patterned DNA oligonucleotides and DNA “origami”.[13-16]

Despite these examples, however, there has been little work in mediating particle packing and orientation in 3-D thin films directly from a substrate.[17-19] We recently showed that highly ordered hexagonally close packed nanocrystal superlattices could be obtained on geometrically and chemically confined DNA patterns on a substrate by using DNA sequences that mediate interparticle hybridization as well as thermal annealing.[20]

This work underscored the proven ability of biomolecules, particularly DNA, to bind specific targets in a tunable, orthogonal, multivalent, and reversible manner.

4.2 Materials and Methods

4.2.1 Dual Subtraction printing

Unpatterned and patterned (3um lines) silicon substrates[20] were cleaned by sonicating in acetone, ethanol, and DI water successively. PDMS substrates were cleaned by sonicating in ethanol and DI water successively. Cleaned PDMS and Si substrates were modified hydrophilic by UVO (Jelight, model 42) treatment with 3 SCFH oxygen gas. The PDMS substrates were then inked with 1ul of 20uM DNA solutions (Integrated DNA Technologies) and incubated in a humid chamber for 20 minutes. The DNA inked PDMS substrates were then gently blown dry with nitrogen. The dual subtraction printing was performed by loading a 50g weight on top of the PDMS and bringing it into contact with the silicon pattern for 30 seconds. The subtracted DNA patterns on PDMS were then brought into conformal contact with planar Si and transferred. The DNA patterned Si substrates were next vapor coated with hexyltrimethoxysilane(Gelest Inc.) in a 45^{o}C oven for 15hrs.

4.2.2 DNA-conjugated gold nanoparticles

10nm gold nanoparticles (Ted Pella) were first reacted with bis-(p-sulphonatophenyl) phenylphosphine dihydrate dipotassium salt (Strem Chemicals) and concentrated.[27] The phosphine stabilized nanoparticles were then reacted with either 5’ or 3’ thiolated DNA at 200:1 molar ratios of DNA to gold and incubated by salt aging.[28] Excess salts and DNA were then removed by microcentrifuge filtration (NANOSEP, Pall corp.). Gold nanoparticle assembly on Si substrates: 6ul of DNA

conjugated gold nanoparticles (10nM-80nM) in 125mM $MgCl_2$ were adsorbed to the DNA printed Si substrates for 60min in a humid environment. To remove excess nanoparticles and salts, the substrates were next briefly rinsed in 1xTAE buffer with 125mM $MgCl_2$ followed by a 5 s 50% ethanol rinse and a 30min immersion in 90% ethanol. The gold nanoparticle arrays next underwent thermal annealing at 70 ^oC in a humid environment for 2.5hrs and samples were then slowly cooled down for 1.5 hours ($0.4^oC\ min^{-1}$)

4.2.3 Characterization and analysis

Fourier Transformation (FT) analyses were done using ImageJ. Experimental d spacings were determined by FT and plot profile analyses of SEM images. Film thickness measurements were conducted by tapping mode atomic force microscopy (Digital Instrument MultiMode Nanoscope IV). Cross-sectional SEM images were prepared by cleaving the samples and imaged at approximately 6^o tilt.

4.2.4 Small angle X-ray diffraction

Small angle X-ray scattering experiments were performed with monochromatic X-rays of beam energy 10 keV and calibrated using silver behenate as a standard. Samples were prepared on glass substrate and were vertically mounted for analysis. Scattered radiation was collected using a MAR Research CCD area detector (pixel size, 79 μm). 2D SAXS patterns were integrated using the Nika 1.2 package and FIT2D. The data are depicted as the structure factor S(q) versus scattering vector, $q=(4\pi/\lambda)\sin(\theta/2)$, where θ is the scattering angle. Scattering of DNA was negligible compared the gold

nanoparticles.

4.3 Results and Discussion

4.3.1 Design of DNA sets for 3-D cubic structure

In order to investigate substrate-adsorbed DNA for the generation of 3-D cubic nanoparticle arrangements, DNA sequences were designed that hybridize specifically to two different sets of DNA conjugated gold nanocrystals (Fig. 4.1).[20, 21] By using two chemically distinct DNA conjugated gold nanoparticles and DNA linkers on the substrate that hybridize to both, BCC packing is thought to be favored because it maximizes the number of DNA hybridization events between the particles, resulting in non-close packed cubic structures with eight coordinated neighbors (CsCl-type superlattices).[11,12] First, 3um square arrays of DNA linkers composed of either 5'-$(AG)_4$-T-AGGAAAGA-3' (Set 1) or 5'-A_{12}-T-$(GA)_6$-3'(Set 2) were dual subtraction printed on UVO cleaned silicon (Fig. 4.1a). The remaining bare silicon surface was then modified with hexyltrimethoxysilane (HTS) through vapor deposition. Next, equimolar amounts of 10nm gold nanocrystals modified with 3'-SH-T_{15}-$(TC)_6$-5' and 5'-SH-T_{15}-TTCCTCTTTCCT-3' (Set 1) or with 3'-SH-T_{31}-5' and 5'-SH-T_{15}-$(TC)_8$-3' (Set 2) were adsorbed to the corresponding linker patterns in 125mM $MgCl_2$ for 1 h, followed with buffer and ethanol rinsing to remove excess particles and salts . This was followed by annealing the substrates at 70 ^{o}C in a humid environment to drive particle assembly toward a thermodynamically favored state (Fig. 4.1b).[11,12]

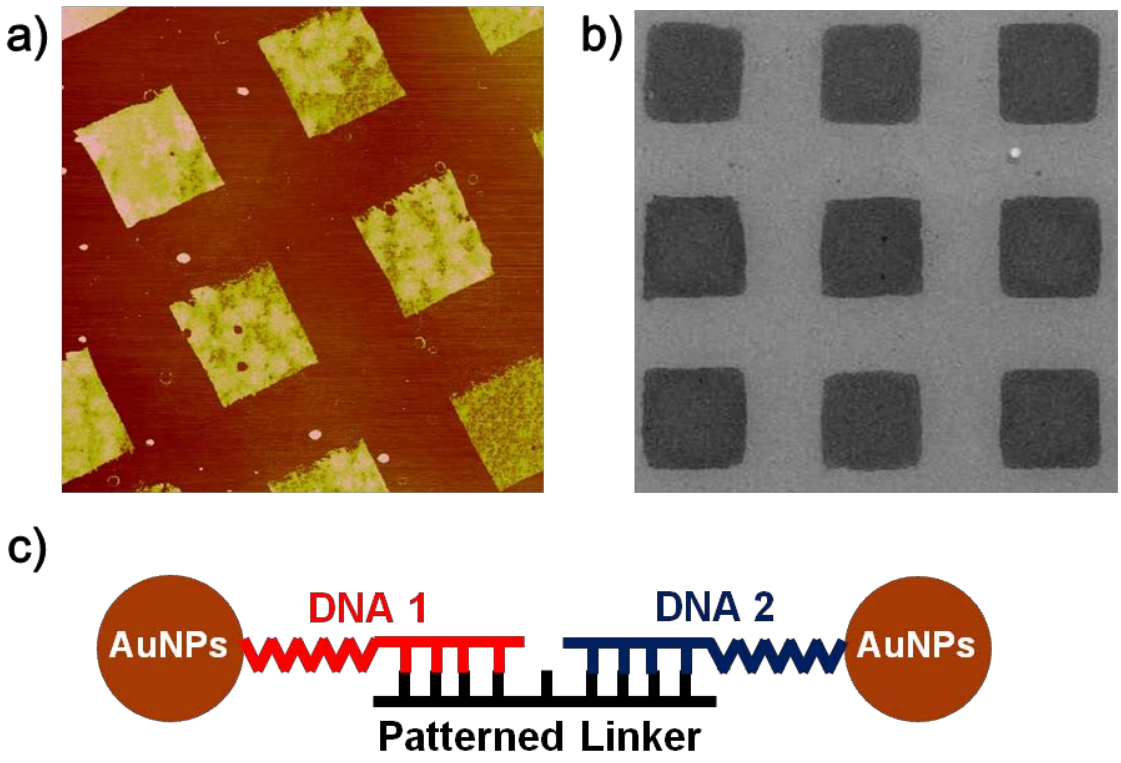

Fig. 4.1 a) AFM images of 3um square arrays prepared by dual subtraction printing (DSP). b) SEM images of 3um square arrays of Au nanoparticles assembled on the linker (5'-$(AG)_4$ -T-AGGAAAGA-3') patterns after thermal annealing. c) Schematic of DNA linkers on the substrate hybridizing between two different DNA modified gold nanocrystals.

4.3.2 Fourier transformation and SEM analysis of ordered AuNPs structure

After adsorbing 20 to 40 nM gold nanocrystal concentrations to the DNA arrays and annealing for 4 h, highly ordered, close-packed nanocrystal arrays were clearly observed from both sets of DNA conjugated gold and DNA linkers (Fig. 4.2). In order to determine the crystallographic orientation of each superlattice, Fourier transform (FT) analyses of individual SEM images of representative arrays (Fig. 4.2a,b and Fig. 4.2c,d) were conducted, demonstrating BCC arrangement with the (110) plane, the most densely packed and lowest energy crystal plane, displayed at the surface. For comparison, a schematic depicting the (110) plane of a BCC structure is shown in Fig. 4.3 with pertinent spots in its FT labeled by the corresponding Miller indices. The planar spacings d(200), d(220), d(1 ½ ½) and d(222) were also determined for both sets and were measured to be 8.28nm, 11.79nm, 13.44nm and 14.29nm and 10.76nm, 15.29nm, 17.48nm and 18.69nm, respectively, for sets 1 and 2. Furthermore, the d(220)/d(200) and d(1 ½ ½)/d(200) ratios for both sets were 1.42 and 1.62, close to the theoretical values of 1.41 and 1.63. While FT analyses of SEM images with different gold nanoparticle concentrations (Fig. 4.4) showed some variability in the distance between the nanoparticles with a range of +2%, the BCC (110) plane was the predominant facet observed at the surface of all of the arrays.

The d(222) values of 14.29nm and 18.69nm correspond to center-to-center interparticle spacings and are close to the theoretical ranges of 14.38nm<d<18.84nm and 16.38nm<d<20.84nm for Sets 1 and 2 respectively. The lower limits were determined by assuming the hybridized segment to be rigid A-form DNA (0.25nm per base) [22] and the flexible polyT spacers to be random coils of persistence length 0.75nm.[23] Since a total

of 16 bases would be hybridized in the case of Set 1 but 24 bases in Set 2, the different ranges of d spacings for Sets 1 and 2 are appropriate. The upper limits were obtained by assuming scaling predictions in which the chain dimensions follow scaling power laws in the limit of high interface curvature.[24] While interparticle distances in Set 1 were close to what would be assumed for 10nm particles separated by a perfectly rigid length of A-form DNA plus two flexible coils of ssDNA, in Set 2 the d(222) value was slightly larger than estimated values. This difference in interparticle lengths between the two different sets of DNA linkers (5'-AGAGAGAG-T-AGGAAAGA-3'(1) and 5'-AAAAAAAAAAAA-T-GAGAGAGAGAGA-3'(2)) may be explained by considering that the intermolecular repulsive forces of stacked purine molecules such as adenine are known to introduce more delocalized π electron densities and polar side groups and thereby increase electrostatic repulsion.[25,26] The results of the FT analysis of the gold nanoparticle arrays obtained using Set 1 linker DNA (Table 4.1) was consistent with the interparticle distances found in the first diffraction peak of small angle X-ray scattering (SAXS), showing strong ordering and uniform interparticle distances within the nanoparticle films (Fig. 4.5). However, these arrays were too thin (<100nm) to obtain enough signal to observe higher order peaks using our instrumentation. The relative degree of ordering and BCC packing through a single nanoparticle film was explored using cross-sectional SEM images of nanocrystal arrays generated from 40nM gold nanoparticle solutions. As shown in Fig. 4.6, approximately 80nm thick film arrays were obtained with strong ordering both parallel and normal to the surface. While the top plane clearly showed a BCC (110) face, obtaining absolute vertical (220) facets along the z-axis of the cross section was difficult due to multiple grain boundaries within an array as well

as issues of substrate cleaving. Because the ordering within a nanoparticle superlattice is induced by the DNA at the surface, it is not surprising that the ordered assembly is seen throughout the film as it would be highly unlikely for the surface alone to show BCC packing with the underlying layers showing disordered or non BCC packing with the same DNA interactions used throughout.

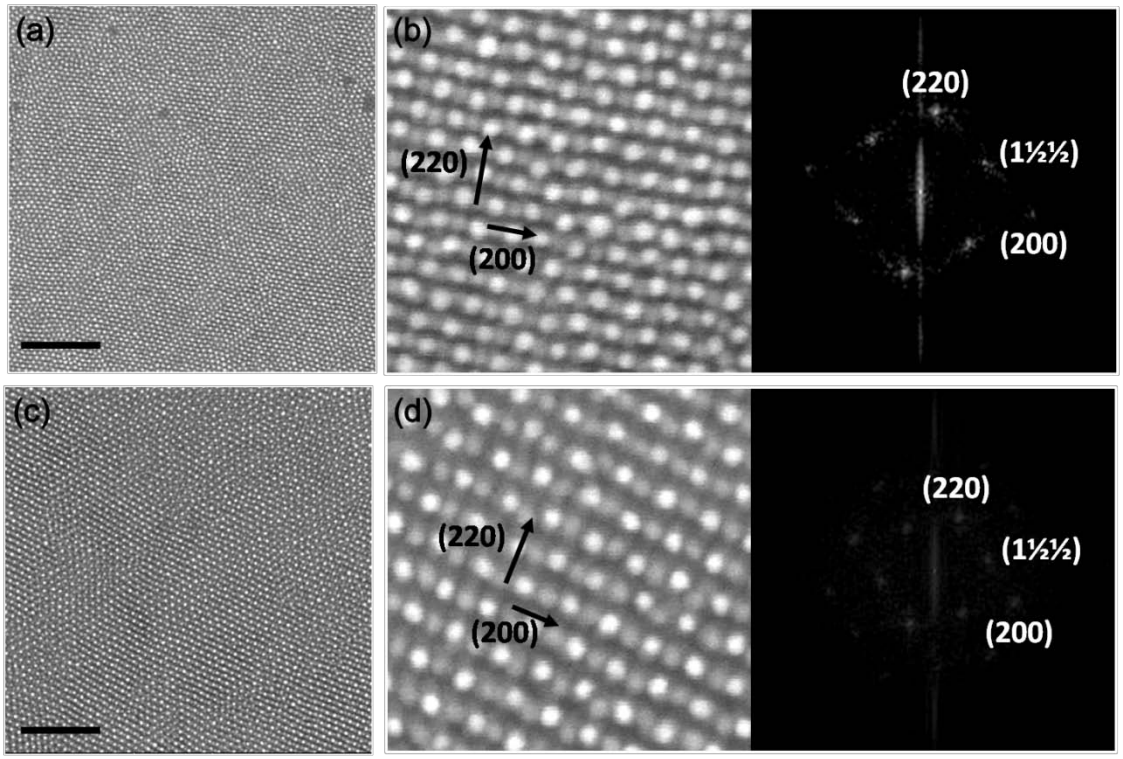

Fig. 4.2 Representative SEM images of gold nanoparticle superlattices obtained using two different DNA linkers (a, b: 5'-$(AG)_4$-T-AGGAAAGA-3', c, d: 5'-A_{12}-T-$(GA)_6$-3'). b) SEM image and FT analysis of a nanoparticle superlattice assembled using 20nM set 1 conjugated gold and printed linker (5'-$(AG)_4$ -T -AGGAAAGA-3'). d) SEM image and FT analysis of a nanoparticle array assembled using 40nM set 2 conjugated gold and printed linker (5'-A_{12}-T-$(GA)_6$-3'). Scale bar corresponds to 200nm

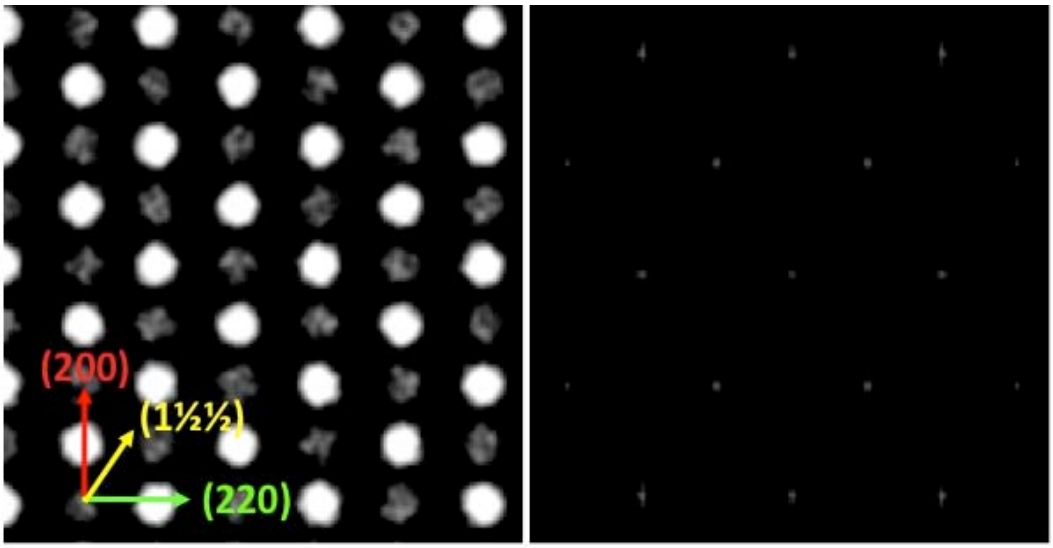

Fig. 4.3 Image and FT analysis of BCC (110) schematic array.

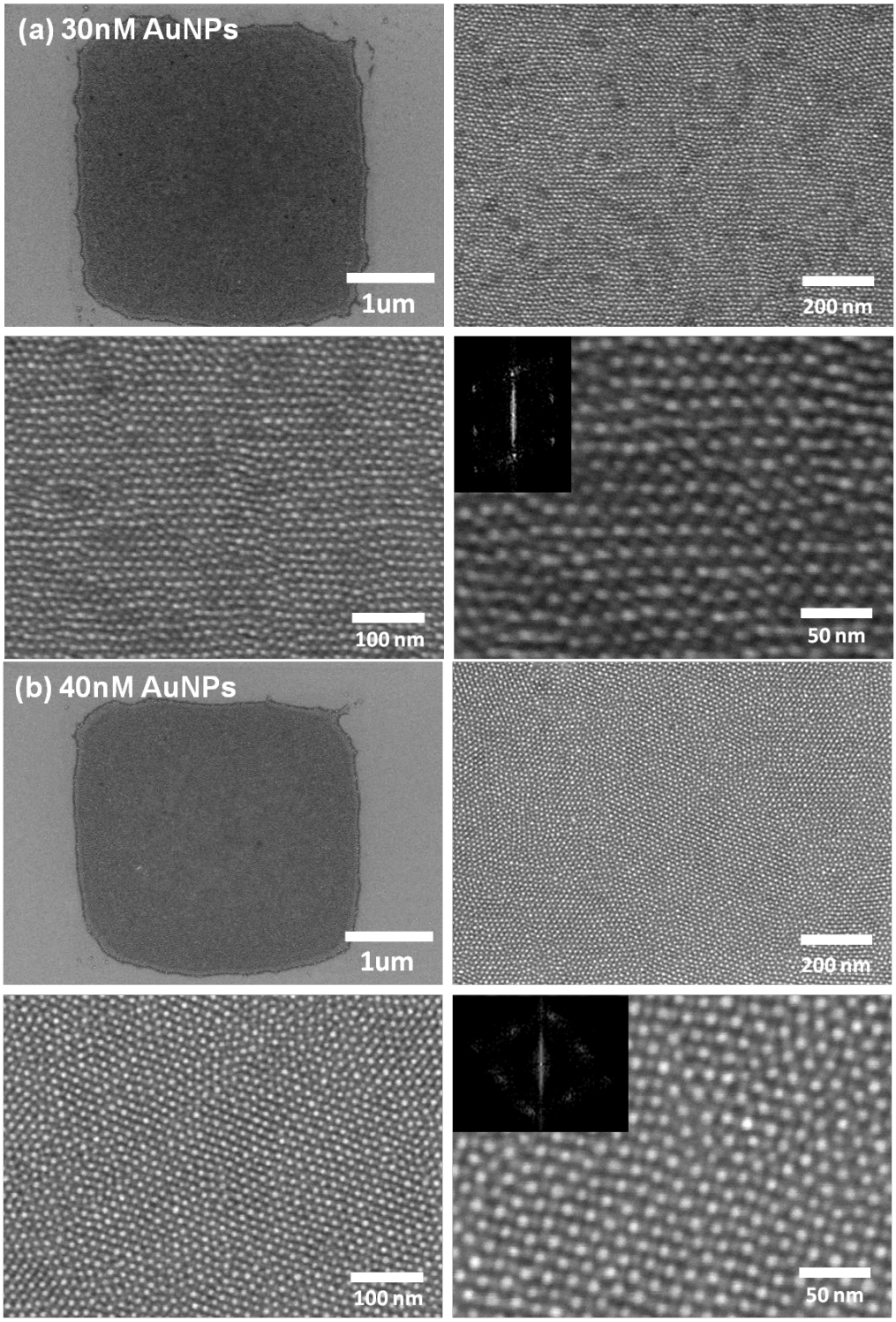

Fig. 4.4 SEM images of gold nanoparticle superlattices obtained on DNA linker 5' - $(AG)_4$ -T-AGGAAAGA - 3' from 30nM(a) and 40nM(b) gold nanoparticle solutions. Insets show FT analyses.

Table 4.1 d-spacings and ratios obtained from different concentrations of DNA-conjugated gold adsorbed to the subtraction printed 5'-$(AG)_4$-T-AGGAAAGA-3' linkers.

DNA on Substrate	Au Conc.	d(200)	d(220)(ratio)	d(1½½)(ratio)	d(222)(ratio)
5'-$(AG)_4$ -T-AGGAAAGA-3'	10nM	8.46nm	12.95nm (1.53)	14.54nm (1.71)	N/A
	20nM	8.28nm	11.79nm (1.42)	13.44nm (1.62)	14.29nm (1.72)
	30nM	8.83nm	12.49nm (1.41)	14.49nm (1.64)	15.52nm (1.75)
	40nM	8.70nm	12.44nm (1.42)	14.18nm (1.63)	15.25nm (1.75)

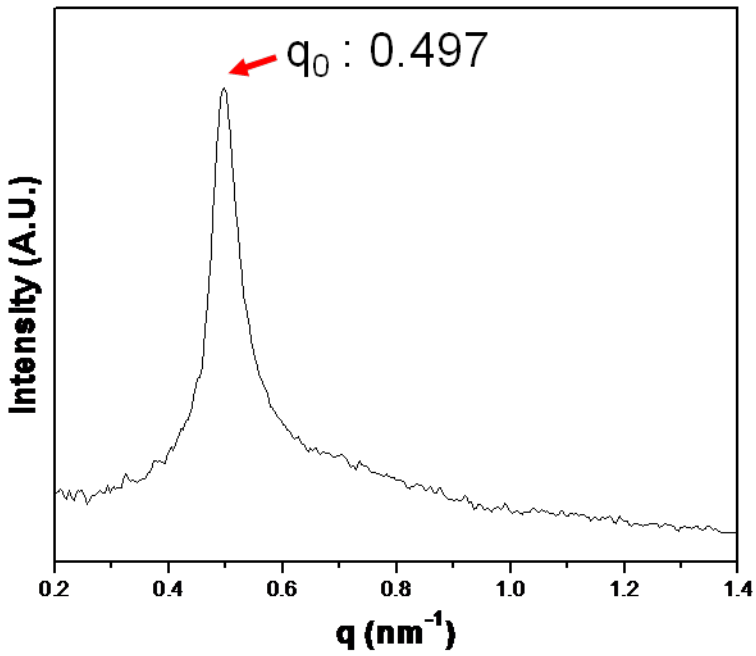

Fig. 4.5 Small angle x-ray scattering (SAXS) data of nanocrystal thin films obtained using 40nM gold nanoparticle concentration and DNA linker 5'-$(AG)_4$-T-AGGAAAGA-3'. Scattering intensity is plotted as a function of the magnitude of the scattering vector $q = 4\pi\sin(\theta) / \lambda$. A first strong corresponding peak is explained as a relatively uniform interparticle distance calculated by d_{Au} = sqrt.(6)* 3.14 / q_0 =15.48nm

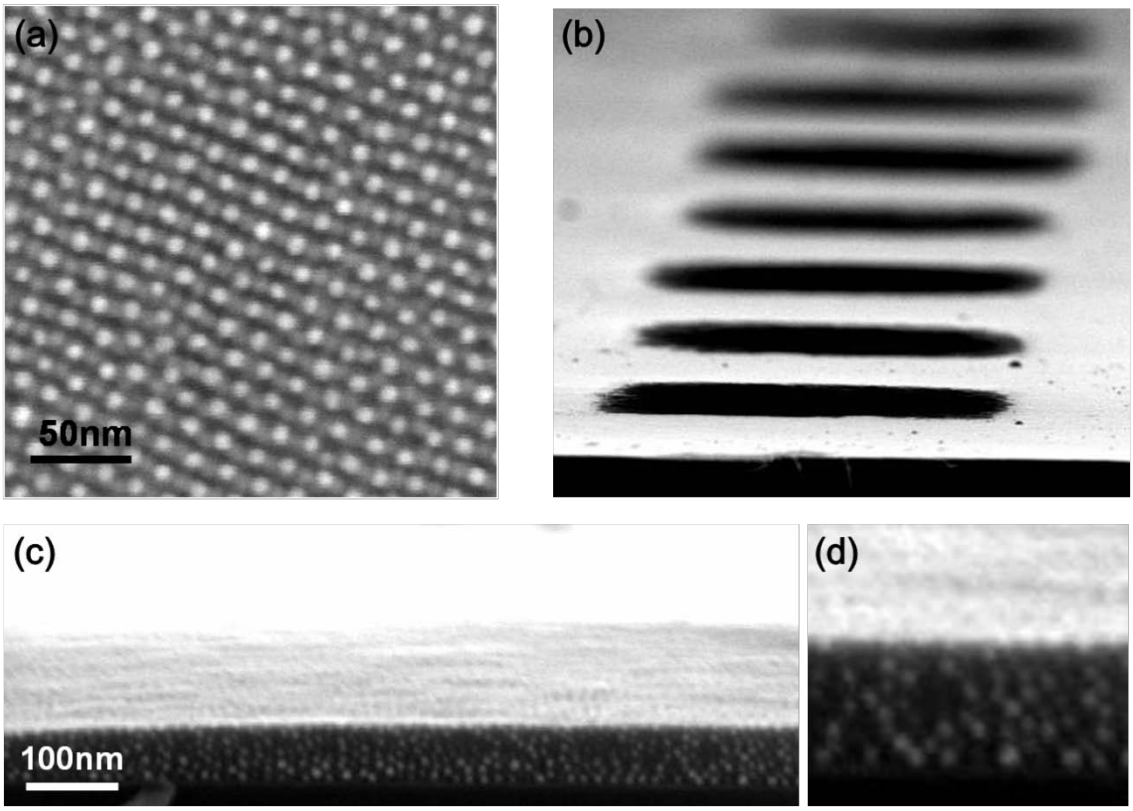

Fig. 4.6 SEM images of top (a) and cross sections of nanocrystal films obtained from 40nM of 3'-SH-T_{15}-$(TC)_6$-5' and 5'-SH-T_{15}-TTCCTCTTTCCT-3' conjugated gold nanoparticles on DNA linker (5'-$(AG)_4$ -T-AGGAAAGA-3'). Low (b) and high mag (c, d) images are shown. Samples were tilted 6^o for imaging

4.3.3 Controllability of AuNPs film thickness

Because there is no physical or chemical boundary in the z-direction, such as an air-liquid interface, that can limit the film thickness, highly-ordered nanocrystal films from 20 to 100 nm can be generated simply by controlling the gold nanoparticle concentrations from 10nM to 80nM. Although there was some variation in the exact DNA-conjugated gold nanocrystal concentrations, on average a linear correlation was observed between nanoparticle concentrations and the final array thicknesses obtained (Figs. 4.7, 4.8).

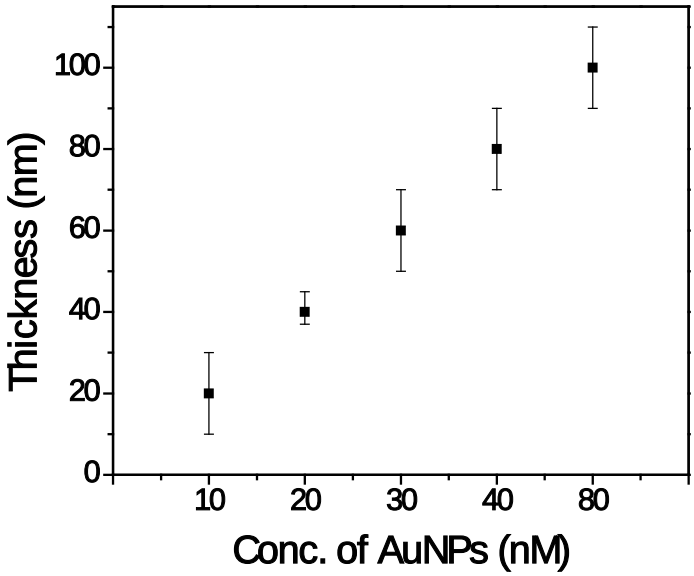

Fig. 4.7 Thicknesses obtained of gold nanoparticle thin film assemblies on the subtraction printed 5'-$(AG)_4$-T-AGGAAAGA-3' linkers as a function of gold concentrations used.

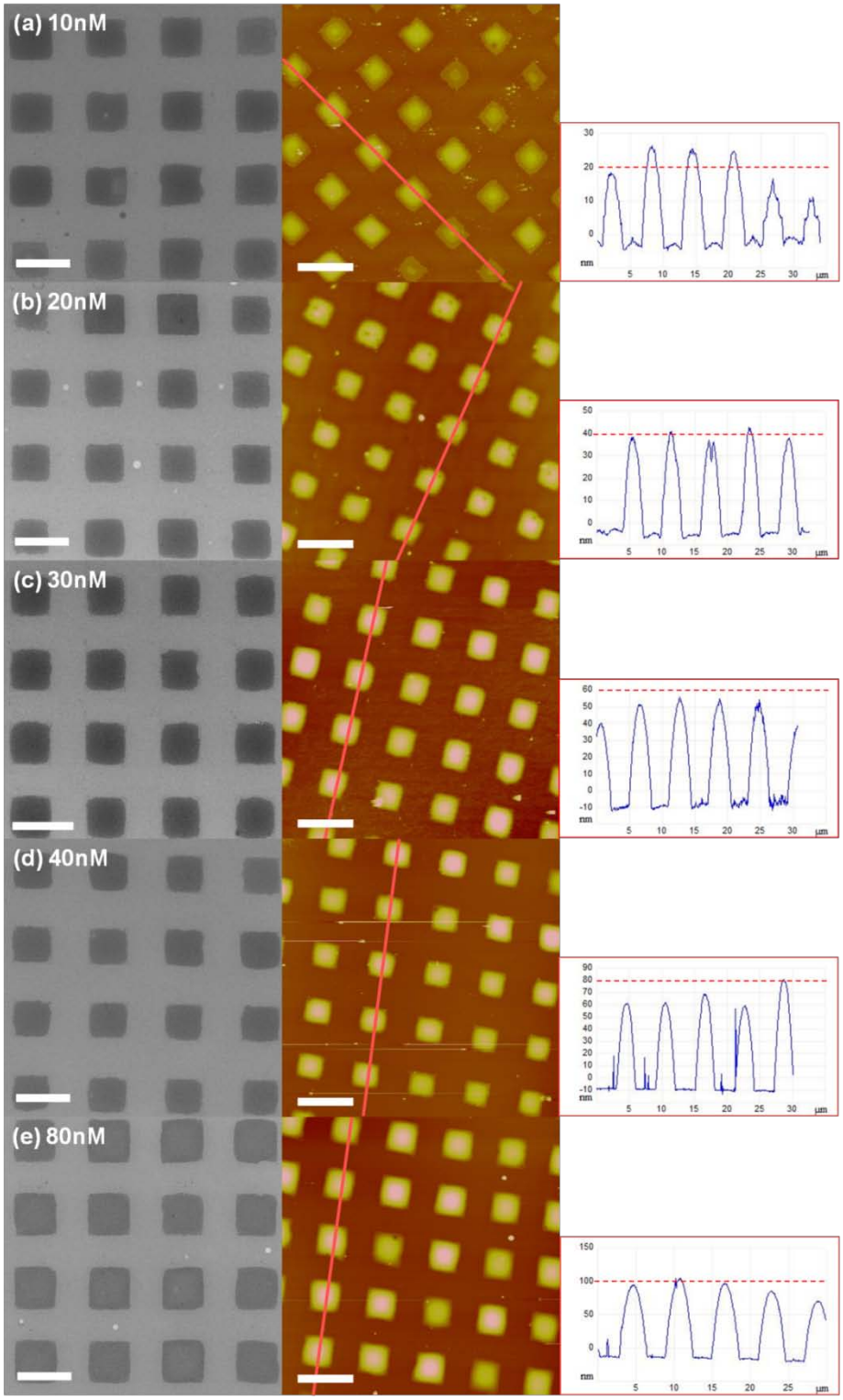

Fig. 4.8 SEM and AFM images with corresponding height profiles of gold nanoparticle superlattices obtained on printed 5'-$(AG)_4$-T-AGGAAAGA-3' using gold nanoparticle concentrations ranging from 10nM to 80nM. Scale bar: 6um

4.3.4 The effect of AuNPs concentration on formation of 3D cubic structure

The d spacings of samples prepared using different concentrations of gold nanoparticles (Set 1) were also determined by FT analyses (Table 1). At 10nM gold concentrations, both the d(220)/d(200) and d(1½½)/d(200) ratios were higher than theoretical ones, resulting in a distorted lattice with mixed and random orientations. It is thought this occurs because the layers are only 1-2 nanoparticles in thickness that is not enough to generate a highly stable BCC crystal. This was also verified by the observation of a transition domain between a monolayer of particles at the edges of each array and a stacked multilayer (2-3 layers) of particles in the middle of each film (Fig. 4.9). It is also possible that at smaller concentrations there is not enough gold present to trap the physisorbed surface-bound DNA, causing some of the initially printed DNA to wash off. However, as the concentration of gold nanocrystals increased to 40nM, nanoparticle superlattices could easily be observed with d-space ratios d(220)/d(200) and d(1 ½ ½)/d(200) for both sets equaling 1.42 and 1.63 indicating BCC (110) packing within an error range of ~2%. Having the areas surrounding the initial DNA patterns be strongly hydrophobic furthermore forces the particles to stack on top of one another as opposed to assembling laterally out. As the gold nanoparticle concentrations increased further to 80nM, BCC packing was not seen in the uppermost layers of the films; instead mixed domains of partial BCC and disordered arrays were observed (Fig. 4.10). It is presumed that by driving larger amounts of gold nanoparticles to the printed DNA, the DNA on the surface became consumed eventually, resulting in weaker interactions between the nanoparticles in the top layers due to the existence of less linker DNA per particle.

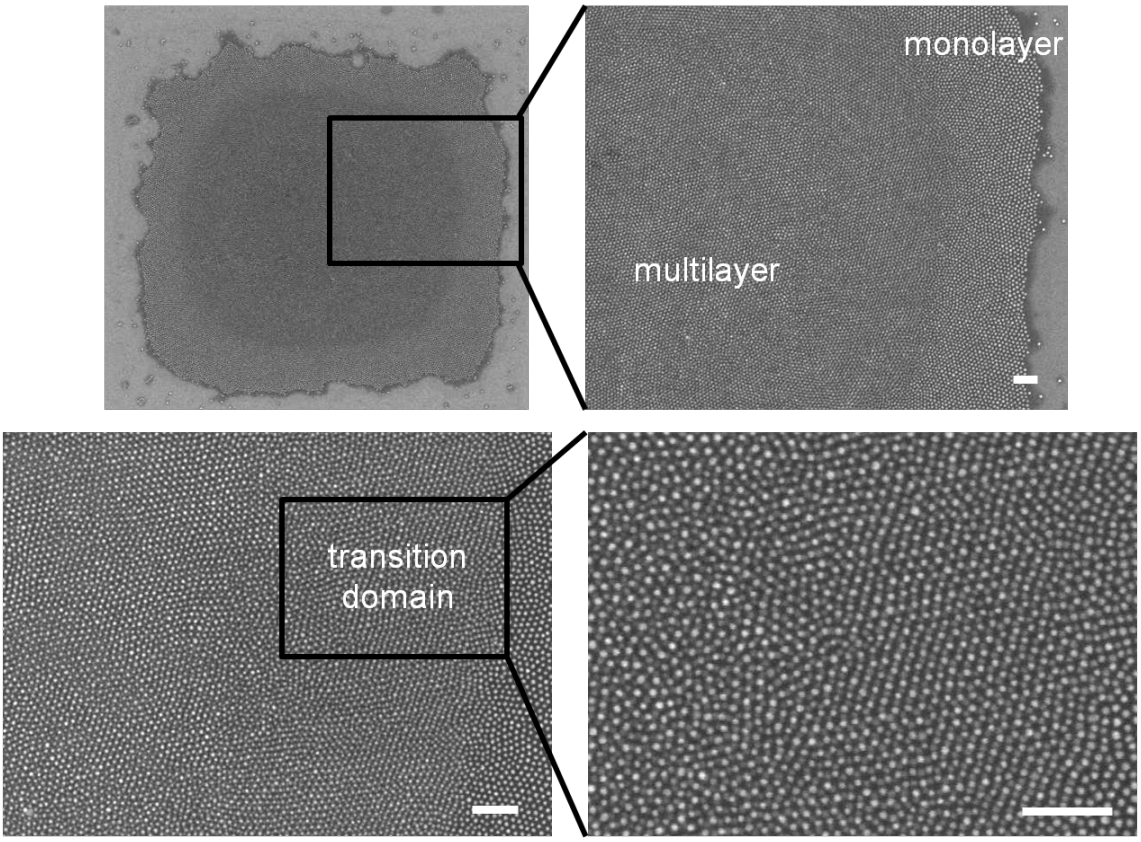

Fig. 4.9 SEM images showing a transition from a hexagonally packed monolayer to a BCC structure when absorbing 10nM DNA conjugated nanoparticles to printed 5'-$(AG)_4$-T-AGGAAAGA-3' DNA linkers. Scale bar: 100nm

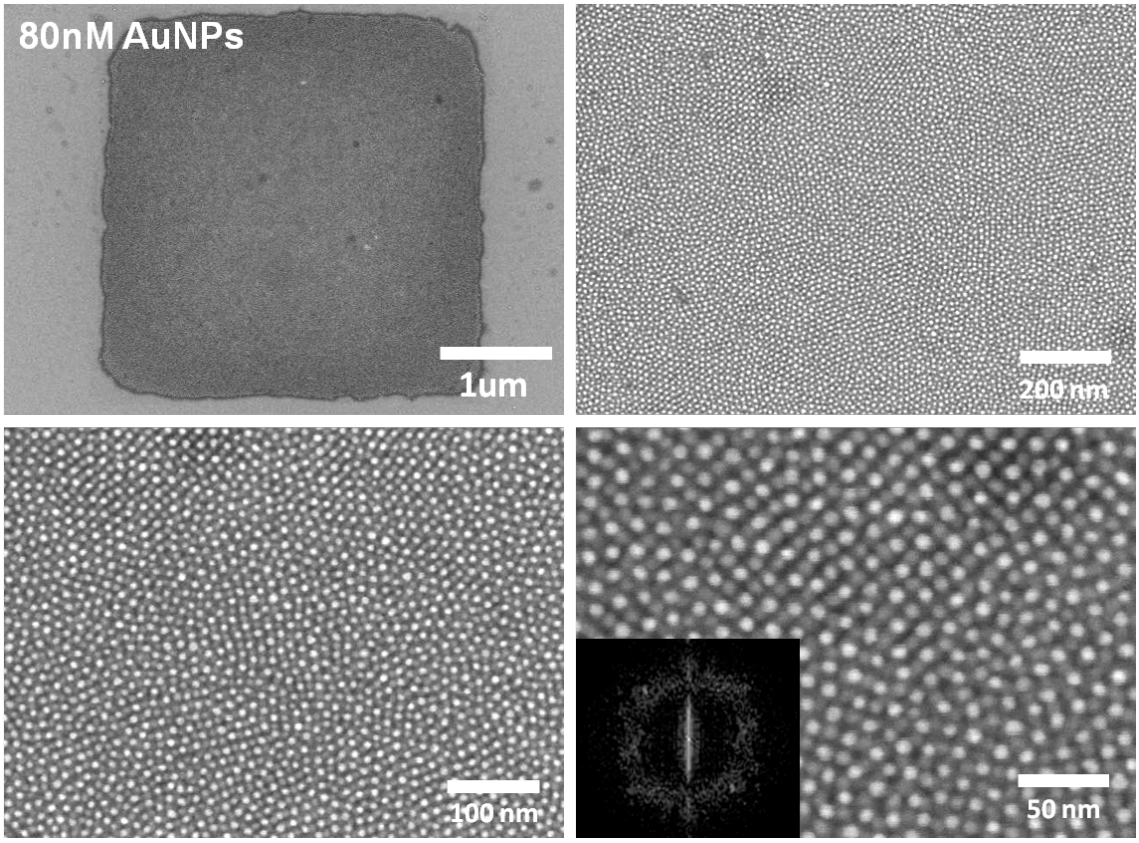

Fig. 4.10 SEM images of 80nM AuNPs superlattice obtained after adsorbing 80nM DNA conjugated gold on printed DNA linker 5'-$(AG)_4$-T-AGGAAAGA-3'. Many more grain boundaries are observed with only partial ordering, resulting in random orientations and less crystallinity.

4.3.5 Variability of nanoparticle size and the role of linker DNAs for formation of 3D cubic structure

In addition to using 10nm gold, generating BCC packing from 5nm gold was also tried. By switching from 10nm gold to 5nm gold while keeping the DNA sequences used exactly the same, it was found the highly ordered BCC superlattices of 5nm gold nanoparticles could also be produced (Fig. 4.11). Finally, control experiments using DNA strands that would only enable hybridization between one set of gold and one of the two DNA strands on the substrate produced close packed particles but no particular ordering within the array (Fig. 4.12).

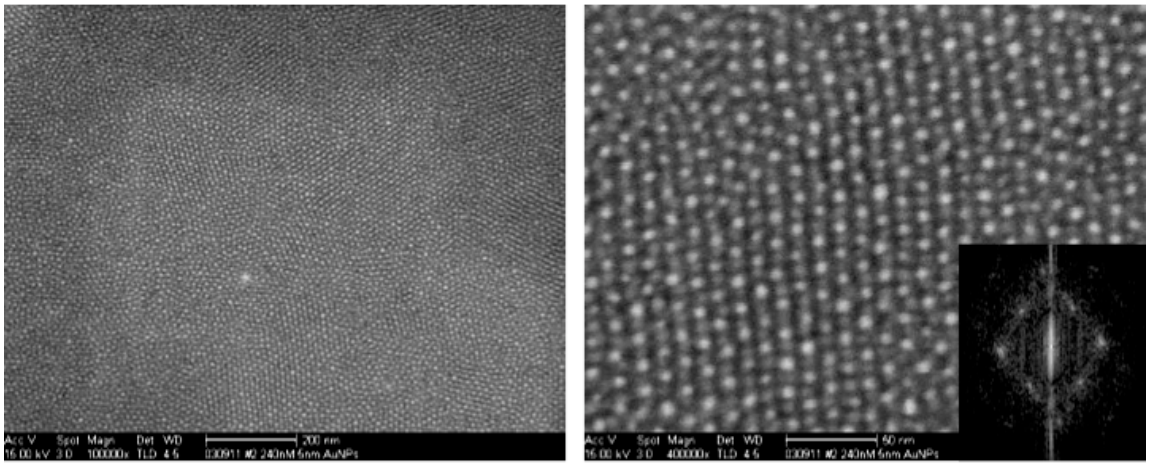

Fig. 4.11 SEM images of gold nanoparticle superlattices obtained after adsorbing 240nM DNA conjugated 5nm gold on printed DNA linker 5'-$(AG)_4$-T-AGGAAAGA-3'.

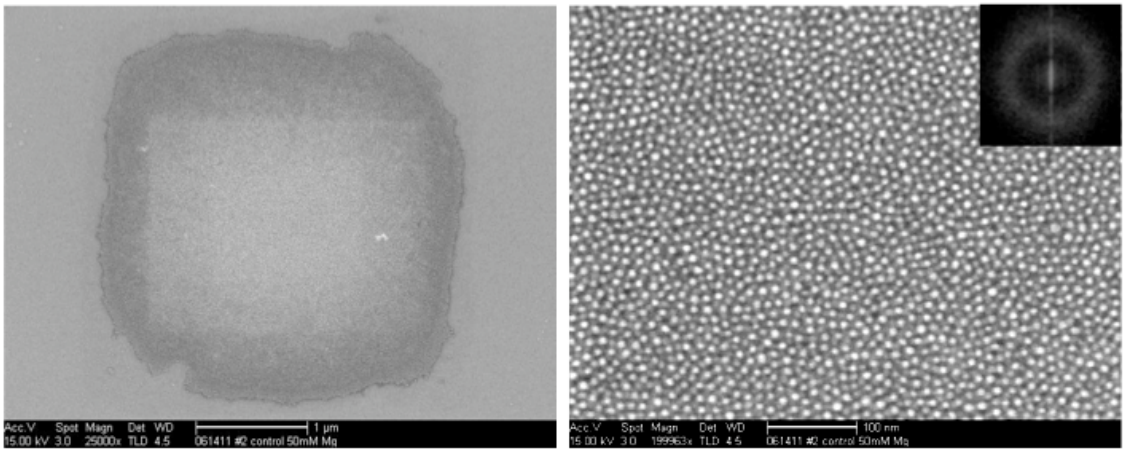

Fig. 4.12 Low and high magnification SEM images of control experiment using gold nanoparticles modified with 5'-SH-T_{10}-AAGACGAATATTTAACAA and 3'-SH-T_{15}-TCTCTCTCTCTC adsorbed to printed DNA 5'-AGAGAGAG-3' and 5'-TTGTTAAA-3'. Because each DNA on the gold could only hybridize to a single DNA sequence on the substrate, no ordering was observed within the nanoparticle arrays.

4.4 Conclusion

The results shown here demonstrate the first guiding principles of obtaining binary type superlattices through substrate mediated information and assembly. Through careful balance of the attractive and repulsive forces between the particles, the array, and the outside surface, binary sets of nanoparticles were assembled into well ordered 3-D BCC superlattices simply by annealing different DNA conjugated gold nanocrystals with DNA-stamped surfaces. To control the crystallographic alignment of each particle with its neighbors, the nanoparticles were assembled using a mixture of DNA base pairing interactions. The surface adsorbed DNA produced binary BCC arrays using DNA linkers that hybridized specifically between two different types of DNA-modified nanocrystals. Because the entire thermodynamically-driven process depended only on the amount of DNA on the surface, nanoparticle films of tunable thicknesses were easily produced simply by tuning the initial concentration of the nanoparticle solutions. By doing so, BCC nanocrystal films ranging in heights from 20 to 100nm were engineered site specifically on a surface with good order throughout. As the assembly is controlled through the DNA sequences employed, this methodology should be easily applicable to a wide variety of pure and binary nanocrystal superlattices for new advances in energy and computing

4.5 Acknowledgments

This, in full, is a reprint of the material as it appears in Small, Volume 7, 2011. Noh, Hyunwoo; Hung, Albert M.; Cha, Jennifer N. The dissertation author was the primary investigator and author of this paper.

4.6 References

1. Whitesides, G. M.; Grzybowski, B. Self-Assembly at All Scales. *Science* **2002**, *295*, 2418-2421.

2. Crespo-Biel, O.; Ravoo, B. J.; Reinhoudt, D. N.; Huskens, J. Noncovalent Nanoarchitectures on Surfaces: from 2D to 3D Nanostructures. *J. Mater. Chem.* **2006**, *16*, 3997-4021.

3. Murray, C. B.; Kagan, C. R.; Bawendi, M. G. Self-Organization of CdSe Nanocrystallites into Three-Dimensional Quantum Dot Superlattices. *Science* **1995**, *270*, 1335-1338.

4. Sun, S.; Murray, C. B. Synthesis of Monodisperse Cobalt Nanocrystals and Their Assembly into Magnetic Superlattices. *J. Appl. Phys.* **1999**, *85*, 4325-4330.

5. Norris, D. J.; Arlinghaus, E. G.; Meng, L.; Heiny, R.; Scriven, L. E. Opaline Photonic Crystals: How Does Self-Assembly Work? *Adv. Mater.* **2004**, *16*, 1393-1399.

6. Urban, J. J.; Talapin, D. V.; Shevchenko, E. V.; Kagan, C. R.; Murray. C. B. Synergism in Binary Nanocrystal Superlattices Leads to Enhanced p-type Conductivity in Self-Assembled PbTe/Ag_2Te Thin Films. *Nat. Mater.* **2007**, *6*, 115-121.

7. Dong, A.; Chen, J.; Oh, S. J.; Koh, W. K.; Xiu, F.; Ye, X.; Ko, D. K.; Wang, K. L.; Kagan, C. R.; Murray, C. B. Multiscale Periodic Assembly of Striped Nanocrystal Superlattice Films on a Liquid Surface. *Nano Lett.* **2011**, *11*, 841–846.

8. Akey, A.; Lu, C.; Yang, L.; Herman, I. P. Formation of Thick, Large-Area Nanoparticle Superlattices in Lithographically Defined Geometries. *Nano Lett.* **2010**, *10*, 1517-1521.

9. Shevchenko, E. V.; Talapin, D. V.; O'Brien, S.; Murray, C. B. Polymorphism in AB_{13} Nanoparticle Superlattices: An Example of Semiconductor−Metal Metamaterials. *J. Am. Chem. Soc.* **2005**, *127*, 8741-8747.

10. Shevchenko, E. V.; Talapin, D. V.; Kotov, N. A.; O'Brien, S.; Murray, C. B. Structural Diversity in Binary Nanoparticle Superlattices. *Nature* **2006**, *439*, 55-59.

11. Park, S. Y.; Lytton-Jean, A. K. R.; Lee, B.; Weigand, S.; Schatz, G. C.; Mirkin, C. A. DNA-Programmable Nanoparticle Crystallization. *Nature* **2008**, *451*, 553-556.

12. Nykypanchuk, D.; Maye, M. M.; van der Lelie, D.; Gang, O. DNA-Guided Crystallization of Colloidal Nanoparticles. *Nature* **2008**, *451*, 549-552.

13. Hung, A. M.; Micheel, C. M.; Bozano, L. D.; Osterbur, L. W.; Wallraff, G. M.; Cha, J. N. Large-Area Spatially Ordered Arrays of Gold Nanoparticles Directed by Lithographically Confined DNA Origami. *Nat. Nanotech.* **2010**, *5*, 121-126.

14. Noh, H.; Hung, A. M.; Choi, C.; Lee, J. H.; Kim, J. -Y.; Jin, S.; Cha, J. N. 50 nm DNA Nanoarrays Generated from Uniform Oligonucleotide Films. *ACS Nano* **2009**, *3*, 2376–2382.

15. Kannan, B.; Kulkarni, R. P.; Majumdar, A. DNA-Based Programmed Assembly of Gold Nanoparticles on Lithographic Patterns with Extraordinary Specificity. *Nano Lett.* **2004**, *4*, 1521–1524.

16. Lalander, C. H.; Zheng, Y.; Dhuey, S.; Cabrini, S.; Bach, U. DNA-Directed Self-Assembly of Gold Nanoparticles onto Nanopatterned Surfaces: Controlled Placement of Individual Nanoparticles into Regular Arrays. *ACS Nano* **2010**, *4*, 6153-6161.

17. Yin, Y.; Li, Z. Y.; Xia, Y. Template-Directed Growth of (100)-Oriented Colloidal Crystals. *Langmuir* **2003**, 19, 622-631.

18. Cui, Y.; Björk, M. T.; Liddle, J. A.; Sönnichsen, C.; Boussert, B.; Alivisatos, A. P. Integration of Colloidal Nanocrystals into Lithographically Patterned Devices. *Nano Lett.* **2004**, *4*, 1093-1098.

19. Cheng, W.; Park, N.; Walter, M. T.; Hartman, M .R.; Luo, D. Nanopatterning Self-Assembled Nanoparticle Superlattices by Moulding Microdroplets. *Nat. Nanotech.* **2008**, *3*, 682-690.

20. Noh, H.; Choi, C.; Hung, A. M.; Jin, S.; Cha, J. N. Site-Specific Patterning of Highly Ordered Nanocrystal Superlattices through Biomolecular Surface Confinement. *ACS Nano* **2010**, *4*, 5076–5080.

21. Coyer, S. R.; Garcia, A. J.; Delamarche, E. Facile Preparation of Complex Protein Architectures with Sub-100-nm Resolution on Surfaces. *Angew. Chem. Int. Ed.* **2007**, *46*, 6837-6840.

22. Park, S. J.; Lazarides, A. A.; Storhoff, J. J.; Pesce, L.; Mirkin, C. A. The Structural Characterization of Oligonucleotide-Modified Gold Nanoparticle Networks Formed by DNA Hybridization. *J. Phys. Chem. B* **2004**, *108*, 12375-12380.

23. Smith, S. B.; Cui, Y.; Bustamante, C. Overstretching B-DNA: The Elastic Response of Individual Double-Stranded and Single-Stranded DNA Molecules. *Science* **1996**, *271*, 795-798.

24. Dan, N.; Tirrell, M. Polymers Tethered to Curves Interfaces: a Self-Consistent-Field Analysis. *Macromolecules* **1992**, *25*, 2890-2895.

25. Cysewski, P. Intra-Strand Stacking Interactions in B-DNA Crystals Characterized by Post-SCF Quantum Chemistry Computations. *New J. Chem.* **2009**, *33*, 1909-1917.

26. Santalucia, J. A Unified View of Polymer, Dumbbell, and Oligonucleotide DNA Nearest-Neighbor Thermodynamics. *Proc. Natl. Acad. Sci. USA* **1992**, *95*, 1460-1465.

27. Loweth, C. J.; Caldwell, W. B.; Peng, X.; Alivisatos, A. P.; Schultz, P. G. DNA-Based Assembly of Gold Nanocrystals. *Angew. Chem. Int. Ed.* **1999**, *38*, 1808-1812.

28. Hurst, S. J.; Lytton-Jean, A. K. R.; Mirkin, C. A. Maximizing DNA Loading on a Range of Gold Nanoparticle Sizes. *Anal. Chem.* **2006**, *78*, 8313–8318.

CHAPTER 5: Scalable assembly of 3D excitonic nanocrystal assemblies by using DNA interactions and DNA mediated charge transport

5.1 Introduction

Semiconductor nanocrystals such as quantum dots (QDs) have been heavily investigated in recent years as potential building blocks for optoelectronic devices.[1-9] The tunable, size-dependent bandgap of QDs has afforded methods to optimize device performance and enhance photon adsorption. In addition, the solution processibility of nanomaterials allows fabrication techniques that are less expensive and time-consuming than methods like vacuum deposition. Despite some of these key advantages, however, common deposition techniques to produce films remain challenging due to inherent surface defects of nanocrystals[10] and difficulties in producing close-packed films with minimal roughness and smooth interfaces. Although methods such as slow evaporation have been explored to orient and arrange nanoparticles (*e.g.* CdSe, Fe_3O_4, CdTe, PbSe, PbS and PbS/CdS) on surfaces,[11-14] these processes require long deposition times and provide limited control over film thickness and roughness. Other methods such as spin-coating or dip-coating often require many steps and low vapor pressure organic solvents, and they ultimately waste substantial amounts of material.

Due to these challenges, there would be a distinct advantage in using a single ligand that could not only assist in the assembly of NPs on substrates but also permit electron transport for device applications. Common ligands for synthesizing semiconductor nanocrystals, and in particular highly insulating hydrocarbon chains,

typically have deleterious effects on carrier mobility in devices. Methods to replace or remove the surfactants typically reduce interparticle distances, which often lead to macroscopic defects (i.e. cracks) in the thin films.[15,16] In contrast, biochemically-driven processes such as those reported in this work have may use as environmentally friendly, scalable, and manufacturable methods to obtain high-quality films. Furthermore, many conductivity studies with double stranded DNA have been run to demonstrate the possibility of using DNA not only as self-assembling material but also as mediators for charge transport.[17-21] For example, several groups have recently reported that electrons can be transported through DNA π stack as well as through 34nm long dsDNA.[22-26]

We recently demonstrated that DNA conjugated onto spherical gold nanoparticles (AuNPs) can drive self-organization into highly ordered gold nanoparticle superlattices on predefined surface sites through tunable, orthogonal, and controllable DNA interactions between nanoparticles.[27, 28] Film defects in the AuNP lattices were removed by utilizing a thermal annealing step to reorganize particles on the surface, rather than relying on kinetic deposition processes. To use DNA for close-packed uniform QD films, we first had to develop methods for conjugating DNA directly to the nanocrystals while avoiding the highly-insulating lipid bilayers or polymer coatings typically used in QD bioconjugates[29-32] and maintaining the stability to high divalent salt concentrations critical to obtaining close-packed nanoparticles.[33]

In this work, we report high-yielding chemical conjugation strategies to attach DNA strands directly to QDs that also retain stability up to 125mM $MgCl_2$. Furthermore, we show that these DNA conjugated QDs can be used to produce uniform thin films with

controllable film thicknesses in just two steps. Finally, in order to study the effect of DNA on charge separation for solar applications, we fabricated test ITO/TiO_2/DNA-CdTe/Au devices to show that the incorporation of DNA in the QD thin films did not impede electron-hole separation and that photovoltaic effects could be observed.

5.2 Materials and Methods

5.2.1 Synthesis of CdTe quantum dots

CdTe quantum dots were prepared with minor modifications following the method reported by Chen et al.[34] The TOP-Te solution was prepared dissolving 0.035g tellurium (Alfa Aesar, 99.99%) in 0.313g TOP under nitrogen at 250^{o}C for 3hrs until the solution turned light yellow. The CdO solution was prepared by mixing 0.035g cadmium oxide, 0.275g octadecylphosphonic acid (Sigma-Aldrich, 97%) and 3.725g trioctylphosphine oxide in a 100mL flask at 100^{o}C for 3hrs under nitrogen. The CdO solution was then heated to 325^{o}C and injected with the TOP-Te solution shortly thereafter. The reaction was then cooled to 315^{o}C followed by a growth step. Running the growth reaction for 1.5 minutes, 6 minutes and 8 minutes yielded ~4.81 nm, 5.69nm and 6.53nm CdTe QDs, respectively. The size was determined both by absorbance[35] and TEM images. Toluene was added to a batch of CdTe QDs when cooled to 60^{o}C. To remove excess organics, the CdTe QDs were precipitated out using methanol followed by bulk centrifugation for 3times.

5.2.2 QD-DNAs conjugation

DNA Conjugated CdTe QDs: The CdTe QDs were dissolved in chloroform. A thioglycerol (Sigma Aldrich, 99%) solution in 5mM phosphate buffer was added to the CdTe QDs in chloroform using CdTe:thioglycerol molar ratios of 1:10^{5} (0.35M thioglycerol for 4.81nm CdTe). Biphasic solutions formed and were mixed vigorously until the CdTe QDs were completely transferred to the aqueous phase. The water soluble

CdTe QDs were then collected and the excess thioglycerol was removed by using a 30K centrifuge filter. At the same time, thiolated DNA (5'HS-T_{10} and 3'HS-T_{10}) was prepared by first reducing the commercially purchased DNA (Integrated DNA Technologies) with TCEP-HCl (Thermo Scientific) for 1 hr followed by removing excess TCEP by dialysis (2K MWCO, Thermo Scientific). The reduced DNA was immediately added to the thioglycerol conjugated CdTe QDs in 0.1M NaOH using CdTe:DNA ratios of 1:250 for a size of 4.81nm CdTe QDs. A ratio of CdTe:DNA varied as proportional to r^2. After overnight reaction, excess DNAs were filtered out using a 30K centrifuge filter and CdTe-DNAs solution was stored in 5mM phosphate buffer.

5.2.3 Device fabrication

TiO_2 film deposition: TiO_2 nanoparticles (Ti-Nanoxide HT/SC) were purchased from Solaronix Inc. The TiO_2 films were prepared on ITO glass (Delta Technologies, 10 Ω/cm^2) by spin coating at 3000 rpm for 15s. One end of the TiO_2 film was wiped with ethanol for ITO contact during current-voltage measurements followed by annealing at 450^oC for 10min. The TiO_2 films were additionally treated with 50mM $TiCl_4$ (Sigma Aldrich) at 70^oC for 30min and followed by a second annealing at 450^oC for 10min.

QD film deposition: Two sets of DNA conjugated QDs one bound with 5'SH-T_{10} and the other with 3'SH-T_{10} were mixed together in 10mM $MgCl_2$ with and without linker DNA A_{10}. First, the area of TiO2 substrate where the DNA-QD film forms was defined by UV exposure with oxygen gas using a shadow mask. The DNA-QD solutions were dropped onto the TiO_2 substrates and adsorbed for 1.5 hrs under humid conditions followed by vacuum treatment for a few minutes to remove excess solvent. The films

were then washed briefly with 90% ethanol to remove excess salts. Next, the DNA-QDs were thermally annealed under humid conditions at 60^{o}C for 1-3hrs to promote ordering and cooled down slowly (0.5^{o}C/min.). The films were further heated under vacuum at 80^{o}C for 40min. to remove any remaining water molecules. Gold metal (Kurt J. Lesker, 99.999%) was next deposited on the DNA-QD film by vacuum evaporation at a rate of 0.4Å/s and 1.5 Å/s with 30nm and 70nm, respectively followed by a vacuum anneal for 40min at 80^{o}C to promote better metal contact.

5.2.4 Current-voltage measurements

Current–voltage measurements were performed using a Keithley 2400 source meter. The solar spectrum at AM1.5 was simulated to within class BBA specifications with a filtered tungsten lamp (PV Measurements). The source intensity (100mW/cm^2) was measured with a calibrated reference solar cell having an 8 mm diameter aperture from PV Measurements. The active area of the devices ranges from 1 mm^2 to 1.5 mm^2, as defined by the overlap of ITO and Au.

5.2.5 Instrumentation

UV-Visible Spectrophotometry (UV-Vis): The UV-Vis absorbance was measured by Beckman Coulter DU 730 Life Science UV-Vis spectrophotometer, which wavelength used for measurements was ranged between 200 and 900 nm.

Scanning Electron Microscopy (SEM): SEM images were taken by JEOL JSM 7401F, which acceleration voltage was 5 kV with a secondary electron mode.

5.3 Results and Discussion

5.3.1 DNA-CdTe QD conjugation

The strategy used for producing stable DNA conjugated CdTe quantum dots (DNA-CdTe) is depicted in Fig. 5.1. First, a buffered thioglycerol (TG) solution was directly added to the as-synthesized CdTe QDs in chloroform to form a biphasic mixture. Once the TG conjugated QDs completely transferred to the aqueous phase, thiolated DNA was added at basic pH (>pKa) to facilitate binding between thiolate (S^-) groups and the Cd surface.[36] By using an intermediate ligand exchange method, we were easily able to conjugate high yields of DNA to each QD without excessive use of DNA as well as impart stability to the DNA-QDs in buffer and salts. After each TG and DNA conjugation, the CdTe QD solutions were run through microcentrifuge filters several times to remove excess ligands and the DNA-CdTe QDs were stored in 5mM phosphate buffer. This modified two-step ligand exchange method could reliably produce stable DNA conjugated QD solutions irrespective of DNA sequence and nanoparticle size. After adding $MgCl_2$ to the DNA conjugated CdTe QD solutions, the nanoparticles were stable without forming any aggregates for at least 48hrs while thioglycerol only coated CdTe QDs left pellets on the bottom of a tube upon the addition of $MgCl_2$. It is believed that the highly negatively charged DNA acts as a buffer layer which keeps the Mg^{2+} ions away from the QD surface as well as provides enough electrostatic repulsion force between particles to prevent aggregation.

Both the optical properties of the DNA(T_{10})-CdTe QDs and the uniformity of DNA coverage on the particles were investigated by UV-Vis adsorption and gel electrophoresis. As shown in Fig. 5.2, after CdTe-DNA(T_{10}) conjugation with

monodisperse CdTe nanocrystals (Fig. 5.2a, b), the excitonic peaks were preserved with less than 5 nm blue shifts observed which correlated to less than 0.22nm decrease (0.18nm for 4.81nm, 0.17nm for 5.69nm and 0.22nm for 6.53nm, respectively) in CdTe dimension (Fig. 5. 2c and Fig. 5.3). All of these observed shifts are smaller than the diameters of the individual Cd (0.3nm) and Te (0.28nm) atoms. These minor blue shifts in absorbance were mainly observed during the thioglycerol ligand exchange in which unpassivated Te atoms on the QD surface could readily react with oxygen, resulting in the formation of singlet oxygen molecules at the CdTe surface.[37] In terms of the uniformity of DNA coating on the CdTe QDs, gel electrophoresis showed very sharp bands of the DNA(T_{10})-CdTe QDs indicating that all the nanocrystals have roughly the same coverage of DNA (Fig. 5.2d). As opposed to the DNA-CdTe QDs, the thioglycerol only conjugated nanocrystals stayed primarily in the well due to its charge neutrality.

.

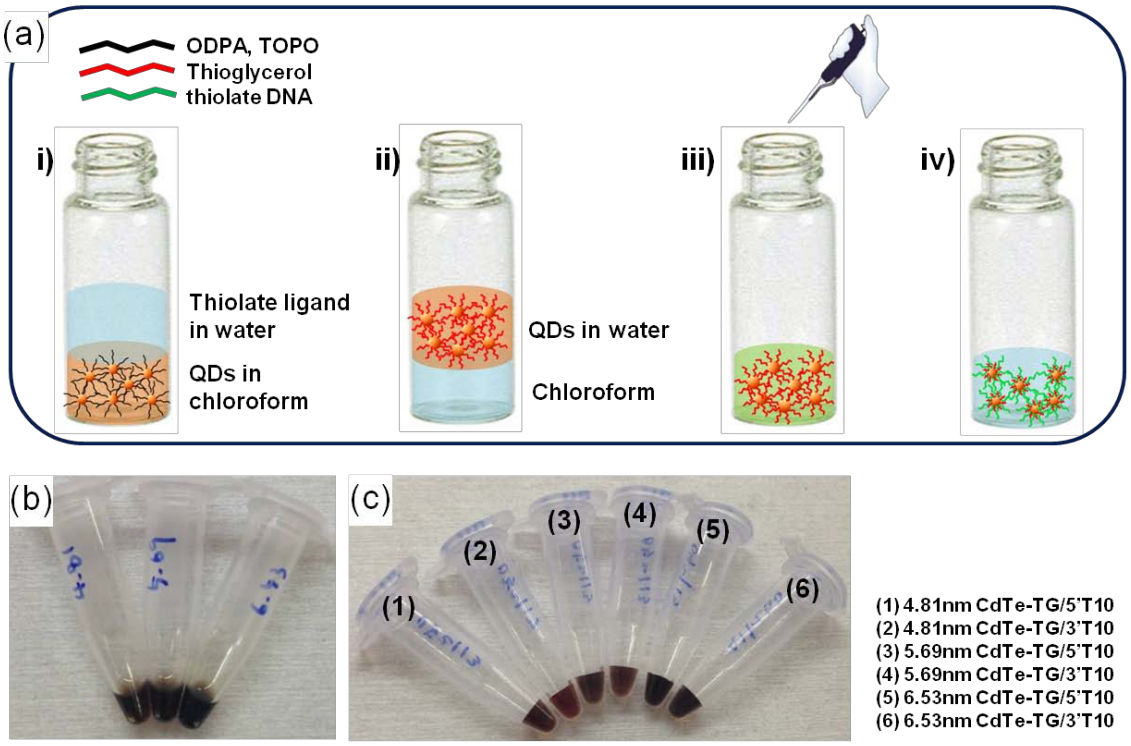

Fig. 5.1. (a) Schematic of DNA-QD conjugation: i) biphasic mixture consisting of QD in chloroform and thioglycerol in 5mM phosphate buffer ii) collection of phase transferred QD-thioglycerol solution followed by filtration of excess thioglycerol iii) addition/reaction of HS-DNA to filtered QD-glycerol pellet and iv) a removal of excess DNA. (b) Optical image of as-synthesized CdTe QD solutions. (c) Optical image of DNA(T_{10}) conjugated CdTe QDs.

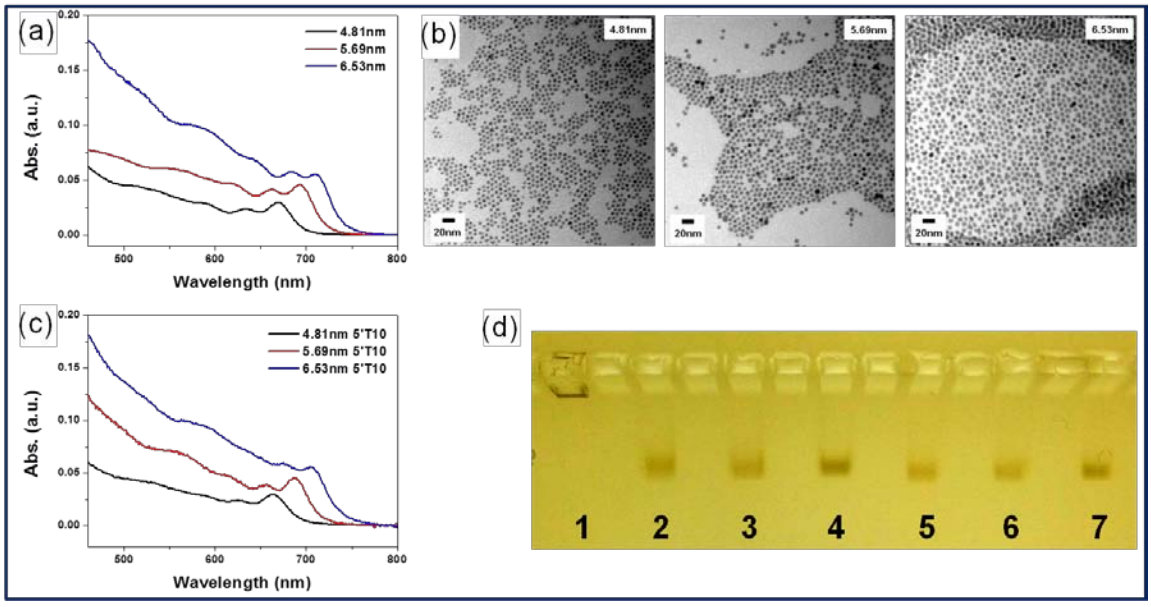

Fig. 5.2 (a) UV-Vis absorbance of as-synthesized CdTe QD solutions. (b) TEM images of as-synthesized CdTe QDs. (c) UV-Vis absorbance of DNA(T_{10})-QD solutions. (d) Agaroase gel electrophoresis of Thioglycerol-QD and DNA(T_{10})-QDs, 1: Thioglycerol-QD, 2: 5'T_{10}-4.81nm CdTe, 3: 5'T_{10}-5.69nm CdTe, 4: 5'T_{10}-6.53nm CdTe, 5: 3'T_{10}-4.81nm CdTe, 6: 3'T_{10}-5.69nm CdTe, 7: 3'T_{10}-6.53nm CdTe.

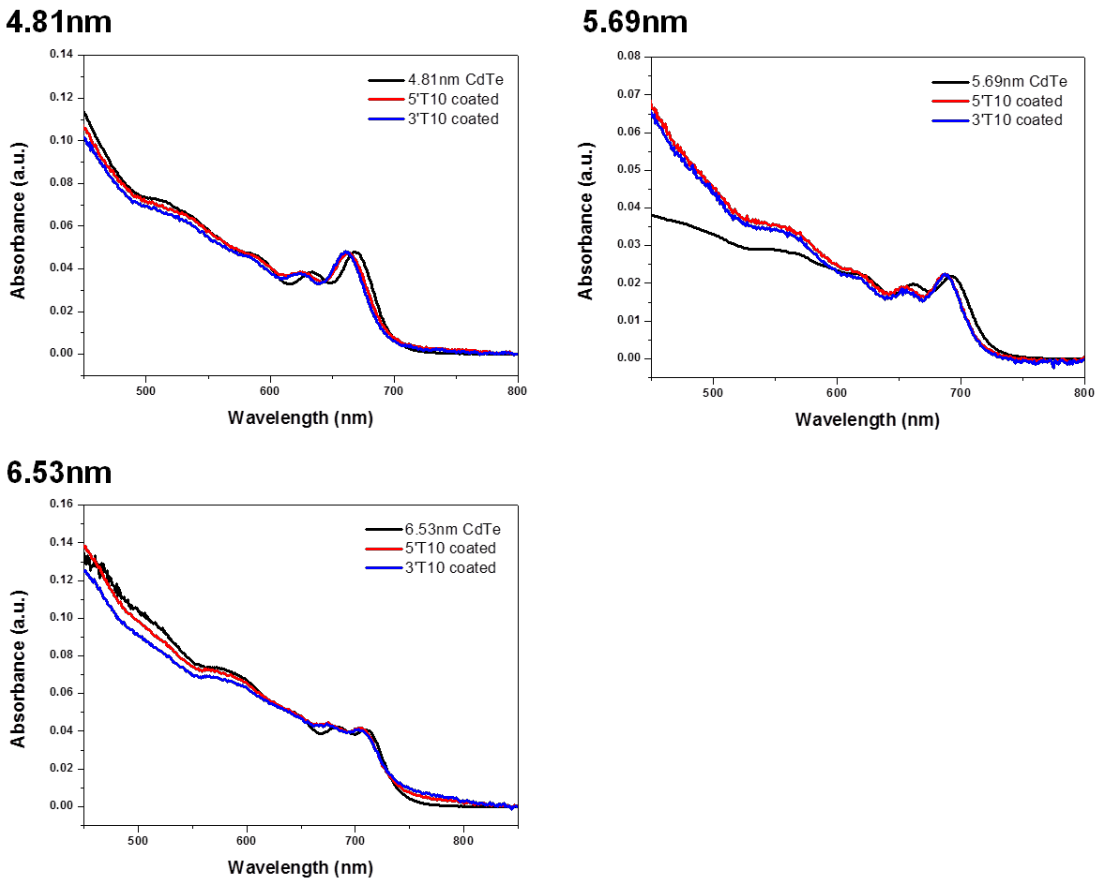

Fig. 5.3 UV-Vis absorbance of organic CdTe QD solution and its DNA(T_{10})-CdTe QD with different sizes of QDs.(4.81nm, 5.69nm and 6.53nm)

5.3.2 Formation of DNA-CdTe QD film and the role of DNA interaction on film uniformity

In order to produce close packed nanoparticle thin films using DNA interactions, we previously found that the use of salt such as $MgCl_2$ was needed as it helped to both screen the negative charges of DNA as well as increase the melting temperature of DNA. However, while we found that the TG-DNA-CdTe QDs could be stable in Mg^{2+} concentrations as high as 125mM $MgCl_2$, because salts could have a negative influence on charge transport, we decided to use the minimum amount of Mg^{2+} needed to facilitate DNA-DNA hybridization which we determined to be 10mM $MgCl_2$. While Na^+ could have been used, the smaller size and divalent nature of Mg^{2+} was found to help yield dense arrays of close packed DNA conjugated nanoparticles on the surface which is critical for optoelectronic thin film devices. To study the use of DNA-QDs for photovoltaic devices, solar cells consisting of ITO/TiO_2/DNA-CdTe/Au were fabricated. TiO_2 films were first deposited on ITO by spin-coating commercial TiO_2 nanoparticle solutions (Solaronix Inc.) at 3000rpm for 15s, sintering at 450^{o}C for 10min followed by treatment with 50mM $TiCl_4$ at 70^{o}C for 30min and a final sintering step. Next, DNA-CdTe QD solutions containing DNA which simultaneously hybridizes with both the 5' and 3' DNA-QDs ("linker DNA") were adsorbed to the sintered TiO_2 surfaces for 1.5 hr followed by drying in vacuum for 5 minutes and rinsing with 90% ethanol to remove excess salts. Comparison studies with no linker DNA were run simultaneously. Immediately, the difference between using linker DNA and no linker DNA was clearly discernable by eye as the films produced with linker DNA which promoted interparticle hybridization produced highly uniform QD films (Fig. 5.4a) whereas in contrast, arrays

generated with no linker DNA yielded visibly rough films where the thickness at the outer edge was much larger than directly in the middle of the film (Fig. 5.4b). After adsorption and vacuum drying, the DNA(T_{10})-CdTe QD films with or without linker DNA underwent humid annealing at 60^{o}Cto further promote order followed by vacuum annealing for 40min to remove water. Finally, a gold electrode was deposited on top of the DNA CdTe QD layer. UV-Vis analysis of the as prepared DNA-CdTe films showed that the QDs were not oxidized as there was no apparent shift in the absorbance onset peak. (Fig. 5.5)

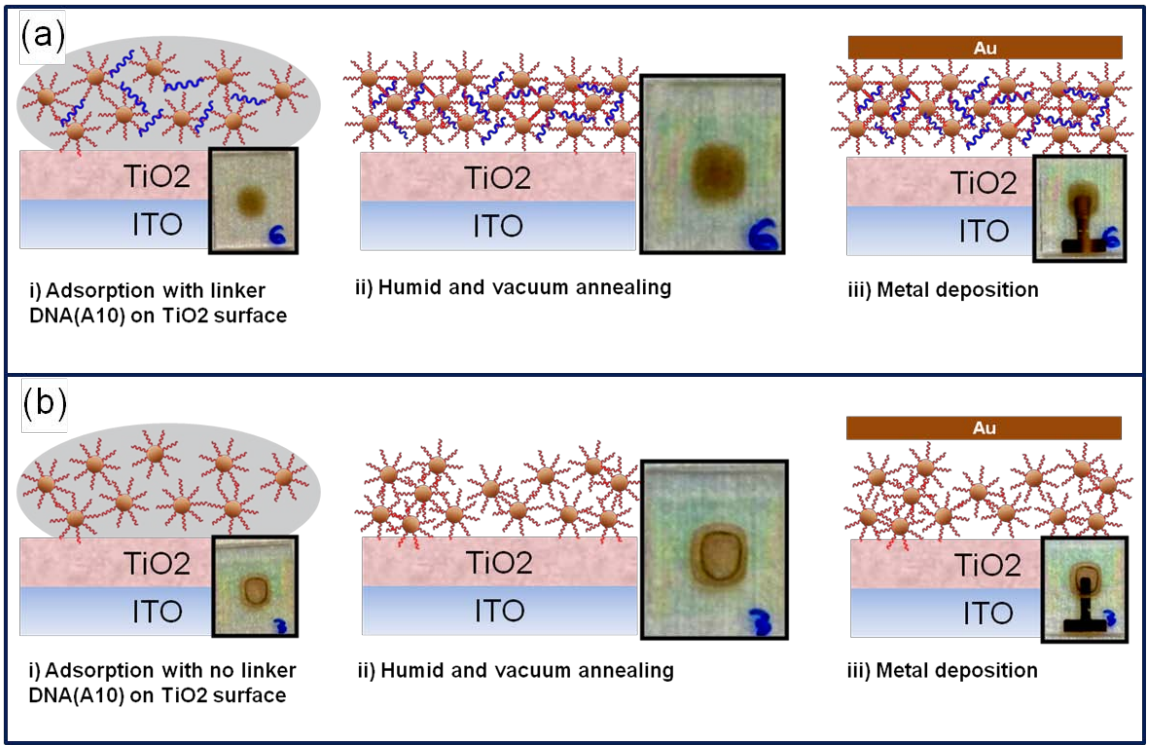

Fig. 5.4. Schematic of DNA(T_{10})-QD film fabrication on TiO_2/ITO film (a) with linker A_{10} DNA (b) with no linker DNA.

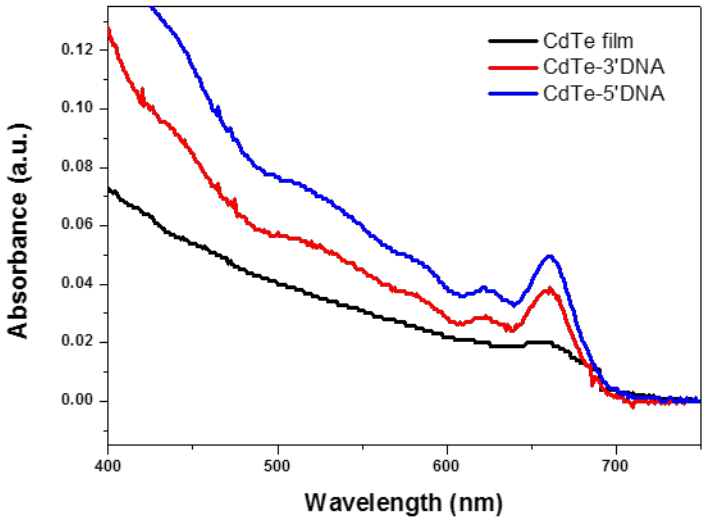

Fig.5.5 UV-Vis absorbance of DNA(T_{10})-CdTe QDs and QD film with linker DNAs(A_{10}) after a deposition on the substrate.

5.3.3 Thickness control of DNA-CdTe QD film

While typical procedures for making thin films either use multi-step spin coating which wastes valuable material or dip-coating which is highly labor intensive and not scalable, the use of biological interactions for assembly greatly facilitated film generation. By using DNA, the entire films could be produced in just a couple steps and under completely benign processing conditions with no waste of material. Furthermore, because the entire process of producing the DNA-QD thin films only involves adsorption of a single solution followed by drying and thermal annealing, it was very simple to produce films of variable thicknesses simply by tuning the DNA-CdTe concentrations (Fig. 5.6b). As shown in Fig. 5.6c, as we increased the QD concentrations from 1uM to 5uM, there was a clear gradation in color that corresponded to increases in film thicknesses. Cross-sectional SEM images (Fig. 5.6c and Fig. 5.7) of the ITO/TiO_2/CdTe/Au film (Fig. 5.6a) showed not only a clear correlation between film thickness and QD concentration but that the films remained relatively smooth and that the QD-DNA layers were intact throughout the film.

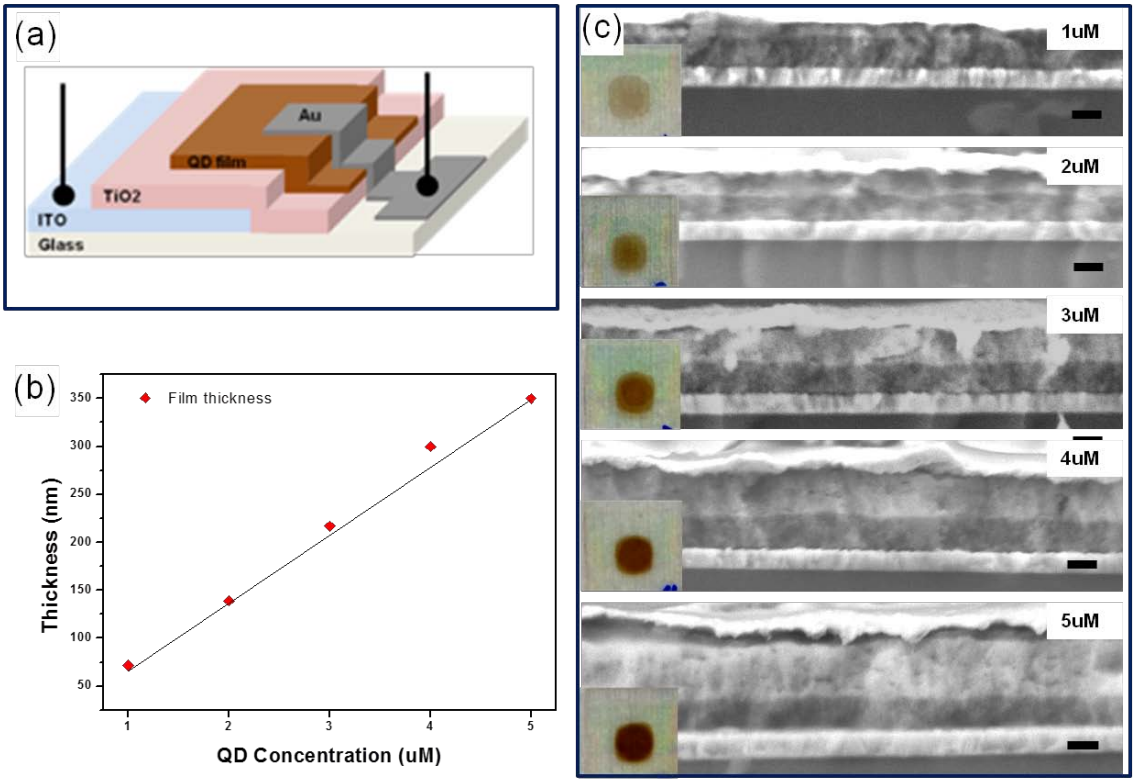

Fig. 5.6 (a) A layout of the ITO/TiO_2/DNA(T_{10})-QD film/Au devices tested. (b) Plot showing the thickness of the DNA(T_{10})-QD films obtained as a function of the concentration of the DNA(T_{10})-QD solutions used. (c) Cross-sectional SEM images and optical images of films obtained using different concentrations (1uM - 5uM) of 6.53nm CdTe-DNA(T_{10}) with A_{10} linker DNA. Scale bar corresponds to 200nm.

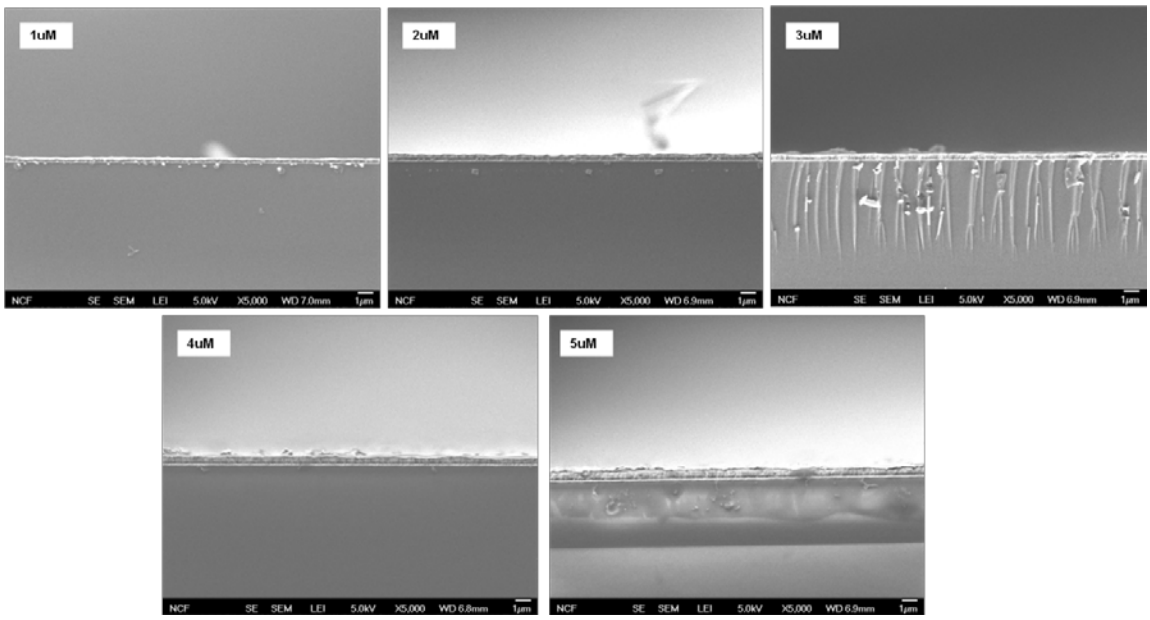

Fig. 5.7 SEM images of low magnification of DNA(T_{10})-QD films with linker DNAs(A_{10}) from all different concentrations.

5.3.4 Current-Voltage characteristics of DNA-CdTe QD film

Based on the relative energy levels of the assembled ITO/TiO_2/DNA-CdTe/Au devices, the DNA-CdTe QDs would act as a hole transport layer while the TiO_2 would accept electrons from the electron-hole pairs generated in the CdTe (Fig. 5.8a). To test this, CdTe QD films composed of different sized nanocrystals (4.81nm, 5.69nm and 6.53nm) were prepared and each device was tested as a function of linker DNA, QD size and film thickness. First as a measure of comparison, films made with no linker DNA showed absolutely little to no consistency in current-voltage characteristics as a function of QD size (Fig. 5.8b). It is hypothesized that the random formation of QD organization within the no DNA linker films could only result in irreproducible and overall poor device performance. The lower open circuit voltage (V_{oc}) values obtained from than that of devices with linker DNA supports this hypothesis because poor film quality is known to lead to more shunt paths.[38] This was supported by the higher shunt resistances (R_{sh}) observed of the linker A_{10} DNA films as opposed to those prepared with no linker A_{10} DNA. In direct contrast, devices with linker DNA showed consistent current-voltage characteristics where in all of the three sets of devices with different QD size, the V_{oc} values were set around 400mV and the short circuit current (J_{sc}) showed an increase as a function of a size of the CdTe QDs (Fig. 5.8c). Overall, the J_{sc} values measured from the films with linker DNA also were comparable to a previous report of pyridine coated CdTe/CdSe nanocrystal solar cell[39] where ligand exchange was run but the nanocrystals were not sintered. One possible reason why J_{sc} would increase with CdTe size is simply that more light is adsorbed with the increase in the CdTe QD size. Based on the reference solar spectra from National Renewable Energy Labs (NREL)

(100mW/cm^2), linear correlations between absorbed input power (P_{input}) and J_{sc} could be observed assuming the overall fill factors (*FF*) and V_{oc} values remain similar enough.

The ease in film fabrication enabled us to study device performance also as a function of the thickness of the CdTe layer. In order to test the affect of film thickness on PV behavior, the 6.53nm CdTe QDs were chosen since they showed the highest performance out of the three sizes of CdTe QDs. As shown in the summarized results of the current-voltage characteristics in Fig. 5.8d, while the device with 1uM CdTe QD film was mostly shunted due to the films being too thin, as we increased from 2uM to 5uM, J_{sc} values decreased although V_{oc} remained stable. As is typically observed with nanocrystal solar cells, having too thick a film are likely to hinder carrier transport due to increased recombination events. Among the devices tested, the use of 2uM CdTe QD (film thickness = 140nm) produced the best photovoltaic effect with J_{sc} of 0.24mA/cm^2, V_{oc} of 0.38V, and *FF* of 0.34.

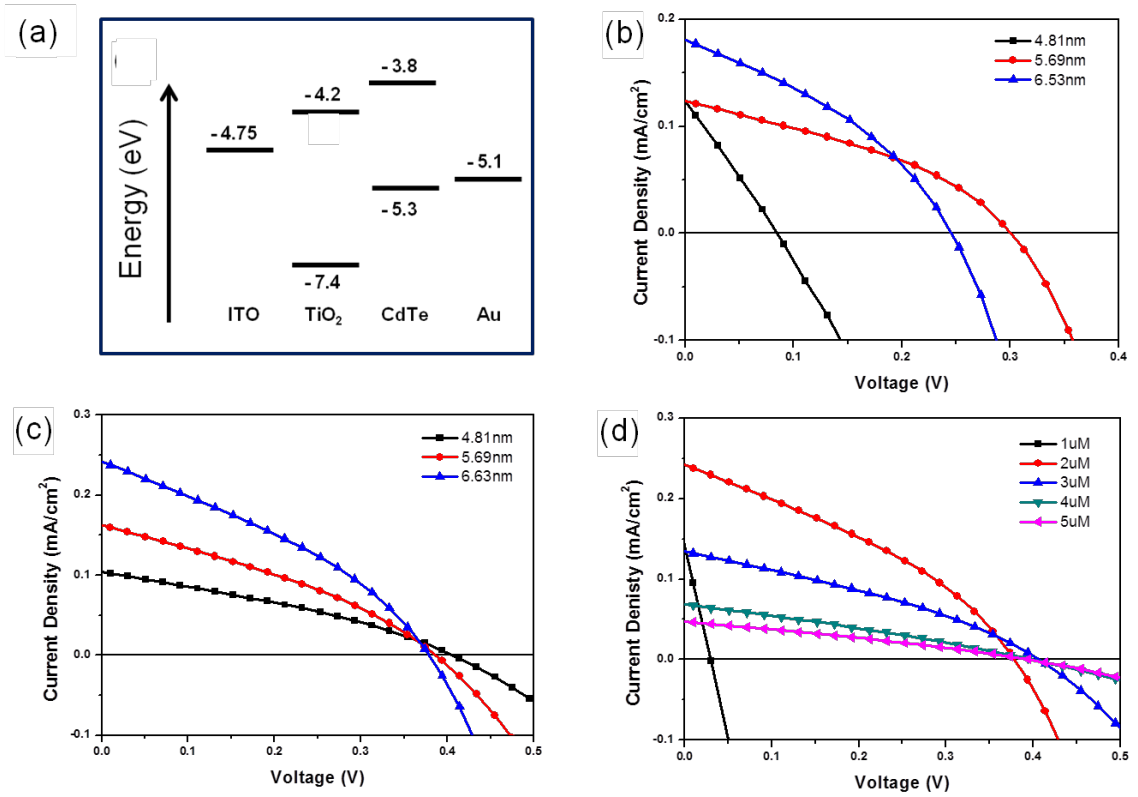

Fig. 5.8 (a) The energy levels with respect to vacuum (E_{vac} = 0 eV). (b) Current-Voltage curves for different sized CdTe QDs-DNA(T_{10}) films with no linker DNA. (c) Current-Voltage curves for different sized CdTe QDs-DNA(T_{10}) film with linker A_{10} DNA. (d) Current-Voltage curves for different thicknesses of the DNA(T_{10})-6.53nm CdTe layer.

5.3.4 Current-Voltage characteristics of DNA-CdTe QD film

Effective separation of electron-hole pairs is critical to achieve a photovoltaic effect. In the case of nanocrystals, the electronic coupling between particles decreases exponentially as a function of interparticle distance.[40] For example, when the ligands on the QDs are the hydrocarbons used for their synthesis the coupling energy diminishes an order of magnitude every ~2Å increase in interparticle distance. In previous work with small area (3-5 micron) DNA-gold nanoparticle superlattice, we determined that the interparticle distance is primarily driven by the lengths of the dsDNA used. If this is roughly maintained with these large area (over 3 x 3mm^2) DNA-QD films, the spacing(surface to surface distance) between the CdTe nanocrystals is theoretically calculated to be ~3nm. Should this be the case, the distance between neighboring CdTe QDs is potentially too long to assume easy carrier hopping from one particle to the next which lends to the possibility that the DNA itself plays a role in enabling carrier migration. Because electron mobility through double stranded DNA has been demonstrated, it is not implausible that an electron generated in a QD could move through the surrounding DNA to the next QD. However, in the case of semiconductors, it is important to also consider the relative HOMO-LUMO energy levels of the DNA attached to the nanoparticle and the Conduction Band(CB)-Valence Band(VB) of the QDs to account for hole mobility. In studies run concurrently with the work shown here, Scanning Tunneling Microscopy (STM) analysis of single DNA conjugated CdTe nanoparticles shows that the relative HOMO level of the double stranded DNA attached may be potentially slightly lower (further away from vacuum level) in energy to the VB of the CdTe nanocrystal, lending to the possibility that the DNA used in this instance

cannot act as a strong hole trap and so the hole generated in the CdTe QD is relatively mobile enough to move between neighboring QDs through the DNA strands. Future studies on QD-DNA clusters will further elucidate the mobility characteristics of the carriers within the DNA strands in between the QDs.

5.4 Conclusion

A new approach to fabricate QD solar cells by DNA hybridization was demonstrated in this work. First, DNA was directly conjugated to CdTe nanocrystals to produce stable DNA-QD solutions with uniform DNA coatings that remain stable in high ionic strength environments and to oxidation. These DNA-QDs and linker DNA were assembled into uniform QD films in a few steps using benign processes with no material waste. These films had minimal surface roughness, and their thickness could be easily tuned by simply changing the initial DNA-QD concentration. In test solar cell devices, current-voltage measurements showed that the DNA strands did not prevent electron-hole separation, and a photovoltaic effect was observed upon illumination. Future studies will investigate carrier mobility through these DNA-QD films as well as discrete nanoparticle structures to understand the influence of DNA on charge separation and energy transfer.

5.5 Acknowledgments

This chapter, in full, is a reprint of the material, currently being prepared for submission for publication. Noh, Hyunwoo; Nagpal, Prashant; Cha, Jennifer N. The dissertation author was the primary investigator and author of this material.

5.6 References

1. Prins, F.; Buscema, M.; Seldenthuis, J. S.; Etaki, S.; Buchs, G.; Barkelid, M.; Zwiller, V.; Gao, Y.; Houtepen, A. J.; Siebbeles, L. D. A.; van der Zant, H. S. J. Fast and Efficient Photodetection in Nanoscale Quantum-Dot Junctions. *Nano Lett.* **2012**, *12*, 5740-5743.

2. Kwak, J.; Bae W. K.; Lee, D.; Park, I.; Lim, J.; Park, M.; Cho, H.; Woo, H.; Yoon, D. Y.; Char, K.; Lee, S.; Lee, C. Bright and efficient full-color colloidal quantum dot light-emitting diodes using an inverted device structure. *Nano Lett.* **2012**, *12*, 2362–2366.

3. Pal, B. N.; Robel, I.; Mohite, A.; Laocharoensuk, R.; Werder, D. J.; Klimov, V. I. High-Sensitivity p-n Junction Photodiodes based on PbS Nanocrystal Quantum dots. *Adv. Func. Mater.* **2012**, *22*, 1741–1748.

4. Sun, L.; Choi, J. J.; Stachnik, D.; Bartnik, A. C.; Hyun,B.-R; Malliaras, G. G.; Hanrath, T.; Wise, F. W. Bright Infrared Quantum-Dot Light-Emitting Diodes through Inter-Dot Spacing Control. *Nat. Nanotech.* **2012**, *7*, 369–373.

5. Kemp, K. W.; Labelle, A. J.; Thon, S. M.; Ip, A. H.; Kramer, I. J.; Hoogland, S.; Sargent, E. H. Interface Recombination in Depleted Heterojunction Photovoltaics based on Colloidal Quantum Dots. *Adv. Energy Mater.* **2013**, *3*, 917-922.

6. Etgar, L.; Zhang, W.; Gabriel, S.; Hickey, S. G.; Nazeeruddin1, Md K.; Eychmüller, A.; Liu, B.; Grätzel, M. High Efficiency Quantum Dot Heterojunction Solar Cell Using Anatase (001) TiO_2 Nanosheets. *Adv. Mater.* **2012**, *24*, 2202-2206.

7. Kim T. -H.; Cho, K. –S.; Lee, E. K.; Lee, S. J.; Chae, J.; Kim, J. W.; Kim, D. H.; Kwon, J. -Y.; Amaratunga, G.; Lee, S. Y.; Choi, B. L.; Kuk, Y.; Kim J. M.; Kim, K. Full-Colour Quantum Dot Displays Fabricated by Transfer Printing. *Nat. Photonics* **2011**, *5*, 176-182.

8. Tang, J.; Liu, H.; Zhitomirsky, D.; Hoogland, S.; Wang, X.; Furukawa, M.; Levina, L.; Sargent, E. H. Quantum Junction Solar Cells. *Nano Lett.* **2012**, *12*, 4889-4894.

9. Kamat, P. V. Quantum Dot Solar Cells. The Next Big Thing in Photovoltaics. *J. Phys. Chem. Lett.* **2013**, *4* 908–918.

10. Ip, A. H.; Thon, S. M.; Hoogland, S.; Voznyy, O.; Zhitomirsky, D.; Debnath, R.; Levina, L.; Rollny, L. R.; Carey, G. H.; Fischer, A.; Kemp, K. W.; Kramer, I. J.; Ning, Z.; Labelle, A. J.; Chou, K. W.; Amassian, A.; Sargent, E. H. Hybrid Passivated Colloidal Quantum Dot Solids. *Nat. Nanotech.* **2012**, *7*, 577-582.

11. Dong, A.; Chen, J.; Oh, S. J.; Koh W. -K.; Xiu, F.; Ye, X.; Ko, D. -K.; Wang, K. L.; Kagan, C. R.; Murray, C. B. Multiscale Periodic Assembly of Striped Nanocrystal Superlattice Films on a Liquid Surface. *Nano Lett.* **2011**, *11*, 841-846.

12. Chen, Z.; O'Brien, S. Structure Direction of II–VI Semiconductor Quan tum Dot Binary Nanoparticle Superlattices by Tuning Radius Ratio. *ACS Nano* **2008**, *2*, 1219-1229.

13. Bodnarchuk, M. I.; Erni, R.; Krumeich, F.; Kovalenko, M. V. Binary Superlattices from Colloidal Nanocrystals and Giant Polyoxometalate Clusters. *Nano Lett.* **2013**, *13*, 1699-1705.

14. Overgaag, K.; Evers, W.; de Nijs, B.; Koole, R.; Meeldijk, J.; Vanmaekelbergh, D. Binary Superlattices of PbSe and CdSe Nanocrystals. *J. Am. Chem. Soc.*, **2008**, *130* 7833-7835.

15. Luther, J. M.; Law, M.; Song, Q.; Perkins, C. L.; Beard, M. C.; Nozik, A. J. Structural, Optical, and Electrical Properties of Self-Assembled Films of PbSe Nanocrystals Treated with 1,2-Ethanedithiol. *ACS Nano* **2008**, *2*, 271-280.

16. Jasieniak, J.; Macdonald, B. I.; Watkins, S. E.; Mulvaney, P. Solution-Processed Sintered Nanocrystal Solar Cell via Layer-by-Layer Assembly. *Nano Lett.* **2011**, *11*, 2856-2864.

17. Roy, S.; Vedala, H.; Roy A. D.; Kim, D. -H.; Doud, M.; Mathee, K.; Shin, H. -K.; Shimamoto, N.; Prasad, V.; Choi, W. Direct Electrical Measurements on Single-Molecule Genomic DNA Using Single-Walled Carbon Nanotubes. *Nano Lett.* **2008**, *8*, 26-30.

18. Porath, D; Bezryadin, A.; de Vries, S.; Dekker, C. Direct Measurement of Electrical Transport through DNA Molecules. *Nature* **2000**, *403*, 635-638.

19. Fink, H. W.; Schoenberger, C. Electrical Conduction through DNA Molecules. *Nature* **1999**, *398*, 407-410.

20. Storm, A. J.; van Noort, J.; de Vries, S.; Dekker, C. Insulating Behavior for DNA Molecules between Nanoelectrodes at the 100 nm Length Scale. *Appl. Phys. Lett.***2001**, *79*, 3881–3883.

21. Kasumov, A. et al. Proximity-Induced Superconductivity in DNA. *Science* **2001**, *291*, 280-282.

22. Slinker, J. D.; Muren, N. B.; Renfrew, S. E.; Barton, J. K. DNA Charge Transport Over 34 nm. *Nat. Chem.* **2011**, *3*, 228-233.

23. Guo, X.; Gorodetsky, A. A.; Hone, J.; Barton, J. K.; Nuckolls, C. Conductivity of a Single DNA Duplex Bridging a Carbon Nanotube Gap. *Nat. Nanotech.* **2008**, *3*, 163- 167.

24. Genereux, J. C.; Barton, J. K. Mechanisms for DNA Charge Transport. *Chem. Rev*. **2010**, *110*, 1642–1662.

25. Cohen, H.; Nogues, C.; Naaman, R.; Porath, D. Direct Measurement of Electrical Transport through Single DNA Molecules of Complex Sequence. *Proc. Natl Acad. Sci. USA* **2005**, *102*, 11589–11593.

26. Xu, B.; Zhang, P.; Li, X.; Tao, N. Direct Conductance Measurement of Single DNA Molecules in Aqueous Solution. *Nano Lett.* **2004**, *4*, 1105-1108.

27. Noh, H.; Choi, C; Hung, A. M.; Jin, S.; Cha, J.N. Site-Specific Patterning of Highly Ordered Nanocrystal Superlattices through Biomolecular Surface Confinement. *ACS Nano* **2010**, *4*, 5076-5080.

28. Noh, H.; Hung, A. M.; Cha, J. N. Surface-Driven DNA Assembly of Binary Cubic 3D Nanocrystal Superlattices. *Small* **2011**, *7*, 3021-3025.

29. Dubertret, B.; Skourides, P.; Norris, D. J.; Noireaux, V.; Brivanlou, A. H.; Libchaber, A. In Vivo Imaging of Quantum Dots Encapsulated in Phospholipid Micelles. *Science* **2002**, *298*, 1759-1762.

30. Wu, X. Y.; Liu, H. J.; Liu, J. Q.; Haley, K. N.; Treadway, J. A.; Larson, J. P.; Ge, N. F.; Peale, F.; Bruchez, M. P. Immunofluorescent Labeling of Cancer Marker Her2 and Other Cellular Targets with Semiconductor Quantum Dots. *Nat. Biotech.* **2003**, *21*, 41-46.

31. Zhou, D. J.; Piper, J. D.; Abell, C.; Klenerman, D.; Kang, D. J.; Ying, L. M. Fluorescence Resonance Energy Transfer Between a Quantum Dot Donor and a Dye Acceptor Attached to DNA. *Chem. Comm.* **2005**, *38*, 4807-4809.

32. Choi, Y.; Kim, H. P.; Hong, S. M.; Ryu, J. Y.; Han, S. J.; Song, R. In situ Visualization of Gene Expression Using Polymer-Coated Quantum-Dot-DNA Conjugates. *Small* **2009**, *5*, 2085-2091.

33. Noh, H.; Hung, A. M.; Choi, C.; Lee, J. H.; Kim, J.-Y.; Jin, S.; Cha, J. N. 50 nm DNA Nanoarrays Generated from Uniform Oligonucleotide Films. *ACS Nano* **2009**, *3*, 2376-2382.

34. Chen, Z.; Moore, J.; Radtke, G.; Sirringhaus, H.; O'Brien, S. Binary Nanoparticle Superlattices in the Semiconductor-Semiconductor System: CdTe and CdSe . *J. Am. Chem. Soc.* **2007**, *129*, 15702-15709.

35. Yu, W. W.; Qu, L.; Guo, W.; Peng, X. Experimental Determination of the Extinction Coefficient of CdTe, CdSe, and CdS Nanocrystals. *Chem. Mater.* **2003**, *15*, 2854-2860.

36. Schapotschnikow, P.; Hommersom, B.; Vlugt, T. J. H. Adsorption and Binding of Ligands to CdSe Nanocrystals. *J. Phys. Chem. C* **2009**, *113*, 12690-12698.

37. Zhang, Y; He, J.; Wang, P. -N.; Chen, J. -Y.; Lu, Z. -J.; Lu, D. -R.; Guo, J.; Wang , C. -C.; Yang, W. -L. Time-Dependent Photoluminescence Blue Shift of the Quantum Dots in Living Cells:Effect of Oxidation by Singlet Oxygen . *J. Am. Chem. Soc.* **2006**, *128*, 13396–13401.

38. Ju, T.; Yang, L.; Carter, S. Thickness Dependence Study of Inorganic CdTe/CdSe Solar Cells Fabricated from Colloidal Nanoparticle Solutions. *J. Appl. Phys.* **2010**, *107*, 104311.

39. Gur, I.; Fromer, N. A.; Geier, M L.; Alivisatos, A. P. Air-Stable All-Inorganic Nanocrystal Solar Cells Processed from Solution. *Science* **2005**, *310*, 462-465.

40. Guyot-Sionnest, P. Electrical Transport in Colloidal Quantum Dot Films. *J. Phys. Chem. Lett.* **2012**, *3*, 1169-1175.